PhD Program in Neuroscience

Instituto de Neurociencias (CSIC-UMH)

A regulatory Prrx1-Snail1 switch controls melanoma development

---

Doctoral Thesis presented by

Francisco Manuel Cabello Torres

Thesis Director

Dr. Berta López Sánchez-Laorden

Universidad Miguel Hernández de Elche

- 2025 -

The Doctoral Thesis, entitled "A regulatory Prrx1-Snail1 switch controls melanoma development" is presented under **the conventional thesis form with the following quality indicators**:

- Abstract publication of poster contribution in THE 18TH INTERNATIONAL CONGRESS OF THE SOCIETY FOR MELANOMA RESEARCH (2021), organized by The Society for Melanoma Research, entitled "Contribution of the epithelial-to-mesenchymal transition transcription factor PRRX1 to melanoma plasticity and progression". **Francisco Manuel Cabello-Torres**; Khalil Kass Youssef; Maria Ángela Nieto Toledano; Berta L. Sánchez-Laorden. *Pigment Cell & Melanoma Research*. DOI: 10.1111/pcmr.13018
- Poster contribution in THE INTERNATIONAL CONGRESS OF THE EUROPEAN ASSOCIATION FOR CANCER RESEARCH (2022), organized by the European Association for Cancer Research, entitled "Contribution of the epithelial-to-mesenchymal transition transcription factor PRRX1 to melanoma progression and plasticity". **Francisco M. Cabello-Torres**; Khalil Kass Youssef; M. Ángela Nieto; Berta L. Sánchez-Laorden.
- Poster contribution in THE EUREOPEAN DEVELOPMENTAL BIOLOGY CONGRESS (2019), organized by International Society for Developmental Biology, entitled "Mechanisms underlying melanoma plasticity. Role of EMT-TFs". **Francisco M. Cabello-Torres**; Khalil Kass Youssef; M. Ángela Nieto; Berta Sánchez-Laorden.
- Oral presentation in 2nd ANNUAL INTERNATIONAL CONGRESS OF DOCTORAL STUDENTS (2022), organized by University Miguel Hernández of Elche, entitled "Contribution of the epithelial-to-mesenchymal transition transcription factor PRRX1 to melanoma plasticity and progression". **Francisco Manuel Cabello-Torres**; Khalil Kass Youssef; M. Ángela Nieto; Berta Sánchez-Laorden.

Sant Joan d'Alacant, 29th July 2025

Dr. Berta López Sánchez-Laorden, director of the doctoral thesis entitled "**A regulatory Prrx1-Snail1 switch controls melanoma development**".

REPORTS:

That Mr. Francisco Manuel Cabello Torres has carried out, under my supervision, the work entitled "**A regulatory Prrx1-Snail1 switch controls melanoma development**" in accordance with the terms and conditions defined in his Research Plan and in accordance with the Code of Good Practice of the University Miguel Hernández of Elche, satisfactory fulfilling the objectives foreseen for its public defence as a doctoral thesis.

I sign for appropriate purposes, at Sant Joan d'Alacant, 29th July 2025.

Thesis director

Dr. Berta López Sánchez-Laorden

Sant Joan d'Alacant, 29th July 2025

Ms. María Cruz Morenilla Palao, Coordinator of the Neuroscience PhD Program at the Institute of Neurosciences in Alicante, a joint centre of Miguel Hernández University (UMH) and the Spanish National Research Council (CSIC).

REPORTS:

That Mr. Francisco Manuel Cabello Torres has carried out under the supervision of our PhD Program the work entitled "**A regulatory Prrx1-Snail1 switch controls melanoma development**", in accordance with the terms and conditions defined in her Research Plan and in accordance with the Code of Good Practice of the University Miguel Hernández of Elche, satisfactory fulfilling the objectives foreseen for its public defence as a doctoral thesis.

Which I sign for the appropriate purposes, in Sant Joan d'Alacant, 29th July 2025.

Dr. María Cruz Morenilla Palao

Coordinator of the PhD Program in Neuroscience

Funding/Grants/Scholarship:

The realization of this Doctoral Thesis has been carried out thanks to a "Formación de Personal Investigador (FPI)" pre-doctoral scholarship financed by the AEI, Ministerio de Economía, Industria y Competitividad, with reference BES-2017-081145 (2018-2022), and a contract of a higher degree in technical and professional activities funded by the Melanoma Research Alliance with reference https://doi.org/10.48050/pc.gr.91574.

The research has been funded by the following research projects: SAF2016-75702R, PID2019-106852-RB100 (MCIN-AEI), the Prometeo Program for Groups of Excellence (CIPROM/2021/045) from Generalitat Valenciana, Melanoma Research Alliance and Fero Foundation.

1 Table of contents

2 Abbreviations

4-HT: 4-hydroxytamoxifen

Bb: Hair bulb

Bg: Hair bulge

EMT: Epithelial-to-mesenchymal transition

EMT-TF: Epithelial-to-mesenchymal transition transcription factor

gDNA: Genomic DNA

HF: Hair follicle

Hg: Hair germ

KM: Kaplan-Meier

Mc: Melanocyte

MSC: Melanocyte stem cell

PBS: Phosphate-buffered saline

PBSTx: Phosphate-buffered saline and Triton X-100

PBSTw: Phosphate-buffered saline and Tween 20

PCR: Polymerase chain reaction

PFA: Paraformaldehyde

qRT-PCR: Quantitative reverse-transcription polymerase chain reaction

RT-PCR: Reverse-transcription polymerase chain reaction

SEM: Standard error of the mean

TA: Transit-amplifying cells

TF: Transcription factor

TPA: 12-O tetradecanoyl phorbol 13-acetate

3 Abstract

Cutaneous melanoma is a highly aggressive skin cancer characterized by phenotypic plasticity and intratumoural heterogeneity. While a role of epithelial-to-mesenchymal transition transcription factors (EMT-TFs) in melanoma progression has been proposed, their contribution to melanomagenesis remains poorly understood. This study investigates the contribution of the EMT-TFs Prrx1 and Snail 1 to melanoma development using genetically engineered mouse models and *in vitro* melanocyte assays. We show that Prrx1 and Snail1 are expressed in melanocytes during the anagen phase of the hair cycle and in early melanomas, but their expression diminishes as tumours progress. Conditional knockout of Prrx1 in melanocytes accelerates melanoma onset and increases tumour number, without affecting proliferation.

Mechanistically, Prrx1 loss leads to upregulation of Snail1, which enhances stem-like properties in melanocytes. In contrast, Snail1 depletion delays melanoma initiation, and combined loss of Prrx1 and Snail1 phenocopies the wild-type phenotype, supporting that the mechanism by which Prrx1 depletion promotes melanomagenesis is driven by Snail1. *In vitro* experiments indicate a unidirectional regulatory axis where Prrx1 attenuates Snail1 expression via the miR-15 family microRNAs. These findings suggest that Prrx1 acts as a tumour suppressor in melanoma and highlight a novel Prrx1–Snail1 axis that regulates early melanocytic transformation. These results refine our understanding of melanoma initiation and suggest that targeting transcriptional reprogramming could offer new avenues for early intervention.

4 Resumen

El melanoma cutáneo es un cáncer de piel altamente agresivo, caracterizado por una notable plasticidad fenotípica y heterogeneidad intratumoral. Aunque se ha propuesto que los factores de transcripción inductores de la transición epitelio-mesénquima (EMT-TFs, por sus siglas en inglés) tienen una función clave en la progresión del melanoma, su contribución a la iniciación tumoral no ha sido totalmente esclarecida. En este estudio hemos investigado la función de EMT-TFs Prrx1 y Snail1 en el desarrollo del melanoma, utilizando modelos murinos modificados genéticamente y ensayos *in vitro* con melanocitos inmortalizados. Nuestros resultados muestran que Prrx1 y Snail1 se expresan en melanocitos durante la fase anágena del ciclo folicular y en lesiones tempranas de melanoma, pero su expresión disminuye a medida que los tumores progresan. La depleción condicional de Prrx1 en melanocitos acelera la aparición del melanoma e incrementa el número de tumores, sin afectar la proliferación.

Mecanísticamente, la pérdida de Prrx1 conduce a una sobreexpresión de Snail1, lo que potencia las propiedades de tipo célula madre en los melanocitos. En cambio, la eliminación de Snail1 retrasa el inicio del melanoma, y la depleción combinada de Prrx1 y Snail1 reproduce el fenotipo observado en animales silvestres, lo que respalda que el mecanismo por el cual la pérdida de Prrx1 promueve la melanomagénesis está mediado por Snail1. Nuestros experimentos *in vitro* indican la existencia de un bucle regulador unidireccional en el que Prrx1 atenúa la expresión de Snail1 a través de microARNs de la familia miR-15. Estos hallazgos sugieren que Prrx1 actúa como un supresor tumoral en el melanoma y destacan un nuevo eje regulador Prrx1–Snail1 que controla la transformación melanocítica temprana. En conjunto, estos resultados refinan nuestra comprensión de la iniciación del melanoma y sugieren que el abordaje de la reprogramación transcripcional podría ofrecer nuevas oportunidades para intervenciones tempranas.

5 Introduction

5.1 Melanoma: Clinical and Molecular context

5.1.1 Epidemiology and clinical relevance of cutaneous melanoma

Melanoma represents a highly aggressive cancer type that originates from cells of the melanocytic lineage, that are pigment-producing cells mostly located in the basal layer of the epidermis in humans (Centeno et al., 2023). These cells derive from neural crest delaminating cells during development (Mort et al., 2015).

Cutaneous melanoma, the most common form of melanoma, occurs in the skin and is highly associated with exposure to ultraviolet radiation. This type of cancer accounts for 90% of skin cancer mortality, even their incidence rate is much lower than other types of skin cancer (Garbe et al., 2022).

Historical records show that over the period of 1990 to 2021, the global melanoma incidence and deaths increased by 182% and 86.1%, respectively (Y. Sun et al., 2025). This incidence varies across different regions, where the higher incidence concentrates in North America, Europe, Russia, Australia and New Zealand (Y. Sun et al., 2025).

In recent years in Europe, a dramatic increase in the incidence of melanoma in patients over the age of 60 has been detected, especially in men. This increase is also accompanied with an increase in all age groups, and its predicted to continue increasing over the next decades (Garbe et al., 2022). Additionally, estimated new cancer cases for melanoma reaches more than 100.000 patients for 2025 in the United States, with around 8000 expected deaths (Siegel et al., 2025).

The risk of developing cutaneous melanoma is strongly correlated with UV exposure, skin phototype and ethnic background (Arnold et al., 2018). The incidence also varies by age and sex, and this factor is also associated with differences in the anatomical site where melanoma develops —adolescent and young adult women have higher incidence rates than men, but mortality rates are higher in males than in females (Raimondi et al., 2020). But among them, intermittent UV-light exposure and accumulated sunburn-derived damage encompass the higher risk factor of cutaneous melanoma (Raimondi et al., 2020).

Together with the increasing risk of developing melanoma, its clinical burden is high due to its aggressive metastatic potential and its resistance to conventional therapies (Garbe & Eigentler, 2007). Historically, advanced melanomas were considered one of the solid tumours most refractory to therapy, although new advances in targeted

therapies and immune checkpoint blockade agents have greatly improved the management of a proportion of melanoma patients (Curti & Faries, 2021; Garbe & Eigentler, 2007).

Even though the current trend of melanoma increase is important, recent evidence suggests that part of the increasing incidence could also be explained by both improved surveillance and earlier diagnosis (Erdmann et al., 2013). New approaches, using advanced imaging diagnosis based on artificial intelligence, could facilitate even earlier melanoma diagnosis (Yan et al., 2025), although these technologies still need refinement (Frasier et al., 2025).

As mentioned above, over the past two decades, new approaches in immunotherapy and targeted therapy has revolutionised the treatment of melanoma, especially for metastatic disease (Curti & Faries, 2021). A rapid decline in death rates for melanoma patients has been reported as these new therapies are used in the clinic (Filho et al., 2025; Sung et al., 2021). However, although much effort has been put into reducing mortality rate and morbidity in melanoma, many patients do not respond or became resistant to these treatments. Melanoma remains as an important public health concern globally, remarking the importance of further research in this area.

5.1.2 Common early genetic mutations

Melanoma has a heterogeneous genetic background, as different signalling pathways can be hijacked to induce tumorigenic features, that could variate during progression among different tumoral subpopulations (Shain et al., 2015). Among them, most common mutations (**Figure 1**) are present in mitogen-activated protein kinase (MAPK) pathway genes and tumour suppressors (Akbani et al., 2015).

MAPK pathway mutations:

- **BRAF**. These mutations are the most common mutations in cutaneous melanoma, present in approximately 50% of patients. These mutations are widely present in nevi and are related to intermittent sun-exposure and prevalently present in younger patients (Akbani et al., 2015; Garbe et al., 2022). The most common variant is $BRAF^{V600E}$, a mutation that constitutively activate the MAPK/ERK pathway, promoting cell proliferation and progression of disease (Akbani et al., 2015).
- **NRAS**. These mutations are present is around 20% of patients, and lead to the activation of the MAPK and PI3K/AKT pathways (Akbani et al., 2015; Chudnovsky et al., 2005). This activating mutation cause dysregulation of the cell-cycle and cellular proliferation signals and has been identified as a predictor of shorter survival (Jakob et al., 2012).

- **NF1**. Mutations in this gene are present in 10-15% of cutaneous melanomas, mostly found in sun-damaged skin of older patients, and associated to a high mutation burden (Akbani et al., 2015). As a RAS repressor, inactivation of this gene results in hyperactivation of the MAPK pathway.

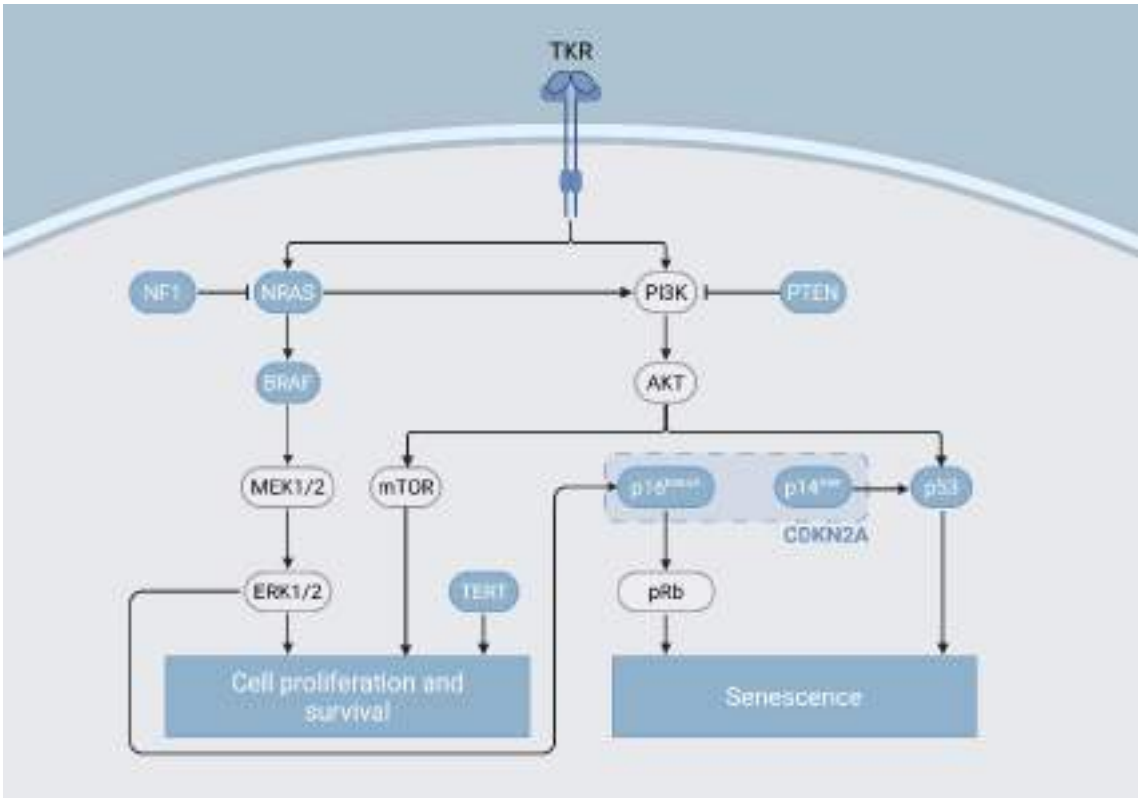

Figure 1. Oncogenic pathways commonly altered in melanoma. Mutations in NRAS and BRAF lead to constitutive MAPK pathway activation, while NRAS and tyrosine-kinase receptors (TKR) can activate the phosphatidylinositol 3' kinase (PI3K), leading to uncontrolled proliferation and survival. PTEN loss leads to failure in repression of the PI3K cascade. NF1 mutations lead to impairment in RAS dephosphorylation. CDKN2A mutations gene leads to loss of $p14^{ARF}$ or $p16^{INK4A}$ proteins, or both, compromising senescence pathways. In addition, p53 mutation facilitates senescence scape. TERT promoter mutations enhance cell survival independently. Adapted from Davis et al., 2019. Created with BioRender.com.

Interestingly, depending on the melanoma anatomical site and the level of UV radiation exposure, different molecular signatures have been identified as oncogenic drivers for melanoma. For instance, melanoma in trunk and limbs with low UV exposure are associated with BRAF mutations, but melanomas in the head and neck with high UV exposure are most likely to have NRAS or other RAS mutations (Garbe et al., 2022).

Commonly lost tumour suppressor genes:

- **TERT**. Among common secondary mutations in melanoma progression, mutations in TERT promoter arises the earliest after oncogene driver mutations (BRAF, NRAS, NF1). These mutations contribute to immortalization by increasing telomerase activity (Shain et al., 2015).
- **CDKN2A**. This gene is a well-known melanoma tumour suppressor that encodes for two proteins by alternative splicing: $p16^{INK4A}$, that indirectly inhibits cell cycle progression; and $p14^{ARF}$, which inhibits a negative regulator of TP53 (Hodis et al., 2012).
- **PTEN**. Loss of PTEN expression is found at later stages of melanoma progression, as it is mostly absent in thicker, invasive melanomas (Shain et al., 2015), Inactivation of this gene leads to PI3K/AKT pathway activation, promoting survival and therapy resistance (Dankort et al., 2009; Paraiso et al., 2011). PTEN mutations and deletions were more frequently found in BRAF-driven melanomas (Akbani et al., 2015).
- **TP53**. Mostly present in later stages of melanoma progression, close to metastatic dissemination stages (Shain et al., 2015), this mutation is less frequently found in melanoma than in other cancer types —genetic pressure to mutate TP53 directly is reduced due to frequent deletion of the CDKN2A locus (Hodis et al., 2012). Even though, UV radiation could directly mutate TP53 in a BRAF melanoma background, increasing tumour burden (Viros et al., 2014).

5.1.3 Melanoma Progression

Melanoma develops due to a series of mutations and alterations, enabling melanocytic lesions to progress to malignant stages. Primary melanomas are often found in association with precursor lesions (benign nevi and dysplastic nevi), from where in situ melanomas arise (Shain & Bastian, 2016).

To study melanoma progression, Clark proposed a model to classify changes across melanoma development (Clark et al., 1984), that was later simplified in five phases (**Figure 2**). The current model is described below:

- **Nevi acquisition**. Benign nevi, either congenital or acquired, have very low likelihood to progress to melanoma, although its high prevalence makes them contributors to a considerable portion of melanomas (Shain & Bastian, 2016). MAPK pathway mutations are present in this stage: BRAF mutations are associated with acquired nevi, while NRAS mutations are associated with congenital nevi (Roh et al., 2015). During this phase of early proliferation,

senescence program is activated to retain proliferation, thus other mutations are necessary for melanoma to progress (Roh et al., 2015).

- **Dysplastic nevi**. Hyperactivation of the MAPK pathway leads to the transformation of benign nevi to dysplastic nevi, harbouring variable pigmentation, asymmetry and/or irregular borders (Shain & Bastian, 2016). In addition to MAPK driver mutations, loss of tumour suppressors such as CDKN2A (Melnikova et al., 2004) or PTEN (Dankort et al., 2009) are detected, favouring malignant transformation.
- **Radial growth phase** (**RGP**). This phase, also known as melanoma *in situ*, shows melanocytic hyperproliferations contained inside the epidermal regions (Miller & Mihm, 2006). It have been linked to the presence of TERT mutations (Shain & Bastian, 2016) and increased levels of Cyclin D1 (Miller & Mihm, 2006).

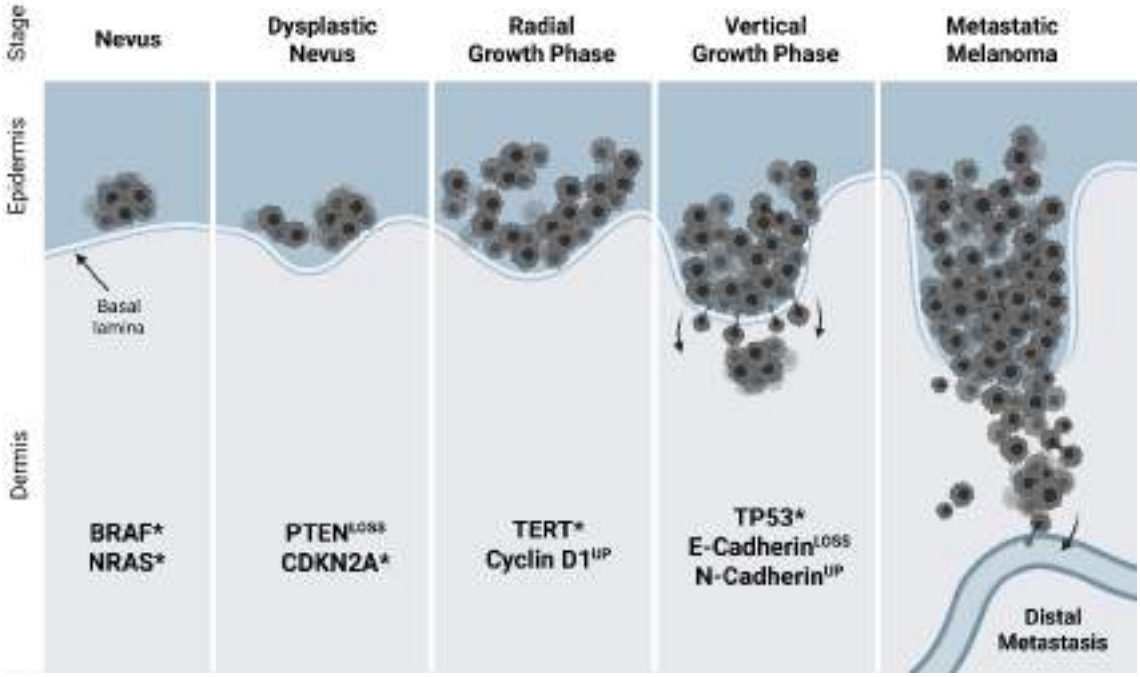

Figure 2. Stages of melanoma progression. Different stages of cutaneous melanoma development from nevus to metastatic melanoma, following the revised Clarck model. Most common mutations and molecular signatures are shown in each stage. Created with BioRender.com.

- **Vertical growth phase** (**VGP**). Also known as invasive melanoma, this phase is characterized by the invasive capabilities that lead to dermal invasion and proliferation, associated with high number of acquired molecular changes, including TP53 mutations (Akbani et al., 2015), that make possible this behaviour (Miller & Mihm, 2006; Shain & Bastian, 2016). In addition, loss of E-cadherin expression and acquisition of N-cadherin expression, common

hallmark of epithelial-to-mesenchymal transition (Nieto et al., 2016), facilitates invasion of these cells (Miller & Mihm, 2006).

- **Metastatic melanoma** (**MM**). At this phase, melanoma cells are able to detach from the primary tumour and disseminate to other organs, where they can successfully proliferate and stablish a metastatic lesion (Miller & Mihm, 2006). Similarly to other solid tumours, metastases generally appear first in sentinel lymph nodes, that later will spread to distant organs (Shain & Bastian, 2016).

During melanoma progression, molecular alterations accumulate to promote melanocyte transformation, dermal invasion and metastatic dissemination. As a result, melanomas show high genetic and phenotypic heterogeneity, which enhances inter-tumoral diversity and complicates prognosis and treatment (Rambow et al., 2018; Shain & Bastian, 2016).

5.1.4 Melanoma plasticity and phenotypic switching

Phenotypic plasticity is a defining hallmark of melanoma, representing one of the most formidable barriers to effective and durable treatment of the disease. Unlike other solids tumours, melanoma cells undergo reversible non-genetic transitions between transcriptionally and functionally distinct cell states (Florian Rambow et al., 2019; Rambow et al., 2018). These transitions are influenced by intrinsic transcriptional programs (Wouters et al., 2020), tumour microenvironment and therapeutic stress (Rambow et al., 2018).

A central regulator of this plasticity is the microphthalmia-associated transcription factor (MITF), the master regulator of the melanocyte lineage. MITF expression follows a rheostat model, where different levels of MITF correspond to distinct cell states (Hoek et al., 2008). Melanoma cells expressing $MITF^{high}$ levels are typically associated with proliferation, pigmentation and sensitivity to therapy, while $MITF^{mid}$ and $MITF^{low}$ cells are associated with dedifferentiation, invasiveness and therapy resistance (Rambow et al., 2018). $MITF^{low}$ cells frequently express markers of neural crest or mesenchymal programs, which makes them more motile and invasive, supporting metastatic dissemination (Karras et al., 2022).

In addition to MITF, other factors have been proposed to modulate proliferative/invasive balance in melanoma cells. For instance, TFAP2 may control proliferative versus invasive profiles, and also it has been shown that these two populations may cooperate during blood circulation forming heterotypic clusters, leading to increased metastatic burden (Campbell et al., 2021).

This transcriptional and phenotypic heterogeneity account for different cell populations among the tumour, but also for temporal changes (Rambow et al., 2018;

Rowling et al., 2020). Single-cell transcriptomic studies have revealed the co-existence of multiple phenotypic states within a single tumour, supporting the idea of intra-tumoral heterogeneity as a tumour survival strategy (Karras et al., 2022; Wouters et al., 2020). This plasticity allows subpopulations of melanoma cells to evade immune surveillance, often through downregulation of antigen presentation machinery (Pozniak et al., 2024) or upregulation of immune checkpoint molecules such as PD-L1 (Jerby-Arnon et al., 2018).

Importantly, melanoma phenotypic switch plays a major role in resistance to targeted therapies. For instance, treatment with BRAF and MEK inhibitors often show an initial response to tumour regression, but this also leads to a phenotypic selection of a subset of cells that are resistant to therapy. Selection maintains cells that shift towards a slow-cycling (or quiescent) and drug-tolerant state, often associated with $MITF^{low}$ and AXL^{high} expression (Kemper et al., 2014; Rambow et al., 2018). This resistance is due to transcriptional or epigenetic mechanisms, as drug withdrawal often results in cells reverting to proliferative states (Rambow et al., 2018).

Among different subpopulations of melanoma cells, there is a particularly plastic one that exhibits features of cancer stem-like cells (CSCs). Interestingly, the presence of CSCs, theorized as a rare subpopulation of cells within the tumour that are the only cells with the capacity to initiate and sustain tumour growth, has not been confirmed in melanoma. However, plastic neural-crest stem-like cells with dynamic behaviour that show stem cell properties could fulfil this role. These cells, enriched in dedifferentiated markers, display self-renewal, drug resistance and quiescence (Arozarena & Wellbrock, 2019), and may dynamically arise under stress conditions, contributing to minimal residual disease and late relapse (Rambow et al., 2018).

Altogether, literature highlights the importance of understanding the role and mechanisms of phenotypic plasticity of melanoma, as it takes a major role in modulating melanoma progression, immune evasion and therapy resistance.

5.1.5 Challenges in early detection and current therapeutic approaches

Early detection remains the cornerstone of melanoma outcomes, as survival rate strongly depends on tumour stage at diagnosis. The most used histopathological diagnostic factor is Breslow thickness, that measures tumour vertical depth of invasion, from the granular layer of epidermis to deepest tumoral cell: stage I (<1mm), stage II (1 - 2mm), stage III (2.1 - 4mm), stage IV (>4mm). Proposed initially by Breslow (Breslow, 1970), has been revised and updated including ulceration, tumour-associated inflammation and regression in the latest AJCC staging manual. Histological diagnosis is typically confirmed by biopsy followed by immunohistochemistry (Davis et al., 2019). In addition, sentinel lymph node biopsy

plays a key role in staging patients with intermediate-thickness melanoma and provides additional prognostic insight (Wong et al., 2012).

Despite the efficacy of clinical and dermoscopic screening, melanoma remains challenging due to its broad phenotypic heterogeneity. Artificial intelligence-based algorithms have demonstrated high sensitivity and specificity, comparable to experts (Yan et al., 2025), although it still needs to overcome some problems with overrepresentation of certain types of skin (Frasier et al., 2025).

In advanced disease, metastasis detection involves a multimodal approach. Whole body PET/CT and brain MRI are standardized for identifying metastasis (Horton et al., 2025). In parallel, liquid biopsy techniques such as circulating tumour DNA (ctDNA) analysis are emerging as promising tools for detecting minimal residual disease and monitoring therapy response (Sacco et al., 2020).

On the therapeutic front, targeted therapies have been developed to combat molecular alterations present in melanoma. BRAF-mutant melanoma (approximately 50% of patients) is commonly treated with dual BRAF and MEK inhibitors, which has substantially improved patient outcomes. However, primary resistance, no initial response, and acquired resistance, relapse after initial benefit, remain major obstacles (Robert et al., 2019).

The most effective treatments for metastatic melanoma to date are immune checkpoints inhibitors, the first of which was approved for clinical use in 2011 (Davis et al., 2019). PD-1 inhibitors have demonstrated durable clinical responses in up to 40% of metastatic melanoma patients, even better when in combination with CTLA-4 inhibitors, in expenses of increased immune-related adverse effects (Davis et al., 2019). Immunotherapy resistance may also arise, through mechanisms such as loss of antigen presentation mechanisms (Sade-Feldman et al., 2017), T-cell exclusion, or WNT/β-catenin signalling, among others (Restifo et al., 2016).

Emerging strategies aim to overcome resistance via novel immunomodulatory agents, including LAG-3 inhibitors, oncolytic viruses, personalized cancer vaccines and adoptive T-cell therapy (Chan & Corrie, 2024). Other strategies tend to enhance immunotherapy response, including modulation of tumour microenvironment cells (Rodriguez-Baena et al., 2025) and metabolic rewiring (Redondo-Muñoz et al., 2023).

5.2 Melanocyte biology and origin

In the skin, melanocytes and keratinocytes at the basal layers of the epidermis create the epidermal-melanin unit, which is a photo-barrier that provides protection against the harmful effects of UV radiation (Lin & Fisher, 2007). Upon UV exposure, keratinocytes release melanocyte-stimulating hormone (α-MSH), which activates

cAMP signalling pathway in melanocytes via melanocortin-1 receptor (MC1R) (Rodríguez & Setaluri, 2014). The activated melanocytes produce melanin in specialized vesicles known as melanosomes, which are then transported to the keratinocytes to provide the protective pigment (Mort et al., 2015). The accumulation of melanin in keratinocytes provides thermoregulation, skin pigmentation and protection against UV-induced genomic alterations (Lin & Fisher, 2007). Aberrations in melanocyte biology can lead to proliferation disorders, benign melanocytic neoplasms (moles or nevi), or malignant lesions like melanoma (Centeno et al., 2023).

5.2.1 Embryonic origin of melanocytes from the neural crest

During embryonic development, neural crest cells (NCCs) delaminate from the neural tube undergoing EMT. These cells migrate to distinct locations in the embryo, where they differentiate into various cell types, including neural, cartilage, bone and melanocytic cells (Brombin & Patton, 2024).

Melanocytes classically arise from dorsolaterally migrating NCCs, upon activation of MITF, the master regulator of melanocyte lineage, committing cell fate towards the melanocytic lineage (Brombin & Patton, 2024). In addition to this stream of NCCs, Schwann cells precursors could serve as a secondary source of melanocytes, as they can detach form distal end of nerves and differentiate into melanocytes (Adameyko et al., 2009). This additional source of melanocytes explains the origin of melanocytes located in heart, meninges, inner ear and other locations different from skin (Kaucka et al., 2021).

Migratory MITF expressing cells, termed as melanoblast, undergo proliferation, directional migration and differentiation, regulated by key signalling pathways such as KIT and WNT, among others. These cells will populate the basal layer of epidermis and developing hair follicles (Brombin & Patton, 2024).

In mouse, melanoblast colonize both interfollicular epidermis and follicular regions, but maintenance of this populations changes towards adulthood. Follicular melanoblasts, that will stablish melanocyte stem cells (MSCs) pool in the bulge of the outer root sheath of the hair follicle, will serve a resource for melanocytes during adulthood (Brombin & Patton, 2024). Interfollicular melanoblast, by contrary, will completely disappear at few days after birth in hairy skin (Mort et al., 2015), but will be maintained in tail skin (Glover et al., 2015). In contrast, human skin retains melanocytic cells in both compartments in adulthood, though density varies by anatomical site an phototype (Slominski et al., 2004).

5.2.2 Maintenance of the melanocytic lineage in adult skin

In adult mammals, the maintenance of the melanocytic lineage relies on the persistence and cyclic activity of melanocyte stem cells (MSCs), primarily located in specialized niches within the hair follicle.

In humans, melanocytes are present both in the interfollicular dermis, under basal lamina in the epidermis, and within hair follicles, contributing to constitutive skin pigmentation and hair colour (Lin & Fisher, 2007). Within the interfollicular compartment, a melanocytic subpopulation characterized by $cKit^{-}/CD90^{+}/TYRP1^{-}$ profile has been detected, proposed as a reservoir population for interfollicular melanocytes (Michalak-Mićka et al., 2022). Within the hair follicles, MSCs reside in the bulge region of the outer root sheath (Bedogni & Paus, 2020).

In mice, interfollicular melanocytes are lost within the first postnatal week, with the exception of tail skin interfollicular melanocytic cells (Glover et al., 2015). In the follicular compartment, MSCs residing in the bulge give rise to transit-amplifying cells (TA), that will migrate and differentiate into melanocytes in the hair bulb, contributing to hair pigmentation (Bedogni & Paus, 2020). However, recent studies indicate that this population is not a static stem-cell reservoir, but in fact MSCs toggle between transit-amplifying (TA) and stem cells states for both self-renewal and generation of mature progeny (Q. Sun et al., 2023).

The hair follicle functions as a cyclic unit composed of three major phases (**Figure 3**):

- **Anagen** (growth phase). During this phase, MSCs exit quiescence and divide, giving rise to transit-amplifying cells. This process is controlled by the activation of WNT/β-catenin signalling pathway in coordination with epithelial stem cells residing in the bulge (Rabbani et al., 2011), and MSC proliferation depends on CRAF and BRAF activation (Valluet et al., 2012). Later, these progenitors actively migrate to the newly forming secondary hair germ, where they differentiate into mature melanocytes. However, it has been shown very recently that transient-amplifying cells, that already express differentiation markers such as Tyrp1, can dedifferentiate back into MSCs. (Q. Sun et al., 2023).
- **Catagen** (regression phase). During this phase, the hair follicle undergoes massive apoptosis and involution. Lower and middle parts of the hair follicle undergo apoptosis and are eliminated, while a subset of progenitors in the bulge survives this remodelling process (Schneider et al., 2009).
- **Telogen** (resting phase). During this phase, the pigmentary unit is inactive, and the follicle awaits cues to activate WNT/β-catenin pathway and re-enter anagen (Rabbani et al., 2011). TGF-β produced by multipotent hair follicle stem cells residing in the bulge maintain stemness properties of MSCs in the

niche, by promoting quiescence, survival and inhibiting differentiation (Blanpain & Sotiropoulou, 2010; Nishimura et al., 2010).

Understanding the anatomical location and functional behaviour of melanocytes across distinct skin compartments is essential to elucidate the cellular origins of melanoma. Recent studies have revealed that melanoma may arise from both terminally differentiated melanocytes (Köhler et al., 2017) and MSCs/progenitor cells residing the in the hair follicle niche (Q. Sun et al., 2019). Given this dual potential, comprehensive characterization of both interfollicular and follicular melanocytic populations is critical for deciphering the mechanisms of tumour initiation and heterogeneity.

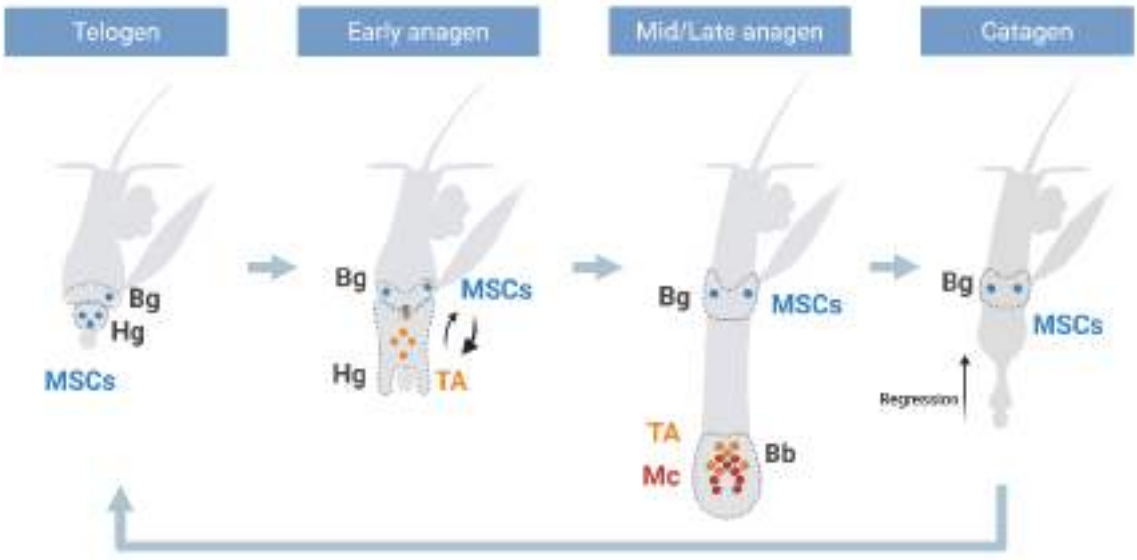

Figure 3. Simplified overview of hair cycle progression. Hair is maintained stable during telogen, where MSCs remain quiescent waiting for hair cycle initiation cues. During early anagen, activated MSCs migrate and divide giving rise to TA cells, that populate the hair germ or revert to MSCs to refuel stem cell niche. Later in anagen, TA cells will differentiate to melanocytes, that are necessary for hair pigmentation or reverse back to MSCs. Once new hair is generated, during catagen, hair bulb degeneration and regression prepares the hair follicle for the next telogen stage. Bb: Hair bulb, Bg: Hair bulge, Hg: Hair germ, Mc: Melanocytes, MSCs: Melanocyte stem cells, TA: Transit-amplifying cells. Created with BioRender.com.

5.2.3 Melanoma initiation and contribution of the melanocytic lineage

Melanoma initiation is a highly context-dependent process that can originate from multiple cellular sources within the melanocytic lineage, including melanocyte stem cells (MSCs), melanoblasts and terminally differentiated melanocytes. Understanding how these cell types respond to oncogenic induction across anatomical sites and differentiation states is key to elucidate melanoma heterogeneity and therapeutic resistance.

Zebrafish models have provided critical insights into melanoma initiation dynamics. Due to their transparency and genetic tractability, this model allows real-time visualization of melanoma initiation upon melanocyte transformation. Taking this in advantage, Zon laboratory elegantly described how melanocytes harbouring $BRAF^{V600E}$ mutations were not able to transform into melanoma until they recover the expression of neural-crest like signatures (Crestin, SOX10), detecting clonal melanoma outgrowth from these cells —thus highlighting the reemergence of progenitor-like identity as an additional step for melanoma initiation (Kaufman et al., 2016).

Another study directly tackles the propensity for melanocytic cells to undergo melanomagenesis. Using zebrafish with a $BRAF^{V600E}$/ $TP53^{-/-}$ background combined with different cell-stage dependent promoters, the authors observed that neural crest and melanoblast, but not melanocytes, can be readily transformed. The propensity seems to depend on the expression of chromatin-remodelling factors that are reduced during melanocyte differentiation (Baggiolini et al., 2021).

Studies using mouse models have tried to resolve the controversy among the cell of origin of melanoma. For instance, some studies using the *Tyr*::Cre-ER^{T2}/ *Braf*^{V600E}/ *Pten*$^{fl/fl}$ mouse model (Dankort et al., 2009) indicate that melanoma can arise from MSCs that reside in the bulge region of the hair follicle, upon activation of these cells. In this case, melanoma induction required an activating stimulus, either intrinsic hair follicle anagen or UV radiation stress. However, the activation of the Cre recombinase during or in the progression to telogen was not able to induce melanoma indicating that bulge-residing quiescent MSCs during telogen are resistant to melanoma induction (Moon et al., 2017). In addition, another study using *c-Kit*::Cre-ER/ *Braf*^{V600E}/ *Pten*$^{fl/fl}$ model, that targets MSCs and not differentiated melanocytes, also showed that MSCs give rise to melanoma during anagen stage. This study detected local proliferation and migration of MSCs progeny towards interfollicular epidermis, where they progressed to melanoma (Q. Sun et al., 2019).

By contrast, another study performed in the *Tyr*::Cre-ER^{T2} / *Braf*^{V600E}/ *Pten*$^{fl/fl}$ model showed that terminally differentiated melanocytes, residing in the interfollicular compartments of tail skin, could give rise to melanoma. These cells undergo transformation in the epidermis and acquire dedifferentiation traits prior to dermal invasion (Köhler et al., 2017). The use of mouse tail melanoma model, as it generates melanomas similar to what occurs in melanoma *in situ* in humans, can be used to understand melanoma initiation in patients. Nevertheless, the ability of MSCs residing in the bulge of the hair follicle to populate interfollicular regions upon stress makes them still an important candidate for melanoma initiation in humans (Chou et al., 2013).

Altogether, there is evidence that cutaneous melanoma can be derived from either MSCs or their progeny, but in the context of human melanoma this issue needs to be further explored.

5.3 EMT and EMT-like processes in melanoma

Among different steps of melanocyte development and melanoma, the epithelial-to-mesenchymal transition (EMT) plays a major role in fulfilling different functions. Neural crest delaminates from neural tube by undergoing EMT, and migratory progenitors that engender melanoblast express EMT transcription factors (EMT-TFs) during its path to final destination (Nieto et al., 2016). Also, even though melanocytes are not epithelial cells, they express E-cadherin, which expression is lost in crucial points of melanoma progression, a hallmark of EMT (Lade-Keller et al., 2013). This, together with other studies that will be presented across this section, enhance the importance of EMT and EMT-TFs in melanoma.

Epithelial-to-mesenchymal transition is a highly conserved biological program by which cells dynamically lose their epithelial identity. Epithelial cells lose cell polarity, apicobasal organization and intercellular adhesion, while progressively acquiring a mesenchymal phenotype with increased motility, invasiveness and survival (Nieto et al., 2016). Importantly, EMT is not a terminal or unidirectional event; it is an intrinsically reversible process though the mesenchymal-to-epithelial transition (MET), a process crucial for restoring epithelial traits during tissue regeneration and metastatic colonization (Aiello & Kang, 2019; Youssef & Nieto, 2024). This bidirectionality enables cells to cycle through different phenotypic states in response to contextual cues, an important behaviour during development, repair and cancer progression (Nieto et al., 2016).

Recent evidence has challenged the traditional binary model of EMT-MET, proposing instead a continuum model where epithelial and mesenchymal cells features coexist in individual cells or within dynamic cell populations (Nieto et al., 2016). These intermediary states, hybrid or partial EMT states, are characterized by the expression of both epithelial and mesenchymal markers, while enhancing cell adaptability and plasticity (Pastushenko & Blanpain, 2019) (**Figure 4**).

During development, EMT drives important aspects of key early processes and cell motility and survival. It is necessary for gastrulation, neural crest formation and delamination, and organ positioning (Nieto et al., 2016; Ocaña et al., 2017; Rago et al., 2019) On the other hand, adult tissue undergoes EMT during wound healing and regeneration processes. In fact, partial EMT plays a critical role in re-epithelialization during wound healing, as cells in the wound edge migrate without completely losing

their epithelial identity. These cells will later revert via MET, maintaining tissue homeostasis (Nieto et al., 2016).

In the disease context, partial EMT plays an important role in degenerative processes such as renal (Grande et al., 2015) or liver fibrosis (Youssef & Nieto, 2024); in cancer progression, metastatic dissemination and colonization (Pastushenko & Blanpain, 2019; Youssef & Nieto, 2024).

5.3.1 EMT-TFs

EMT is orchestrated by a complex network of transcription factors (EMT-TF) including Snail1/2, Twist1/2, Zeb1/2 and Prrx1. During its activation, they suppress epithelial markers such as E-cadherin and promote mesenchymal gene expression of vimentin (VIM) and fibronectin (FN1), among others (Yang et al., 2020).

Numerous mechanisms are implicated in the activation and regulation of the EMT-TFs, that has been studied thoroughly over the past few decades (Nieto et al., 2016; Peinado et al., 2007). Among them, the TGF-β/BMP pathway is the most extensively studied EMT inducer. TGF-β receptors activate SMAD-dependent (canonical) and SMAD-independent (non-canonical) pathways to activate the expression of EMT-TF. Additionally, WNT and NOTCH pathways act independently or in collaboration to activate the expression of EMT-TFs. Other pathways include JAK-STAT and NF-kB, that can be activated in response to intercellular cues due to cellular stress, inflammation or hypoxia, among others (Ocaña et al., 2012; Youssef & Nieto, 2024). Recent evidence indicates that EMT-TFs may be also regulated through transcriptional regulatory mechanisms orchestrated by miRNAs (Díaz-López et al., 2014) or alternative splicing (Warzecha & Carstens, 2012). In fact, miR200 and Zeb family regulate in a mutually repressive loop (Pastushenko & Blanpain, 2019), while miR34 and Snail1 act in a similar way (Díaz-López et al., 2014). These two regulatory pathways are interconnected, as Snail1 can repress miR200 and Zeb1 represses miR34 expression (Nieto et al., 2016).

Although EMT-TF activation and function is very context-dependent (Aiello & Kang, 2019), studies indicate that there is an activation hierarchy among the EMT-TFs. Snail1 acts a pioneer of EMT induction, with later activation of Snail2, Zeb family and Twist family for consolidation of the epithelial repression, and finally Prrx1 activation for induction of the mesenchymal phenotype (Youssef et al., 2024).

Snail1 is a zinc finger transcription factor that acts as a master regulator of EMT, playing a pivotal role in developmental processes, wound healing and tumour progression. During embryonic development, it is essential for mesoderm formation and neural crest delamination (Nieto et al., 2016). This transcription factor acts mostly as a transcriptional repressor of epithelial-identity genes. In epithelial cancers,

Snail1 drives the repression of E-cadherin, initiating the cascade towards acquisition of mesenchymal traits, necessary for dissemination (Nieto et al., 2016). It also has been linked to promoting cell survival, chemoresistance, immune checkpoint blockade resistance and stem-cell maintenance (Dongre & Weinberg, 2019).

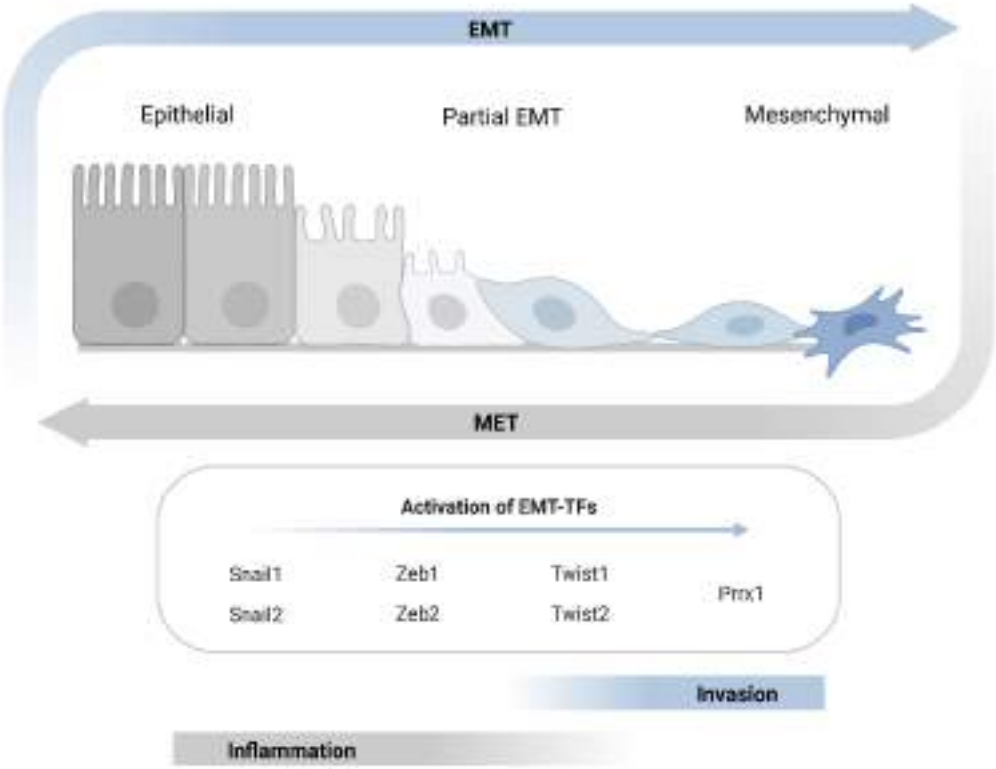

Figure 4. Schematic overview of epithelial-mesenchymal plasticity. During EMT, epithelial cells undergo significant changes, losing their apicobasal polarity and cell to cell contact that enables them to migrate and invade. Also, as a reversible process, through the MET cells can revert to an epithelial phenotype. Notably, cells can stay in an intermediate state, known as partial EMT, where they present a combination of epithelial and mesenchymal traits. EMT-TFs control these processes, activating in a hierarchical way, that can follow distinct EMT programs that control inflammation and invasion independently. EMT: epithelial-to-mesenchymal transition, MET: mesenchymal-to-epithelial transition, EMT-TFs: EMT transcription factors. Created with BioRender.com.

Additionally, Prrx1 is an homeobox transcription factor involved in the regulation of the EMT, cellular plasticity and stemness properties across different cancer types, although these properties are highly context dependent (Youssef & Nieto, 2024). Generally, Prrx1 facilitates a mesenchymal phenotype that enhances invasion but not necessarily metastatic colonization. In epithelial tumours such as breast cancer, Prrx1 drives EMT and cell migration, but its sustained activity represses stemness and metastatic outgrowth, indicating that its downregulation is necessary to enable

colonization at secondary sites (Ocaña et al., 2012). In lung adenocarcinoma, Prrx1 expression in the TME promotes proliferation, immune evasion and increased migratory capacity (Y. Sun et al., 2024). However, in colorectal cancer, Prrx1 supports proliferation, stem-like properties and resistance to chemotherapy (Zhong et al., 2022). Similarly, Prrx1 acts in combination with FOXM1 to induce chemoresistance in bladder cancer (Huang et al., 2022). In contrast, Prrx1 appears to play a role in hepatocellular carcinoma as a tumour suppressor by regulating metabolism (Piorońska et al., 2021).

Interestingly, an important factor regulating interactions among these EMT-TFs is the mutually repressive loop that occurs between Snail1 and Prrx1 expression. Snail1, acting as a repressor, inhibits Prrx1 expression by directly binding to Prrx1 promoter regions. On the contrary, Prrx1 activates the expression of miR-15 family members, that are able to destabilize Snail1 mRNA, reducing its expression. This loop favours the mutually exclusive role of these EMT-TFs, as Snail1 and Prrx1 do not usually co-express at cellular level, at least a mid/high expression levels (Fazilaty et al., 2019; Rago et al., 2019).

Interestingly, recent findings clearly delineate two segregated EMT programs in breast tumours: one governed by Snail1, linked to immune evasion and cytokine signalling, and another driven by Prrx1, which promotes cellular invasion and matrix remodelling (Youssef et al., 2024). These trajectories are transcriptionally exclusive; Snail1 and Prrx1 regulatory loop maintain mutual repression (Fazilaty et al., 2019; Youssef et al., 2024). In this framework, Prrx1 orchestrates the invasive EMT axis, contributing to mesenchymal motility but not inflammatory signalling (Youssef et al., 2024).

5.3.2 EMT-TFs in melanoma

Melanoma, although not of epithelial origin, consistently expresses EMT-TFs contributing to phenotypic switching, therapy resistance and immune evasion. Unlike canonical epithelial tumours, melanoma retains a hybrid epithelial/mesenchymal plasticity, where the EMT-TFs operate independently of classical cadherin switches (Caramel et al., 2013; Tang et al., 2020).

One of the central transcriptional rewiring events involves a Zeb2-to-Zeb1 switch (**Figure 5**), first reported by Caramel in 2013. This switch was described as a change from a proliferative, pigmented state with Zeb2/Snail2 expression, towards an invasive, dedifferentiated state with Zeb1/Twist1 expression (Caramel et al., 2013). While Zeb2 and Snail2 are expressed in lineage-committed melanocytic cells (Denecker et al., 2014; Kim et al., 2013), Zeb1 and Twist1 are hallmark regulators of a mesenchymal, stem-like state, facilitating metastasis and resistance to BRAF/MEK inhibitors (Richard et al., 2016; Tang et al., 2020).

Importantly, these EMT-TFs interact with MITF often in a mutually antagonistic manner. For instance, Zeb2 downregulation induced the repression of MITF and the upregulation of Zeb1, impairing melanocyte pigmentation and differentiation (Denecker et al., 2014; Vandamme et al., 2020, 2020). On the other hand, Zeb1 expression is able to repress SOX10-MITF dependent proliferative state, transitioning cells towards neural-crest like and mesenchymal states (Durand et al., 2024).

Some studies have investigated the role of Snail1-induced EMT in melanoma indicating that it contributes to the transformation of melanocytes *in vitro* (Poser et al., 2001) and promote invasiveness and immunosuppression (Kudo-Saito et al., 2009). Further, in the lab we have described that Snail1 expression in TME-residing fibroblasts promote an immunosuppressive microenvironment facilitating melanoma and metastases growth (Arumi-Planas et al., 2023). However, Snail1 cell-autonomous contribution to melanoma progression *in vivo* is not characterized.

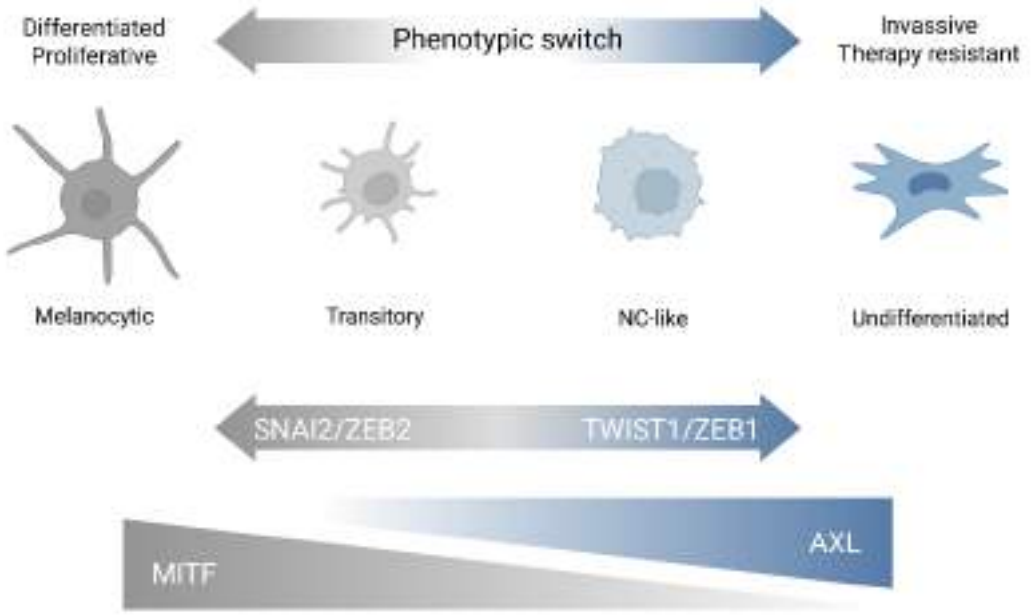

Figure 5. EMT-TFs modulate reversible phenotypic switches in melanoma. Phenotypic switch in melanoma transit from differentiated, proliferative and therapy responsive states to dedifferentiated, invasive and therapy resistant states. MITF, the master regulator of melanocyte lineage, controls axis towards differentiation, while AXL has been related with undifferentiated states. EMT-TFs are able to modulate phenotypic switch, with SNAI2 and ZEB2 associated with proliferative and differentiated states, while expression switch to TWIST1/ZEB1 is related with dedifferentiation, invasion and therapy resistance.

In addition, the role of Prrx1 in melanoma remains incompletely understood and is subject to ongoing debate, highlighting the context-dependent functions mentioned

above. In murine models, Prrx1 expression appears important for metastasis, as suggested in the *Nras*-mutant mice, where a melanoma subpopulation expressing Prrx1 with metastatic potential was identified (Karras et al., 2022). Supporting this, a study in the *Braf*^{V600E}/*Pten*$^{fl/fl}$ mouse model with *Loxl3* deletion suggested that Prrx1 cooperates with LOXL3 to promote melanoma cell survival, mesenchymal identity and enhanced tumour plasticity, potentially facilitating distant metastasis formation, although this was not tested *in vivo* (Vázquez-Naharro et al., 2022). Conversely, another finding suggest that Prrx1 expression must be downregulated to enable melanoma outgrowth and colonization, indicating that sustained Prrx1 activity may constrain late-stage metastatic expansion (Ferreres et al., 2024). These seemingly contradictory observations highlight the dynamic and temporally regulated role of Prrx1 in melanoma progression.

These context-specific functions underscore Prrx1 as a key regulator of tumour plasticity and progression. As mentioned, some efforts, although still controversial have attempted to understand Prrx1 contribution to melanoma progression and metastatic colonization; however, its role in melanomagenesis and its interplay with Snail1 in melanoma remains to be elucidated.

6 Objectives

Although the roles of Prrx1 and Snail1 in cancer progression have been investigated across various cancer types, their specific contributions to melanoma remain poorly characterized. During embryonic development, epithelial-to-mesenchymal transition transcription factors (EMT-TFs) are expressed in neural crest cells, the progenitors of melanocytes and, ultimately, melanoma cells. EMT-TFs have been implicated in regulating the phenotypic plasticity of melanoma, facilitating the reacquisition of neural crest-like traits and acting as key effectors during melanoma initiation. Interestingly, despite being non-epithelial in origin, adult melanocytes express certain EMT-TFs under homeostatic conditions. This thesis aims to investigate whether Prrx1 and/or Snail1 contribute to melanoma onset and progression.

General objective

This thesis aims to understand the cell-autonomous contribution of Prrx1 and Snail1 to melanoma biology *in vivo* using preclinical mouse models.

Specific objectives

1. To characterize the expression of Prrx1 and Snail1 in melanocytic cells in the hair follicle
2. To investigate the functional roles of Prrx1 and Snail1 in melanoma initiation and progression *in vivo*.
3. To understand the molecular mechanisms underlying Prrx1/Snail1 cross-regulation in melanocytic cells.

7 Material and methods

7.1 Experimental animals

7.1.1 Mouse handling

All experiments involving animals were performed in accordance with the European Community Council Directive (2010/63/EU) and Spanish legislation. The protocols were approved by the CSIC and UMH Ethical Committee and the Animal Welfare Committee at the Institute of Neurosciences CSIC-UMH. Mice were hosted in a specific pathogen-free (SPF) facility under controlled temperature and humidity, with a 12 h light/dark cycle. Both male and female C57BL/6 mice, aged 4 weeks for hair follicles analyses and 7-8 weeks for tumour analyses, were used in all experiments. Animal models used are listed in **Table 1.**

7.1.2 Inducible melanoma mouse model

Cg-Tg(Tyr-cre/ERT2)13Bos, $Braf^{tm1Mmcm}$, $Pten^{tm1Hw}$ /BosJ. Abbreviated as BP.

In this study, the BP mouse model was used to experimentally induce melanoma formation in our experimental mice. This model was obtained from The Jackson Laboratory© (RRID: IMSR_JAX:013590).

The murine BP model (Dankort et al., 2009), expresses Cre-ER^{T2} recombinase under the control of the tyrosinase (*Tyr*) promoter, which is active in melanocytes and MSCs when treated with 4-hydroxytamoxifen (4-HT).

In the absence of Cre activity, the wild type form of *Braf* is expressed since $Braf^{V600E}$ mutation is initially silenced by a stop cassette flanked by loxP sites. When Cre is activated, it removes the stop cassette and the mutated $Braf^{V600E}$ allele becomes expressed. Additionally, the $Pten^{loxP}$ model has loxP sites flanking exon 5 of the *Pten* gene. Cre induced removal of the *Pten* gene segment flanked by loxP sites leads to loss-of-function of PTEN protein when recombination occurs. Thus, the administration of 4-HT induces simultaneous expression of $BRAF^{V600E}$ and PTEN loss in melanocytes and MSCs, and triggers melanomagenesis (Köhler et al., 2017).

7.1.3 Inducible melanoma lineage tracing mouse model

Cg-Tg(Tyr-cre/ERT2)13Bos,Braf^{tm1Mmcm},Pten^{tm1Hw}/BosJ, Gt(ROSA)26Sor$^{tm9(CAG-tdTomato)\ Hze}$. Abbreviated as BP-tdTomato.

This model was generated by crossing the *Braf*-driven mouse melanoma model (BP) previously described, with a Ai9 tdTomato reporter line (RRID:IMSR_JAX:007909). This Ai9 is a Cre reporter tool strain designed to have a loxP-flanked STOP cassette preventing transcription of a CAG promoter-driven red fluorescent protein variant (tdTomato).

Under the administration of 4-HT, *Tyr*::Cre-ER^{T2} expressing melanocytes are subjected to simultaneous expression of tdTomato protein, BRAF^{V600E} and PTEN loss in melanocytes, triggering the development of melanomas labelled with red fluorescence.

Given name	Mouse line	Gene expression upon recombination
BP	Cg-Tg(Tyr-cre/ERT2)13Bos, Braf^{tm1Mmcm}, Pten^{tm1Hw} /Bos	*Braf*^{V600E}, *Pten*$^{fl/+}$
BP/Prrx1^{cKO}	Cg-Tg(Tyr-cre/ERT2)13Bos, Braf^{tm1Mmcm}, Pten^{tm1Hw} /Bos, Prrx1^{em1An}	*Braf*^{V600E}, *Pten*$^{fl/+}$, *Prrx1*$^{fl/fl}$
BP/Snai1^{cKO}	Cg-Tg(Tyr-cre/ERT2)13Bos, Braf^{tm1Mmcm}, Pten^{tm1Hw} /Bos, Snai1^{tm2Stjw}	*Braf*^{V600E}, *Pten*$^{fl/+}$, *Snai1*$^{fl/fl}$
BP/Prrx1^{cKO}/Snai1^{cKO}	Cg-Tg(Tyr-cre/ERT2)13Bos, Braf^{tm1Mmcm}, Pten^{tm1Hw} /Bos, Prrx1^{em1An}, Snai1^{tm2Stjw}	*Braf*^{V600E}, *Pten*$^{fl/+}$, *Prrx1*$^{fl/fl}$, *Snai1*$^{fl/fl}$
BP-tdTomato	Cg-Tg(Tyr-cre/ERT2)13Bos, Braf^{tm1Mmcm}, Pten^{tm1Hw} /Bos, Gt(ROSA)26Sor$^{tm9(CAG-tdTomato)Hze}$	*Braf*^{V600E}, *Pten*$^{fl/+}$, tdTomato
BP-tdTomato/Prrx1^{cKO}	Cg-Tg(Tyr-cre/ERT2)13Bos, Braf^{tm1Mmcm}, Pten^{tm1Hw} /Bos, Gt(ROSA)26Sor$^{tm9(CAG-tdTomato)Hze}$, Prrx1^{em1An}	*Braf*^{V600E}, *Pten*$^{fl/+}$, tdTomato, *Prrx1*$^{fl/fl}$
BP-tdTomato/Snai1^{cKO}	Cg-Tg(Tyr-cre/ERT2)13Bos, Braf^{tm1Mmcm}, Pten^{tm1Hw} /Bos, Gt(ROSA)26Sor$^{tm9(CAG-tdTomato)Hze}$, Snai1^{tm2Stjw}	*Braf*^{V600E}, *Pten*$^{fl/+}$, tdTomato, *Snai1*$^{fl/fl}$
Tyr^{+}-tdTomato	Cg-Tg(Tyr-cre/ERT2)13Bos, Gt(ROSA)26Sor$^{tm9(CAG-tdTomato)Hze}$	tdTomato
Tyr^{+}-tdTomato/Prrx1^{cKO}	Cg-Tg(Tyr-cre/ERT2)13Bos, Gt(ROSA)26Sor$^{tm9(CAG-tdTomato)Hze}$, Prrx1^{em1An}	tdTomato, *Prrx1*$^{fl/fl}$
Tyr^{+}-tdTomato/Snai1^{cKO}	Cg-Tg(Tyr-cre/ERT2)13Bos, Gt(ROSA)26Sor$^{tm9(CAG-tdTomato)Hze}$, Snai1^{tm2Stjw}	tdTomato, *Snai1*$^{fl/fl}$

Table 1 Mouse models used for *in vivo* experiments.

7.1.4 Generation of Snai1 and Prrx1 conditional knock out melanomas

Prrx1 ^{em1An} and Snai1^{tm2Stjw}. Abbreviated as Prrx1^{cKO} and Snai1^{cKO} respectively.

To investigate *Prrx1* contribution to melanoma, we crossed the BP model with a newly generated *Prrx1*^{loxP} conditional mutant mouse line (Prrx1 ^{em1An}), that was generated in Angela Nieto's laboratory (Youssef et al., 2024). To investigate *Snai1* contribution to melanoma, we used a similar strategy, crossing the BP model with a *Snai1*^{loxP} (Rowe et al., 2009). To block *Prrx1* and *Snai1* expression simultaneously, we crossed these three models together, to study interdependent relationships between these EMT-TFs in melanoma biology.

7.1.5 Inducible melanocyte lineage tracing mouse model

Cg-Tg(Tyr-cre/ERT2)13Bos, Gt(ROSA)26Sor$^{tm9(CAG-tdTomato)Hze}$. Abbreviated as Tyr^{+}-tdTomato.

In this thesis, we also employed the Tyr^{+}-tdTomato murine model to characterize the expression of EMT-TFs in melanocytes at the hair follicle.

To obtain this model, we backcrossed our BP models to segregate *Tyr*::Cre-ER^{T2} allele together with tdTomato allele from *Braf*^{CA} and *Pten*^{LoxP} alleles. This model, when treated with 4-HT, induces the expression of tdTomato protein in *Tyr* expressing cells.

Additionally, these animals were crossed with Prrx1^{cKO} and Snai1^{cKO} models, as previously described, to inactivate specifically *Snai1* or *Prrx1* in Tyr^{+} cells.

7.1.6 Genotyping

The genotyping of the animals used was performed through collection of distal tail or ear tissue followed by NaOH (50 mM) DNA isolation. The PCRs were carried out using the primers listed in **Table 2**.

7.1.7 Tamoxifen administration for melanoma induction

To obtain a tamoxifen stock solution, tamoxifen (Sigma) was dissolved in a DMSO (50mg/ml). For tamoxifen administration, 4-HT in DMSO solution was diluted in ethanol up to a concentration of 4-HT of 8mg/ml. This solution was administered topically to adult and juvenile mice at a dose of 120ug in a region depilated back skin region of 2cm^2, treated three times with an interval of one day between the treatments. Mice were immobilized until 4-HT dried completely.

Allele	Primer Sequence (5'-3')	Amplicon length
tdTomato	Fw: AAGGGAGCTGCAGTGGAGTA Rv: CCGAAAATCTGTGGGAAGTC Fw: GGC ATTAAA GCA GCG TATCC Rv: CTG TTC CTGTACGGCATGG	ROSA^{WT} allele: 297 bp ROSA^{tdTomato} allele: 196 bp
***Prrx1*^{loxP}**	Fw: TTTCTTTCCCCGTCTTTGGT Rv: AAGGAGATAGCCTTCCCTTCC	*Prrx1*^{WT} allele: 780bp *Prrx1*^{loxP} allele: 850bp
***Snai1*^{loxP}**	Fw: CTGCCAGGTGGGAAGGACT Rv: CAA GGACATGCGGGAGAAGGT	*Snai1*^{WT} allele: 324 bp *Snai1*^{loxP} allele: 424 bp
***Snai1*^{Floxed}**	Fw: CCCGGGCTATGGAGGTATGGT Rv: GGAGGCGCTTGGGAACAGGAA	*Snai1*^{Floxed} allele: 503 bp
***Braf*^{CA}**	Fw: TGAGTATTTTTGTGGCAACTGC Rv: CTCTGCTGGGAAAGCGGC	*Braf*^{WT} allele: 185 pb *Braf*^{CA} allele: 308 pb
***Pten*^{loxP}**	Fw: CAAGCACTCTGCGAACTGAG Rv: AAGTTTTTGAAGGCAAGATGC	*Pten*^{WT} allele: 156 pb *Pten*^{loxP} allele: 328 pb
***Tyr*::CreER^{T2}**	Fw: GGAGCAAACAGTAGCTTCAC Rv: AGCTTCGATGATGGGCTTAC	*Tyr*::CreER^{T2}: 201 pb

Table 2. Primers used to genotype mouse transgenic lines.

7.2 Experimental melanomas analysis and validation

7.2.1 Analysis of tumour onset and progression

Melanoma mouse models treated three times with 4-HT were kept in the animal facilities. Animals bearing *Braf*^{V600E}/*Pten*$^{loxP/+}$ mutations developed tumours at 4-8 weeks, depending on the genotype. Animals were monitored weekly during their whole lifespan after 4-HT treatment.

Tumour initial day was considered when nevi reached 2mm diameter. This new developed tumour, and any new tumour that was developed during the experiment, were measured individually. Tumours that grew very closely were impossible to treat as different entities; therefore, those tumours were measured as one but the number of tumour events responsible for this entity were considered for tumour number analysis.

Animals were kept until tumours collective size reached approximately 1200 mm^3 (formula: length × width × depth × 0.562). At this moment, animals were euthanized, and tumours collected (late melanomas). On the other hand, for the analysis of early melanomas, animals were sacrificed when any tumour reached 2mm and samples collected.

7.2.2 Cell sorting and verification of Cre-ER^{T2}-dependent gene recombination

Tumour cell suspensions were prepared from melanomas mechanically dissociated using a scalpel blade in cold DMEM on ice. Prepared tumour samples were added to 1ml of digesting solution containing 0.25 mg/ml of Liberase DH (Merck, 54010544001), 0.55 mg/ml of Dispase II (Merck, 4942078001) and 150 U/ml of DNAse (Roche, 11284932001), incubated at 37 °C for 30 min and then homogenized with increasing gauge syringes up to 25 G. Then, samples were centrifuged at 300*g* 4°C for 5 min, red-blood lysis buffer (BioLegend, 420301) was applied for 5 min at room temperature (RT) and then filtered through a 40-µm cell strainer.

After red blood cell removal, cancer cells were neutralized and resuspended in 0.5 ml of FACS buffer with DAPI per 10^7 cells and directly sorted using a BD FACSAria3 flow cytometer. For each sample, 100,000 cancer cells were sorted at high purity following a singlet/DAPI^{low}/tdTomato^{high} gating strategy. Post-sorting analysis was performed to verify the purity of tdTomato^{high}-sorted cells.

Sorted cancer cells were centrifuged at 300g for 10 min and further lysed using REDExtract-N-Amp™ PCR kit for tissues (Merk, 41106303) for genomic DNA extraction. PCR was performed using primers listed in **Table 2** and subjected to gel electrophoresis to check CreER^{T2}-dependent gene recombination.

7.3 Hair follicle melanocytic cells lineage tracing

For hair follicle characterization, we treated Tyr^{+}-tdTomato and BP-tdTomato models, including those combined with Prrx1^{cKO} and Snai1^{cKO}, topically with 4-HT (30µl DMSO/ethanol containing 240µg 4-HT). Prior to topical treatment, hair skin was depilated using a hair trimmer to avoid skin irritation. Treatment was administered three times in total, with one day between treatments.

Treatment started at postnatal day 28 (4 weeks). At this stage, synchronized from development HF starts anagen stage (van der Veen et al., 1999). Although depilation induced HF synchronicity is more time-specific, acute inflammation have been detected with this procedure (Müller-Röver et al., 2001), which could lead to undesired effect upon EMT-TF characterization (Youssef et al., 2024).

Treated animals were collected at 7 days post-treatment, for anagen characterization, and 28 days post-treatment, for telogen characterization, following hair follicle cycle guidelines (van der Veen et al., 1999).

7.4 Histology

7.4.1 Skin (hair follicles) processing

For OCT embedding, mouse back skins were dissected (2x3 cm area) and fixed in 4% PFA for 4 h in agitation at 4 °C. After fixation, skins were washed three times with PBS and incubated in 30% sucrose for three days at 4 °C. Before embedding in OCT, samples were checked for tdTomato red fluorescence in Leica Stereoscope and regions with higher density of red-labelled hair follicles were selected and sectioned for embedding. Embedded samples were kept in dry ice and transferred to −80 °C before sectioning. Finally, OCT-embedded skins were sectioned in a cryostat (Leica) at 7 µm-thick sections and stored at −80 °C.

7.4.2 Tumour processing

For OCT embedding, tumours were sectioned in 5mm maximum thickness and fixed in 4% PFA for 4 h in agitation at 4 °C. After fixation, tumours were washed three times with PBS and incubated in 30% sucrose for three days at 4 °C before embedding in OCT. Embedded samples were kept in dry ice and transferred to −80 °C before sectioning. Finally, OCT-embedded tumours were sectioned in a cryostat (Leica) at 7 µm-thick sections and stored at −80 °C.

For paraffin embedding, tumours were sectioned in half and fixed in Formalin 10% overnight in agitation at RT. Samples were incubated in serial dilutions of ethanol in H2O + NaCl 0.83% m/v (25%, 50%, 75% and 100%, 10 minutes each) and butanol (20min, twice). Samples were incubated in low-melting paraffin o/n at 45ºC, incubated with fresh low-melting paraffin six times for 1 hour each and mounted in paraffin blocks for long-term storage at RT. Paraffin samples were sectioned using Leica RM2245 Microtome at 7µm thickness.

7.4.3 Human samples

Stainings were performed at the MD Anderson in Madrid, thanks to our collaboration with Gema Moreno-Bueno. Double immunofluorescence was performed on 2µm tumour sections from human melanoma nevi samples, using a BOND RX Fully Automated Research Stainer and an Opal TM 7-Color Automation IHC kit (Akoya Biosciences). Opal-650 and Opal-520 were used to detect antibodies to HMB45 and PRRX1, respectively. Slides were mounted with Prolong Diamond (Molecular Probes) and imaged using Olympus FV1200 confocal microscope with 40X objective. Samples were acquired from the Biobank of the Anatomy Pathology Department of the MD Anderson Cancer Center, Madrid, Spain. This study was performed following

standard ethical procedures of the Spanish regulation (Ley de Investigación Orgánica Biomédica, 14 July 2007) and was approved by the ethic committees of the MD Anderson Cancer Center, Madrid, Spain.

7.5 Section staining and image analysis

7.5.1 Histopathological analysis of melanomas

Paraffin 7 µm-thick late tumour sections were prepared and stained with Hematoxylin (Abcam, Ab220365) and Eosin (Millipore, HT110116-500ML), then mounted for imaging. Whole sections were imaged using the Axioscan 7 (Zeiss) with a 40X objective.

7.5.2 Immunofluorescence (IF)

OCT frozen sections were dried for 2 hours at RT, then washed three times with PBS at RT to remove OCT and prepared for blocking.

Paraffin sections were deparaffinated using xylol and seriated dilutions of ethanol (100%, 75%, 50% and 25% ethanol in H2O + NaCl 0.83% m/v). Then, antigen retrieval was performed incubating deparaffinated sections in Citrate 10mM + 0.1% Tween20 pH 6 at 95ºC for 20 minutes. Sections were rinsed repeatedly with PBS and prepared for blocking.

Antibody	Clonality	Host	Dilution	Provider	Cat. no.
HMB45	Multiclonal	Mouse	1:500	Abcam	Ab732
IBA1	Polyclonal	Rabbit	1:100	Wako Chem.	019-19741
KI67	Polyclonal	Rabbit	1:500	Abcam	ab15580
PRRX1	Polyclonal	Rabbit	1:100	From Angela Nieto´s lab. Kind gift from Prof. TANAKA (IMP Vienna BioCenter)	
SNAI1	Polyclonal	Rabbit	1:50	Cell Signalling	3879
ZEB1	Polyclonal	Rabbit	1:100	Novus Biologicals	NBP1-05987

Table 3. Primary antibodies used for fluorescence immunolabeling.

Sections were blocked in 5% NGS, 1% BSA and 0.1% Triton x-100 for 1 h at RT and incubated with the primary antibodies overnight at 4 °C in blocking solution. After extensive washing in PBS Tween20 0.1% (PBSTw), slices were incubated with the secondary antibodies and DAPI (Sigma, D9542) in PBST1x for 1 h at RT. After washing the secondary antibody with PBS, slices were mounted in Dako Fluorescence

Mounting Medium (Dako). Slices were imaged using an Olympus FV1200 confocal microscope with 40X objective. Information and dilution of antibodies are listed in **Table 3** and **Table 4**.

Antibody	Host	Dilution	Provider	Cat. no.
Alexa Fluor® Plus 647 anti-rabbit	Goat	1:500	Invitrogen	A32733
Opal 520 anti-rabbit			Akoya Bioscience	NEL811001KT
Opal 650 anti-rabbit			Akoya Bioscience	NEL811001KT

Table 4. Secondary antibodies used for fluorescence immunolabeling.

7.5.3 Quantification of Prrx1 and Snai1 immunolabeled cells

Prrx1$^+$ and Snai1$^+$ cells were quantified after immunofluorescent staining by imaging the sections and processing the with ImageJ software. All IF images were acquired using Olympus FV1200 confocal microscope with 40X objective.

For Hair follicle analyses, anagen and telogen bulb area and bulge areas were imaged (15 to 30 HFs per animal). Then, PRRX1$^+$/TdTomato$^+$ or SNAI1$^+$/TdTomato$^+$ melanocytes were quantified and compared to total TdTomato$^+$ cells (melanocytes) per animal, respectively.

For early tumours analyses (2mm diameter), non-overlapping images (5 to 10 per tumour) were acquired following epidermal edge limit of the tumours. Then, PRRX1$^+$/TdTomato$^+$ or SNAI1$^+$/TdTomato$^+$ melanoma cells were quantified and compared to total TdTomato$^+$ cells (melanoma cells) per animal, respectively.

For late tumours analyses, images were obtained from tumour invasive front, tumour bulk and epidermal tumour edge, three random images in each region for each tumour slice. The same number of pictures were performed in every tumour slice. Then, total PRRX1$^+$/TdTomato$^+$ or SNAI1$^+$/TdTomato$^+$ melanoma cells were quantified and compared to total TdTomato$^+$ cells (melanoma cells) per animal, respectively.

7.5.4 Quantification of proliferation and immune infiltration

Proliferation and immune infiltration were evaluated after IF staining by imaging sections and processing them with the ImageJ software. To analyse tumour proliferation and apoptosis, images were obtained from tumour invasive front, tumour bulk and epidermal tumour edge, three random images in each region for each tumour slice. The same number of pictures were taken in every tumour slice. Immune infiltration was analysed comparing IBA1 immunolabeling fluorescence

covered area compared to total tumour field area of each image. Proliferation was assessed by quantifying $KI67^+$ cells compared to total tumour cell number of each image. All immunofluorescence images were acquired using Olympus FV1200 confocal microscope with 40X objective.

7.6 *In vitro* experiments

7.6.1 Cell culture

Murine melanocyte cell line Melan-a (Bennett et al., 1987) was originally obtained from Jose Carlos García-Borrón and Celia Jiménez Cervantes laboratory (University of Murcia). Cells were maintained in RPMI (Sigma) supplemented with 10% FBS (Sigma) heat inactivated,1% penicillin/streptomycin (Sigma) and 200 mM of 12-O tetradecanoyl phorbol 13-acetate (TPA) (P1585, Merck). Cells were kept at 37 °C in a humid atmosphere containing 5% CO_2 and the media was replaced every 2/3 days. Melan-a cells were passaged when they reached 80% confluency 1:10 every 96 h, using 0,025% trypsin/PBS. Cells were discarded up to six consecutive passages and replaced by fresh stocks. All cell lines were tested and confirmed negative for mycoplasma monthly at the host institution.

7.6.2 Transfection of plasmids and interfering RNAs

For RNA interference in Melan-a cells, siRNA obtained from Silencer® predesigned (Ambion) was used for Prrx1 (Prrx1 siRNA (antisense): UUCUCGAACAAAAGCAUCCgg) and Snai1 (Snai1 siRNA (antisense): AUAUUUGCAGUUGAAGAUCtt). Cells were seeded in six-well plates and transfected 24h after seeding using Lipofectamine™ RNAiMAX (13778075, ThermoFisher) at 60% confluence. At 24h post transfection, cells were lysed for RNA extraction of used in posterior experiments.

For gain-of-function experiments, *SNAI1*-GOF plasmid was transfected in Melan-a cells seeded in six-well plates at 24h after seeding, using Lipofectamine™ 3000 (L3000001, ThermoFisher). At 24h post transfection, cells were lysed for RNA extraction or used in posterior experiments.

7.6.3 *In vitro* soft-agar assay

Cultured Melan-a cells transfected with siRNA or SNAI1 GOF plasmid were collected 24h after transfection. 10000 cells were resuspended in 1ml RPMI supplemented media containing 0.35% agar and seeded in six-well plates previously covered with a thin layer of RPMI supplemented medium containing 0.5% agar. 30 min later, 1 ml of

supplemented RPMI media was added on top of agar-media layers. Melan-a cells were incubated for 50 days at 37 ºC and 5% CO2, and media was refreshed twice per week. At the end of the incubation time, cell cultures were imaged (three non-overlapping fields) and the colonies larger than 50 µm in diameter were counted using ImageJ software.

7.6.4 Total RNA extraction, cDNA synthesis and qPCR analysis

Total RNA extraction from cell line samples was performed using the Illustra RNAspin Mini isolation kit (GE healthcare), following manufacturer's instructions. For cDNA synthesis, Maxima First Strand cDNA Synthesis kit (Thermo Fisher) was used, following the manufacturer's instructions. RT-qPCR was done using the Fast SYBR Green Mastermix (Applied Biosystems) in a Step One Plus machine (Applied Biosystems), using the primers listed in **Table 5**.

Relative levels of expression were calculated using the comparative Ct method normalized to housekeeping genes and then normalized to their respective control samples.

Name	Sequence 5'-3'	Gene
mNgfr f	CCTGGACAGTGTTACGTTCTC	Ngfr
mNgfr r	TCGTCCTGGTAGTAGCCATAG	Ngfr
mPrrx1 f	AGAGTGCAGGTGTGGTTTC	Prrx1
mPrrx1 r	CTGAGTAGGACTTGAGGAGAGA	Prrx1
mSnail1 f	CACGCTGCCTTGTGTCT	Snai1
mSnail1 r	GAATGGCTTCTCACCAGTGT	Snai1
hSnail1 f	CTCTAATCCAGAGTTTACCTTCCAG	SNAI1
hSnail1 r	CCCAGATGAGCATTGGCA	SNAI1

Table 5. Primers used for RT-qPCR analyses.

7.6.5 miRNA extraction, cDNA synthesis and qPCR analysis

Long RNA fraction and miRNA enriched fraction extraction from cell line samples were performed using the mirVana™ miRNA Isolation Kit (Invitrogen), following the manufacturers' instructions.

Long RNA fraction was used for cDNA synthesis, using Maxima First Strand cDNA Synthesis kit (Thermo Fisher). Then, RT-qPCR was done using Fast SYBR Green Mastermix (Applied Biosystems) in a Step One Plus machine (Applied Biosystems), using the primers listed in **Table 5**.

For miRNA expression assays, reverse transcription reactions were performed using TaqMan® MicroRNA Assay (Applied Biosystem) according to the manufacturers' instructions. Later, RT-qPCR was performed using specific probes from TaqMan® MicroRNA Assay (Applied Biosystem), listed in **Table 6**. TaqMan® Universal Master Mix II, no UNG (Applied Biosystems) was used in a Step One Plus machine (Applied Biosystems) according to the manufacturers' instructions. Relative levels of expression were calculated using the comparative Ct method normalized to the internal control U6 snRNA.

Name	Assay ID	Assay name	Cat. number
U6	001973	Control U6 snRNA	4427975 001973
Mir15a	000389	hsa-miR-15a	4427975 000389
Mir15b	000390	hsa-miR-15b	4427975 000390
Mir195	000494	hsa-miR-195	4427975 000494

Table 6. TaqMan® MicroRNA Assay probes used for miRNA analyses.

7.7 Statistical analysis

All statistical tests were performed using GraphPad Prism 9 software. Mann-Whitney test or Kruskal-Wallis with Dunns's multiple comparison test were performed to determine the significant values of the data. Kaplan-Meier data were analysed with the comparison of survival curves using the Long-rank (Mantel-Cox) test. All the values were shown as Mean values ± SEM (Standard Error of the Mean). Significant differences between groups were represented as follows: * = $p \leq 0.05$, ** = $p \leq 0.01$, *** = $p \leq 0.001$ and **** = $p \leq 0.0001$.

8 Results

8.1 Expression of Prrx1 and Snai1 in the hair follicle

Cutaneous melanoma arises from melanocytes that reside in the skin. This type of cancer is characterized by its high degree of inter and intratumoral heterogeneity and phenotypic switching capabilities (Rambow et al., 2018; Tirosh et al., 2016). Although numerous studies have focused on investigating these characteristics during melanoma progression, understanding the early events underlaying melanocyte transformation may provide critical insight into the origins of these complex traits.

In murine models, although some melanocytic populations exist in the interfollicular dermis (Glover et al., 2015), most back skin cells of melanocyte lineage reside in different niches in the hair follicle (HF) (Hirobe, 1984; Nishimura et al., 2002). These cells comprise three different cell populations: undifferentiated melanocyte stem cells (MSCs), that resides specifically in a stem cell niche in the hair bulge region; transit-amplifying cells and intermediate population in the outer root sheath of the hair follicle; and fully differentiated melanocytes, that resides in the hair bulb and actively produce melanin (Nishimura et al., 2002). These niches can dynamically change during the progression of hair cycle, as MSCs can migrate between compartments and switch between transit-amplifying cells, what is considered an intermediate state, and stem cell states (Q. Sun et al., 2023).

During development, melanocyte arises from different populations of neural crest cells (Mort et al., 2015). In these stages, migratory cells express some EMT-TFs, including Prrx1, Snai1/2, Zeb1/2 and Twist1 (Candido-Ferreira et al., 2023). At later stages, when the hair follicle is fully developed, differentiated melanocytes express Zeb2 and Snai2 in homeostatic conditions (Denecker et al., 2014; Gupta et al., 2005). However, Prrx1 and Snai1 expression have not being explored in these cell populations at the hair follicle.

8.1.1 Prrx1 and Snai1 are expressed in melanocytic cells in anagen

To characterize the physiological expression of Prrx1 and Snai1 in the hair follicles, we used the conditionally activated Tyr^{+}-tdTomato murine model. This model was generated by isolating the Tyr:Cre-ER^{T2} allele from the BP melanoma murine model (Dankort et al., 2009) and crossing the resulting mice with the tdTomato reporter mouse model (Madisen et al., 2010).

With the aim of analysing different stages of hair cycle, 4 weeks aged mice were treated with 4-hydrotamoxifen (4-HT) three times. Skin was collected 7- and 28-days

post-treatment for the characterization of anagen and telogen hair follicle states, as these two stages show different populations of melanocytic cells (**Figure 6a, b**).

During the active anagen phase, we could detect the presence of PRRX1⁺/tdTomato⁺ cells at the hair follicle (17.83% of total TdTomato⁺ cells, n=5). However, this expression was restricted to the hair bulb region **(Figure 6c, d**). On the other hand, in the resting telogen phase we could detect very few PRRX1⁺/tdTomato⁺ cells (1.52% of total TdTomato⁺ cells, n=3) in the bulge region and no expression was detected in the hair germ (**Figure 6c, e**).

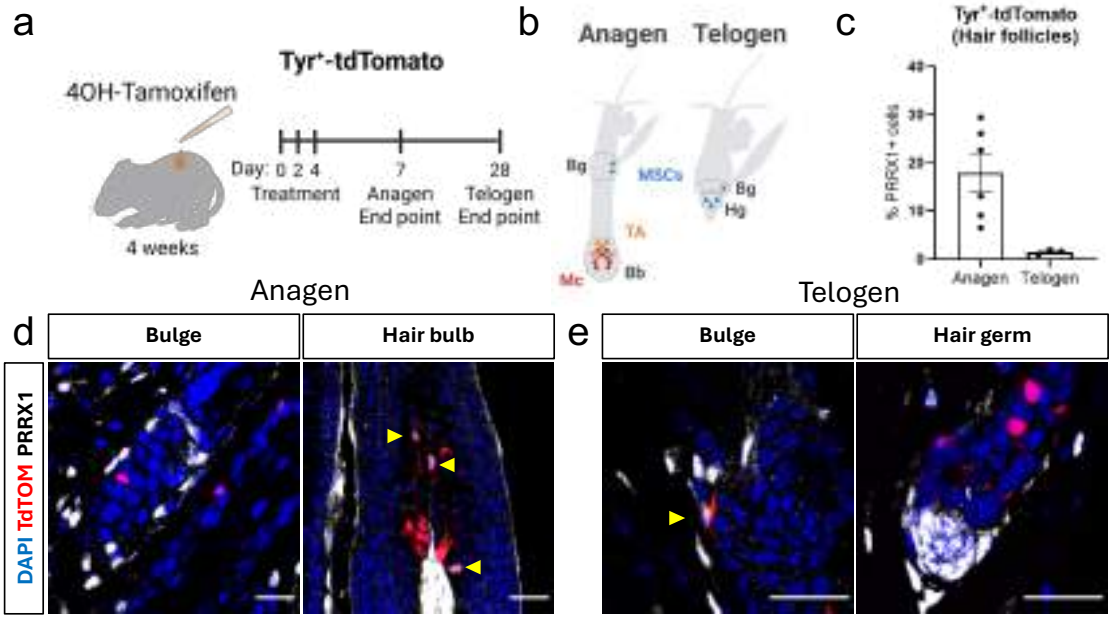

Figure 6. Prrx1 is expressed in the hair bulb of the mouse hair follicle. (**a**) Schematic representation of the treatment performed in mice in which hair follicle samples were analysed. (**b**) Brief illustration of anagen and telogen phases in the hair follicle (Bg: Bulge, Bb: Hair bulb, Hg: Hair germ, Mc: Melanocytes, MSCs: Melanocyte stem cells, TA: Transit-amplifying cells) (**c**) Quantification of % PRRX1⁺tdTomato⁺/total tdTomato⁺ cells in hair bulbs at anagen and telogen phases (n=5, n=3). (**d, e**) Representative images of the hair follicles in anagen or telogen showing PRRX1 immunolabeling (white) in Tyr⁺-tdTomato mice (tdTomato⁺ cells labelled in red). Yellow arrowheads indicate Prrx1 expression in tdTomato⁺ cells. Data are represented by Mean ± SEM and statistically significant differences are tested by unpaired two-tailed Mann-Whitney test. Each dot represents one animal (* = $p < 0.05$, ** = $p < 0.01$, *** = $p < 0.001$, **** = $p < 0.0001$). Scale bars: 25 µm. Illustrations created with BioRender.com.

Additionally, Snai1 expression was also analysed in hair follicles from the Tyr⁺-tdTomato model (**Figure 7a**). During anagen phase, SNAI1 immunolabeling shows the presence of SNAI1⁺/tdTomato⁺ cells residing in the hair bulb (9.04% of total tdTomato⁺ cells, n=5) (**Figure 7b, c**) whereas we could not detect any SNAI1⁺/tdTomato⁺ cells in telogen phase (0% of total tdTomato⁺ cells, n=3) (**Figure 7b, d**).

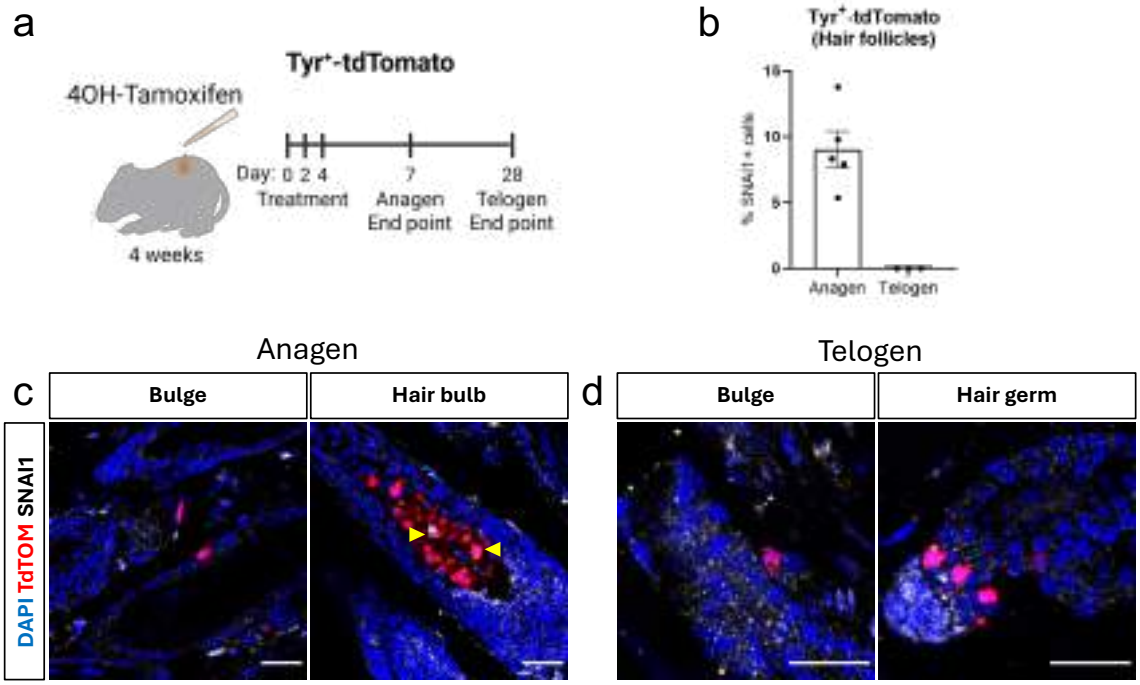

Figure 7. Snai1 is expressed in the hair bulb of the mouse hair follicle. (**a**) Schematic representation of the treatment performed in mice in which hair follicle samples were analysed. (**b**) Quantification of % SNAI1$^+$ tdTomato$^+$/total tdTomato$^+$ cells in in hair bulbs at anagen and telogen phases (n=5, n=3). (**c, d**) Representative images of the hair follicles in anagen or telogen showing SNAI1 immunolabeling (white) in Tyr$^+$-tdTomato mice (tdTomato$^+$ cells labelled in red). Yellow arrowheads indicate Snai1 expression in tdTomato$^+$ cells. Data are represented by Mean ± SEM and statistically significant differences are tested by unpaired two-tailed Mann-Whitney test. Each dot represents one animal (* = $p < 0.05$, ** = $p < 0.01$, *** = $p < 0.001$, **** = $p < 0.0001$). Scale bars: 25 µm. Bg: Bulge, Bb: Hair bulb, Hg: Hair germ, Mc: Melanocytes, MSCs: Melanocyte stem cells. Illustrations created with BioRender.com.

These results suggest that Prrx1 and Snai1 are predominantly expressed in hair follicles in anagen and that Prrx1 is expressed more abundantly than Snai1 in these conditions.

8.1.2 Prrx1 and Snai1 are expressed in the hair follicle of BP mice

Next, we characterized Prrx1 and Snai1 expression in the hair follicle from the BP-tdTomato mouse model. For this, we used the same protocol and 4 weeks mice were treated 3 times with 4-HT and skin was collected 7- and 28-days post-treatment (**Figure 8a**).

In the HF of BP-tdTomato mice, in line with the expression of oncogenic Braf and as previously described (Köhler et al., 2017; Q. Sun et al., 2019), some tdTomato$^+$ cell pools were detected in the hair bulb during anagen, at positions where melanocytes are not usually present. In these locations, Prrx1 expression was detected in approximately 20% of tdTomato$^+$ cells (n=4) (**Figure 8b**), a very similar proportion to

what was found in tdTomato⁺ cells at HF bulb in the Tyr⁺-tdTomato mouse model (**Figure 8c**).

On the other hand, Snai1 was also detected in aberrant melanocytic cells masses in the hair follicles of the BP-tdTomato model at anagen (**Figure 8b**). SNAI1⁺/TdTomato⁺ cells were present in an approximately 10% (n=5) of the total tdTomato⁺ cells at the hair bulb (**Figure 8d**). This proportion was a bit higher that the expression found in Tyr⁺-tdTomato mouse model, but these differences were not statistically significant.

These results suggest that Prrx1 and Snai1 are also expressed at the hair follicle of oncogenic Braf expressing melanocytes, indicating a potential role in melanomagenesis.

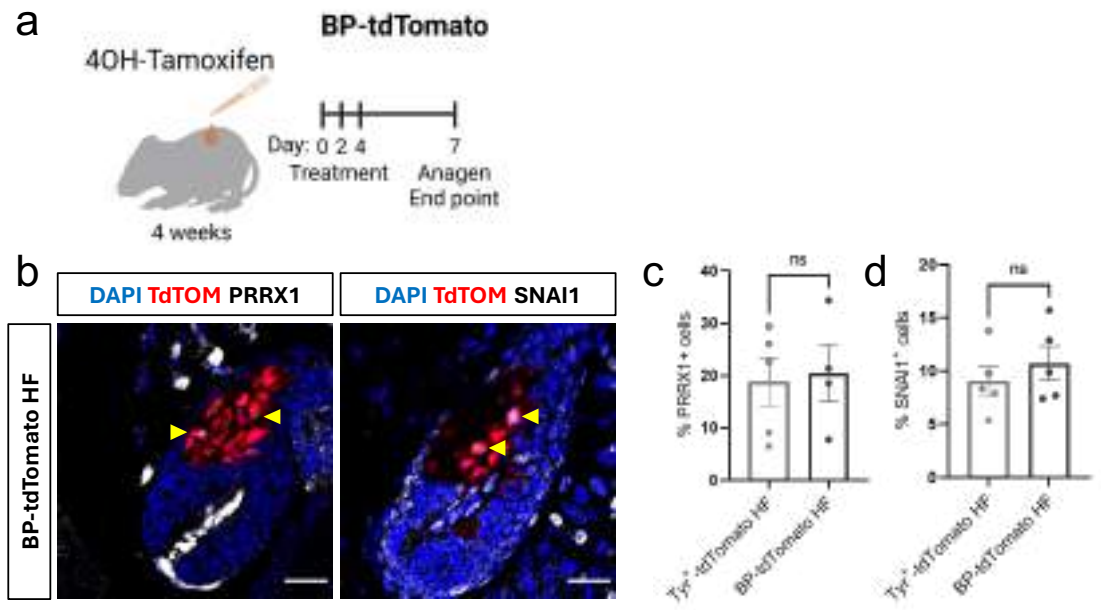

Figure 8. Prrx1 and Snai1 are expressed in the hair bulb of BP mice. (**a**) Schematic representation of the treatment performed in mice in which hair follicle samples were analysed. (**b**) Representative images of immunolabeling (in white) for PRRX1 (left) and SNAI1 (right) in BP-hair follicles (HF) in anagen from BP-tdTomato mice. tdTomato⁺ cells labelled in red. Yellow arrowheads indicate PRRX1 or SNAI1 expression in tdTomato⁺ cells. (**c**) Graph showing percentage of PRRX1⁺/tdTomato⁺ of total tdTomato⁺ cells in the bulb of the hair follicle (HF) in anagen in samples from Tyr⁺-tdTomato mouse model (n=5) and BP-tdTomato mice. (**d**) Graph showing percentage of SNAI1⁺/tdTomato⁺ of total tdTomato⁺ cells in in the bulb of the hair follicle (HF) in anagen in samples from Tyr⁺-tdTomato mouse model (n=5) and BP-tdTomato mice. Data are represented by Mean ± SEM and statistically significant differences are tested by unpaired two-tailed Mann-Whitney test. Each dot represents one animal (* = $p < 0.05$, ** = $p < 0.01$, *** = $p < 0.001$, **** = $p < 0.0001$). Scale bars: 25 µm. Illustrations created with BioRender.com.

8.2 Contribution of Prrx1 to melanoma

8.2.1 Prrx1 is expressed in early melanomas, but its expression is lost as tumour progresses

We first investigated the potential role of Prrx1 in melanoma. As mentioned before, previous studies indicated that some EMT-TFs can regulate and modulate melanoma progression and metastatic dissemination (Caramel et al., 2013; Vandamme et al., 2020).Among them, the EMT-TF Zeb1 plays a major role during melanoma progression, as it has been associated with invasive and stem-like programs (Durand et al., 2024; Vandamme et al., 2020).

Using the melanoma reporter mouse line, the BP-tdTomato model, we could confirm that Zeb1 is expressed by TdTomato$^+$ melanoma cells at different tumour stages (**Figure 9a**): including early (2mm diameter and 1mm thickness), and late melanomas (final point) as defined in the Material and Methods Section (**Figure 9b**). This confirms that this model behaves similarly to what it has been described in previous studies.

Using the same model, we next characterized the expression of Prrx1 at these stages. In early tumours immunolabeling of PRRX1 was detected at around 7% of tdTomato$^+$ cells (n=7) (**Figure 9c left, d**). These PRRX1$^+$/TdTomato$^+$ cells were mostly found under the basal lamina of the epidermis and Prrx1 was also detected in many cells from the tumour microenvironment. Prrx1 expression was next analysed at late stages, when the tumour size reached the criteria for humane end point for the animal. In this case, PRRX1$^+$/tdTomato$^+$ cells were nearly absent (**Figure 9c right, d**), since its expression was only found in a few cells found across all tumours analysed (n=4).

Prrx1 was also present in tumour microenvironment cells, but the location and density of these cells was very heterogeneous even within the tumour.

Our data suggests that Prrx1 expression is lost during melanocytic cells transformation as it is present HFs at anagen in the BP mouse model, but this expression is reduced as tumour progresses and it is eventually lost, indicating that Prrx1 may play a role particularly during melanoma initiation (**Figure 9d)**.

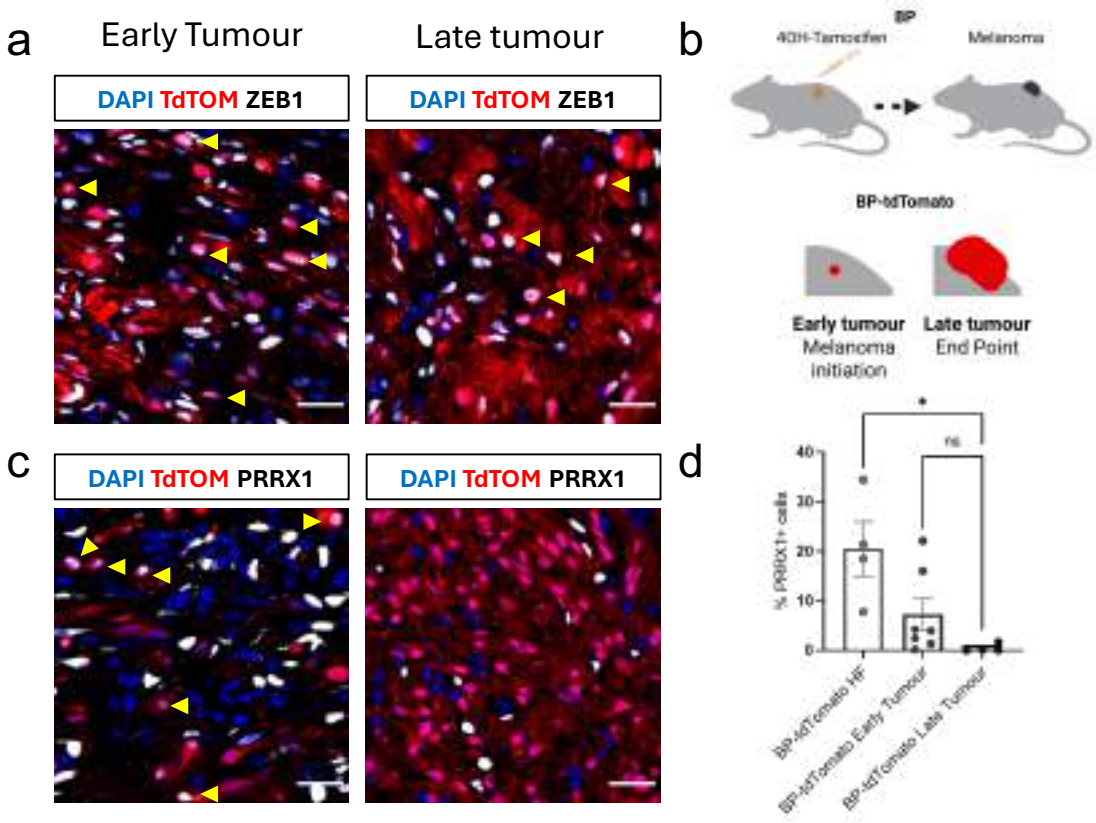

Figure 9. Prrx1 is expressed in early melanomas, but its expression is lost as tumour progresses. (**a**) Representative images of immunolabeling for Zeb 1 (white) in melanomas from BP-tdTomato mice (tdTomato$^+$ cells labelled in red). Early tumours (2mm width, left) and late tumours (experiment end point, right). Yellow arrowheads indicate Zeb1 expression in tdTomato$^+$ cells. (**b**) Schematic representation of the treatment performed in mice to generate melanomas and the different tumour stages analysed. (**c**) Representative images of immunolabeling for PRRX1 (white) in melanomas from BP-tdTomato mice (tdTomato$^+$ cells labelled in red). Early tumours (2mm width, left) and late tumours (experiment end point, right). Yellow arrowheads indicate PRRX1 expression in tdTomato$^+$ cells. (**d**) Graph showing percentage of PRRX1$^+$/tdTomato$^+$ of total tdTomato$^+$ cells in the bulb of hair follicle (HF) in anagen (n=4), early tumours (n=7) and late tumours (n=4) in samples from the BP-tdTomato mouse model. Data are represented by Mean ± SEM and statistically significant differences are tested by unpaired two-tailed Mann-Whitney test. Each dot represents one animal (* = $p < 0.05$, ** = $p < 0.01$, *** = $p < 0.001$, **** = $p < 0.0001$). Scale bars: 25 µm. Illustrations created with BioRender.com.

8.2.2 Human malign nevi show localized Prrx1 expressing melanoma cells

Our melanoma mouse models show Prrx1 expression during melanocyte transformation and tumour initiation, which is lost as tumour progresses. To validate the translational relevance of these findings to human melanoma in the clinical setting, we investigated some human melanoma early lesions (**Figure 10a**).

In these samples, double immunofluorescence shows that PRRX1 is detected in HMB45$^+$ cells (**Figure 10b**). HMB45 is a broad marker for melanoma cells (Gown et al., 1986). Although very few cells were detected on each sample, double

PRRX1^{+}/HMB45^{+} cells were present in all analysed samples (n=3). These results suggest that Prrx1 may also play a role in human cutaneous melanoma.

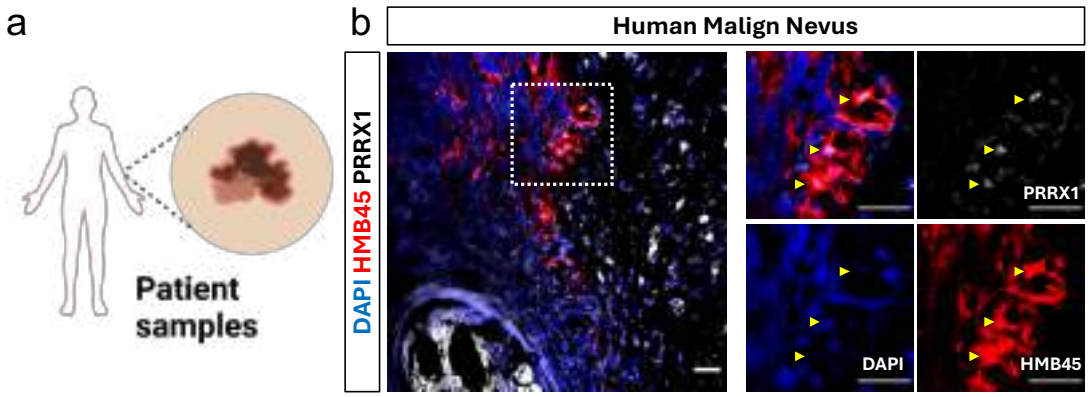

Figure 10. Prrx1 is expressed in early melanoma lesions in human samples. (**a**) Brief illustration of the origin of the melanomas. (**b**) Representative image of an early melanoma (left, higher magnification). Immunolabelling for PRRX1 (white) and HMB45 (red) showing PRRX1 expression in some HMB45^{+} cells in the skin (n=3). Yellow arrowheads indicate Prrx1 expression in HMB45^{+} cells. Scale bars: 25 µm. Illustrations created with BioRender.com.

8.2.3 Generation and validation of a Prrx1 loss-of-function melanoma mouse model

To investigate whether Prrx1 could be implicated in melanomagenesis, we next generated a conditionally activated melanoma murine model unable to express Prrx1. To generate this model and also to trace melanoma cells, we crossed our inducible reporter melanoma BP-tdTomato model (*Tyr*::Cre-ER^{T2}, *Braf*^{CA}, *Pten*$^{loxP/+}$, tdTomato) with the Prrx1^{cKO} model (*Prrx1*$^{loxP/loxP}$), referred as BP-tdTomato/Prrx1^{cKO}.

To validate Cre recombinase activity in this model, BP-tdTomato/Prrx1^{cKO} animals were treated with 4-HT at 6-8 weeks after birth. As described above, treatment consisted in topical application of 4-HT after back skin depilation, three times on alternate days (**Figure 11a**). Animals were kept in the animal facility and monitored until tumour masses arose and reached suitable size for further experiments.

Tumours were collected, homogenized and subjected to fluorescent activated cell sorting (FACS) to isolate TdTomato^{+}-melanoma cells, that were subsequently used to obtain gDNA and perform PCR and electrophoresis to validate Cre recombinase activity.

We confirmed that melanoma cells from BP-tdTomato mice expressed the wild-type Prrx1 allele (Prrx1^{WT}), as expected. In contrast, melanoma cells from BP-tdTomato/Prrx1^{cKO} mice exhibited a PCR band corresponding to the recombined floxed allele (Prrx1^{Floxed}), with a faint residual band corresponding to the

unrecombined allele (Prrx1^{loxP}) (**Figure 11b**). These results confirm that Cre recombinase activity was active at the Prrx1 locus.

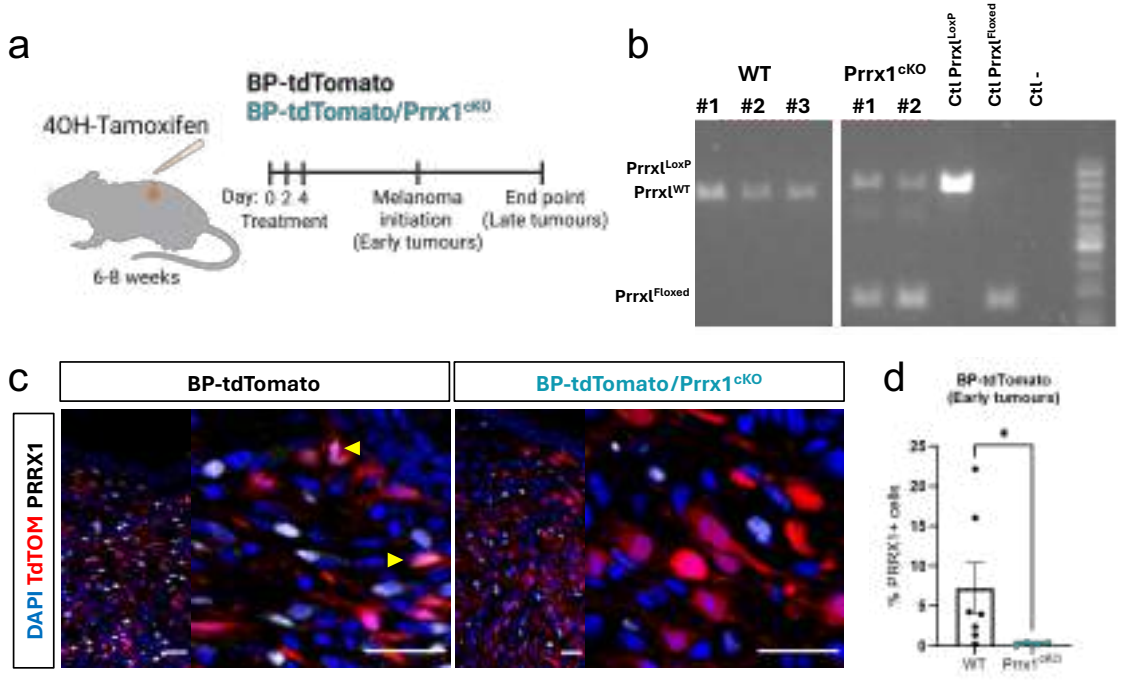

Figure 11. Generation and validation of a Prrx1 loss-of-function mouse melanoma model. (**a**) Schematic representation of the treatment performed in BP-tdTomato/Prrx1^{cKO} mice to generate melanomas. (**b**) Image of a DNA gel electrophoresis confirming CRE-ER^{T2}-dependent recombination of Prrx1^{loxP} gene. Molecular weight marker of 100bp. (**c**) Representative images of immunolabelling for PRRX1 in early melanomas (white) in the BP-tdTomato and BP-tdTomato/Prrx1^{cKO} mouse lines (tdTomato^{+} cells labelled in red). PRRX1^{+}/tdTomato^{+} melanoma cells (yellow arrowheads) appear close to epidermis in BP melanomas, and this is absent in BP-tdTomato/Prrx1^{cKO} models. (**d**) Graph showing percentage of PRRX1^{+}/tdTomato+ of total tdTomato^{+} cells in early tumours in the melanoma BP-tdTomato and BP-tdTomato/Prrx1^{cKO} mouse models (n=7, n=4). Data are represented by Mean ± SEM and statistically significant differences are tested by unpaired two-tailed Mann-Whitney test. Each dot represents one animal (* = $p < 0.05$, ** = $p < 0.01$, *** = $p < 0.001$, **** = $p < 0.0001$). Scale bars: 25 µm. Illustrations created with BioRender.com.

To further check Prrx1 depletion at protein level, we moved to early melanoma tumours. Immunolabeling of PRRX1 in early tumours from BP-tdTomato/Prrx1^{cKO} mice showed very few PRRX1^{+}/TdTomato^{+} cells (less than 0.5%) compared to BP-tdTomato mice (**Figure 11c, d**). These data indicates that PRRX1^{+}/tdTomato^{+} cells were almost absent in BP-tdTomato/Prrx1^{cKO} tumours, validating the suitability of the newly generated Prrx1 loss-of-function melanoma mouse model.

8.2.4 Prrx1 depletion promotes melanomagenesis

Once the newly generated Prrx1 loss-of-function mouse melanoma model was validated, we carried on investigating the impact of depleting Prrx1 in melanoma

initiation. For this, 6-8 weeks BP and BP/Prrx1^{cKO} mice were treated with 4-HT and animals were monitored until lesions appeared. Tumour initiation was registered when tumours reached 2mm diameter and 1mm thickness. Animals were later monitored for new tumour events until the total tumour mass reached the endpoint size, when mice were sacrificed and tumours collected (**Figure 12a**). Representative images of developed tumours of these mouse models 95 days after tamoxifen treatment are shown in **Figure 12b.**

Kaplan-Meier survival plot (**Figure 12c**) shows that the mean melanoma-free-survival time in BP mice was 94.5 days, compared to 61 days in the BP/Prrx1^{cKO} mice. This reduction in the time in which melanoma appears indicates that Prrx1 depletion contributes to melanomagenesis in this model.

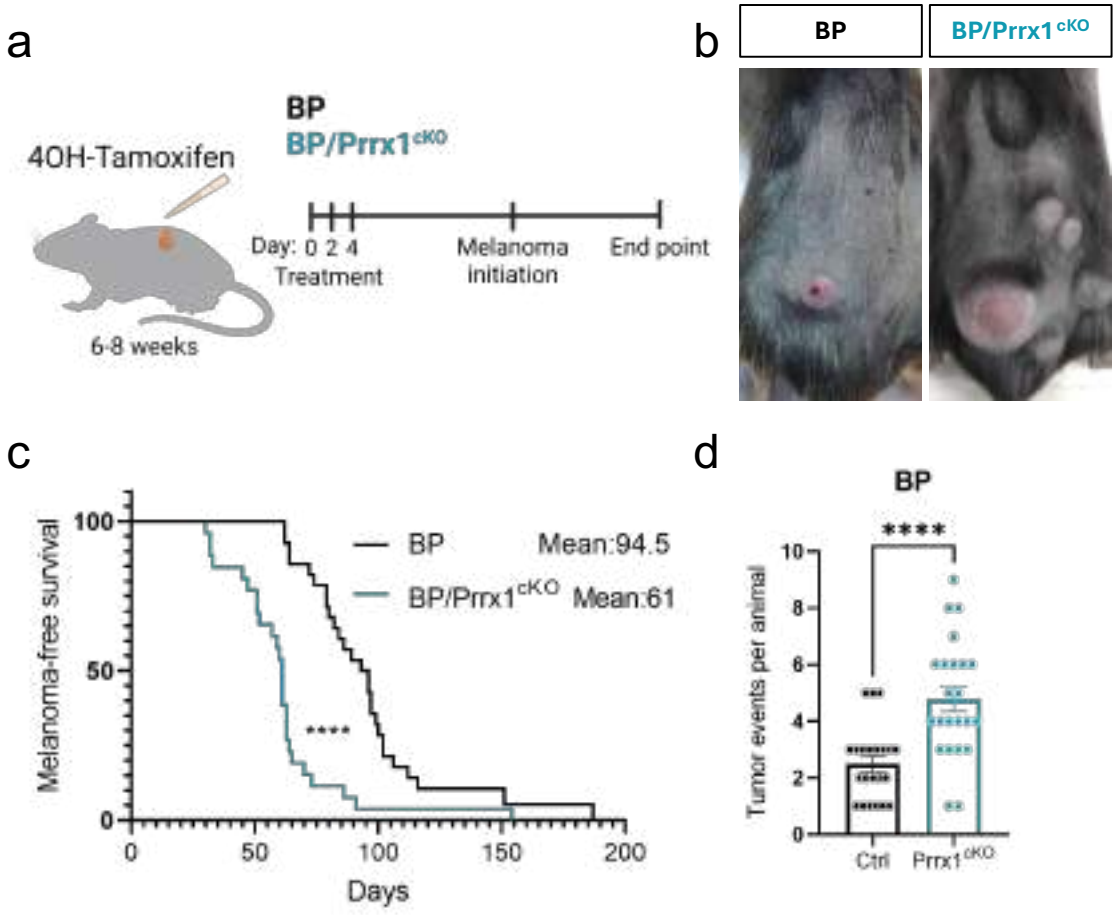

Figure 12. Prrx1 depletion promotes melanomagenesis. (**a**) Schematic representation of the treatment performed in BP and BP/Prrx1^{cKO} mice to generate melanomas. (**b**) Representative images of the back skin of BP and BP/Prrx1^{cKO} mice that have developed melanomas. (**c**) Kaplan-Meier plot showing melanoma-free survival since the start of the 4-HT treatment in the BP and BP/Prrx1^{cKO} melanoma models (n=28, n=27). (**d**) Quantification of tumours developed in BP and BP/Prrx1^{cKO} mice (n=22, n=23). Data are represented by Mean ± SEM and statistically significant differences are tested by unpaired two-tailed Mann-Whitney test. Each dot represents one animal (* = $p < 0.05$, ** = $p < 0.01$, *** = $p < 0.001$, **** = $p < 0.0001$). Illustrations created with BioRender.com.

Together with this acceleration in tumour onset, the number of tumours that appeared until endpoint was almost double in BP/Prrx1^{cKO} mice (mean = 4.78) compared to BP controls (mean = 2.5) (**Figure 12d**). Due to some leakiness of this mouse model, as described previously (*TheJacksonLab - BRaf[CA], Pten[loxP], Tyr::CreER[T2] Strain Details*, n.d.), we only noted as tumour events those that appeared in the back skin surrounding the treatment zone, even though leaky tumours appeared more frequently in BP/Prrx1^{cKO}.

These findings suggest that Prrx1 may play a protective role in melanoma, as downregulation of this gene accelerates the ability of BRAF expressing melanocytes to accelerate and promote tumour development.

8.2.5 Prrx1 loss does not impact on tumour histopathological characteristics or proliferation

To investigate potential differences between melanomas developed in BP/Prrx1^{cKO} mice compared to BP controls, tumours were fixed, processed and sectioned after collection (**Figure 13a**). Haematoxylin-eosin contrast staining showed that these tumours presented high inter- and intra-tumoural heterogeneity, with few pigmented cells mostly located at surface regions of the tumour, and no major differences between BP and BP/Prrx1^{cKO} late tumours were found (**Figure 13b**).

To investigate proliferation levels of these tumours, we performed immunolabeling for KI67, a nuclear protein used as a proliferation marker (Gerdes et al., 1983). Quantification of KI67^{+} cells in tumours showed no significant differences between tumours from the BP and BP/Prrx1^{cKO} models (**Figure 13c, d**). Analyses were performed taking pictures at difference sites of the surface, the inner part and the invasive front of the tumours, and the total tumour cell number was taken in account to calculate KI67^{+} cell ratio.

We also analysed the presence of immune myeloid cells in the tumours. For this, we performed immunofluorescence and quantified the amount of IBA1^{+} cells in the tumour. As mentioned above, Analyses were performed taking pictures at difference sites of the surface, the inner part and the invasive front of the tumours, and the total tumour cell number was taken in account to calculate Iba1^{+} cell ratio. However, no significant differences between BP and BP/Prrx1^{cKO} tumours were found (**Figure 13e, f)**.

These data suggest that the role of Prrx1 in melanoma is independent of the ability of melanoma cells to proliferate or the infiltration of myeloid populations in tumours.

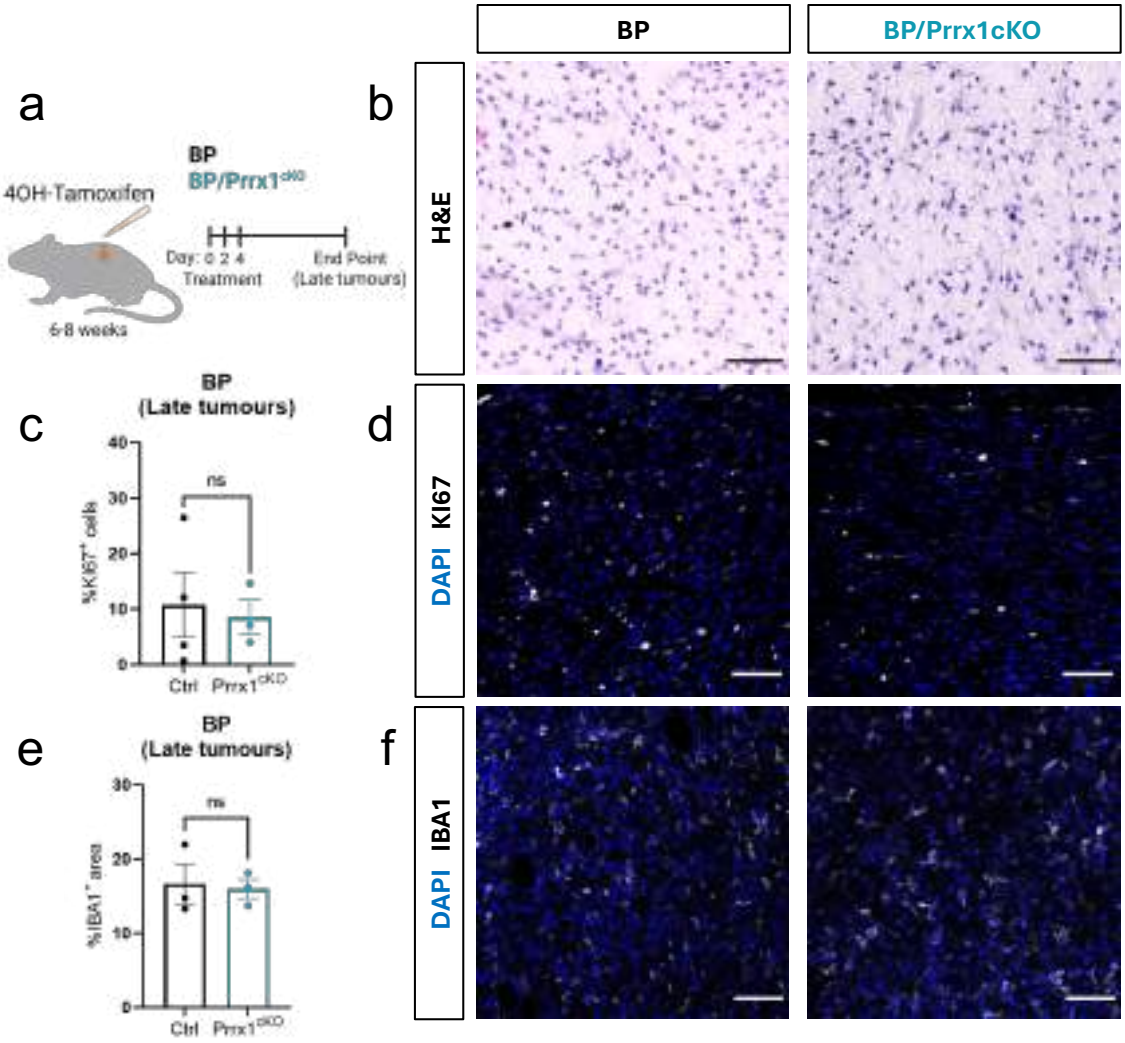

Figure 13. Prrx1 loss does not impact on tumour histopathological characteristics or proliferation. (**a**) Schematic representation of the treatment performed in BP and BP/Prrx1^{cKO} mice to generate melanomas. (**b**) Representative image of haematoxylin-eosin (H&E) staining in melanomas from BP and BP/Prrx1^{cKO} mice. (**c**) Graph showing percentages of KI67^{+} cells in tumour cells in melanomas from BP and BP/Prrx1^{cKO} mice. (**d**) Representative image of KI67 immunolabeling (white) in melanomas from BP and BP/Prrx1^{cKO} mice. (**e**) Graph showing percentages of IBA1^{+} cells in tumour cells in melanomas from BP and BP/Prrx1^{cKO} mouse models. (**f**) Representative image of immunolabeling for IBA 1(white) in melanomas from BP and BP/Prrx1^{cKO} mouse models. Data are represented by Mean ± SEM and statistically significant differences are tested by unpaired two-tailed Mann-Whitney test. Each dot represents one animal (* = $p < 0.05$, ** = $p < 0.01$, *** = $p < 0.001$, **** = $p < 0.0001$). Scale bars: 50 µm. Illustrations created with BioRender.com.

8.2.6 Prrx1 depletion activates Snai1 expression

As previous results suggest, the acceleration of tumour initiation and the higher propensity to develop tumours does not seem related to a higher proliferation of melanoma cells in the BP/Prrx1^{cKO} model. As previous studies indicate that Prrx1 inhibition induces the activation of Snai1 through a regulatory loop (Fazilaty et al., 2019), we next investigated whether Prrx1 depletion may increase Snai1 expression. For this, we next compared Snai1 expression in melanoma cells from the BP-tdTomato and the BP-tdTomato/Prrx1^{cKO} mice in early melanomas (**Figure 14a**)

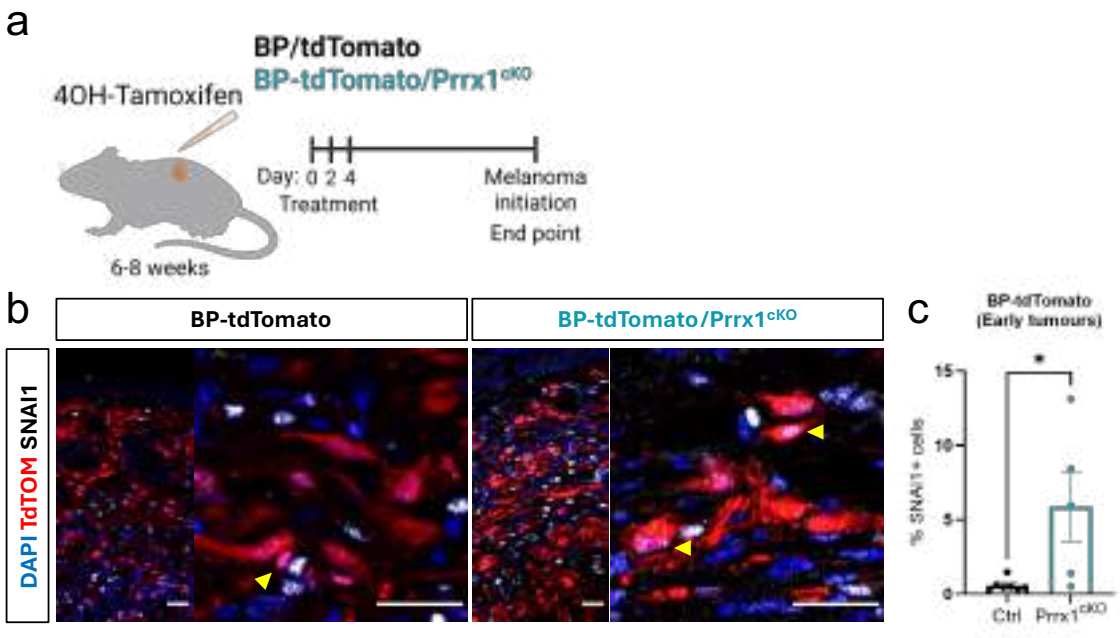

Figure 14. Prrx1 depletion activates Snai1 expression in early melanomas. (**a**) Schematic representation of the treatment performed in BP-tdTomato and BP-tdTomato/Prrx1^{cKO} mice to generate early melanomas. (**b**) Representative images of immunolabeling for SNAI1 (white) in early melanomas from BP-tdTomato and BP-tdTomato/Prrx1^{cKO} mice (tdTomato^{+} cells labelled in red). SNAI1^{+}/tdTomato^{+} melanoma cells appear rarely in BP-tdTomato melanoma tumour, while its frequency is greatly increased in BP-tdTomato/Prrx1^{cKO} model. (**c**) Graph showing percentages of SNAI1^{+}/tdTomato^{+} cells of total tdTomato^{+} cells in early tumours on BP-tdTomato and BP-tdTomato/Prrx1^{cKO} mouse models (n=7, n=5). Data are represented by Mean ± SEM and statistically significant differences are tested by unpaired two-tailed Mann-Whitney test. Each dot represents one animal (* = $p < 0.05$, ** = $p < 0.01$, *** = $p < 0.001$, **** = $p < 0.0001$). Scale bars: 25µm. Illustrations created with BioRender.com.

Interestingly, immunolabeling for SNAI1 in early melanomas show increased number of SNAI1^{+}/tdTomato^{+} cells in BP-tdTomato/Prrx1^{cKO} (5.88% compared with 0.59% in BP-tdTomato control tumours) (**Figure 14b, c**). These cells were located close, but not adjacent, to basal lamina of epidermis or in the interfollicular dermis.

We next compared Snai1 expression in hair follicles from BP-tdTomato and BP-tdTomato/Prrx1^{cKO} mice (**Figure 15a**). Immunolabeling for Snai1 in the bulb of hair

follicles during anagen confirmed an increase of SNAI1^{+}/tdTomato^{+} cells upon Prrx1 depletion (11.19% vs 24.65%) (**Figure 15b, c**), in line with the situation in early tumours.

These results indicate that the mechanism by which Prrx1 depletion promotes melanomagenesis can be mediated by an increase of Snai1 expression. Snai1 upregulation can be identified at the early stages of melanocytic transformation.

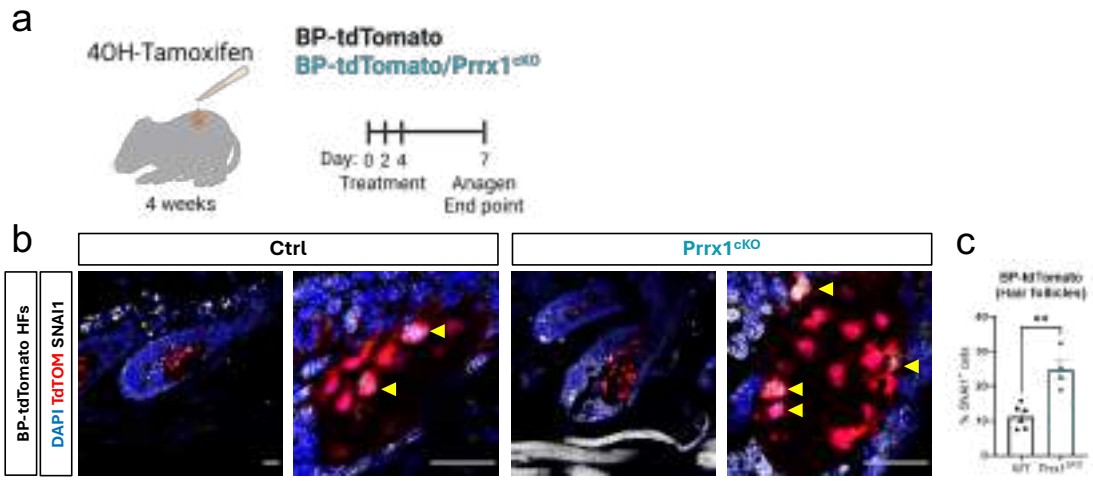

Figure 15. Prrx1 depletion activates Snai1 expression in Tyr^{+} cells in the hair bulb upon oncogenic insult. (**a**) Schematic representation of the treatment performed in BP-tdTomato and BP-tdTomato/Prrx1^{cKO} mice in which hair follicle samples were analysed. (**b**) Representative images of immunolabeling for SNAI1 (white) in BP-hair follicles (HF) in anagen from BP-tdTomato and BP-tdTomato/Prrx1^{cKO} mice. tdTomato^{+} cells labelled in red. Yellow arrowheads indicate SNAI1 expression in tdTomato^{+} cells. (**c**) Graph showing percentages of SNAI1^{+}/tdTomato^{+} of total tdTomato^{+} cells in the bulb of the hair follicle (HF) in anagen in samples from BP-tdTomato (11.19%) and BP-tdTomato/Prrx1^{cKO} (24.65%) mice (n=6, n=4). Data are represented by Mean ± SEM and statistically significant differences are tested by unpaired two-tailed Mann-Whitney test. Each dot represents one animal (* = $p < 0.05$, ** = $p < 0.01$, *** = $p < 0.001$, **** = $p < 0.0001$). Scale bars: 25µm. Illustrations created with BioRender.com.

8.3 Role of Snai1 in melanoma initiation

As an increase in Snai1 expression is associated to melanomagenesis, we next investigated whether Snai1 have a role in melanoma initiation. Snai1 is linked to different cellular programs related to tumorigenesis, metastasis and resistance to therapies across several cancer types.(Kaufhold & Bonavida, 2014; Qing et al., 2023; Tsirigoti et al., 2022). Interestingly, it has also been reported to enhance stemness properties and tumour initiating capacities in epithelial cancers (Mani et al., 2008; Morel et al., 2008). However, whether Snai1 contributes to melanoma initiation is unknown.

As shown previously, our data indicates that Snai1 expression is detected in tdTomato$^+$ cells during anagen phase in the hair bulb in both homeostatic and oncogenic contexts, as analysed in the Tyr$^+$-tdTomato (**Figure 7**) and the BP-tdTomato (**Figure 8**), respectively.

We next investigated whether Snai1 is expressed in tumours (**Figure 16a**). Analysis of early melanomas arising in the BP-tdTomato model detected 1% SNAI1$^+$/TdTomato$^+$ cells (n=7) (**Figure 16b left**). Further, at late tumour stages, immunolabeling for Snai1 detected nearly zero SNAI1$^+$/TdTomato$^+$ melanoma cells within all analysed tumours (n=3) (**Figure 16b right**). Number of SNAI1$^+$/TdTomato$^+$ cells in the hair follicles and melanomas at different stages is shown in **Figure 16c**.

Altogether, these results suggest that Snai1can be expressed in melanocytic cells in the hair follicle and its expression is lost as tumour begins to emerge, suggesting that Snai1 may also play a role during melanoma initiation.

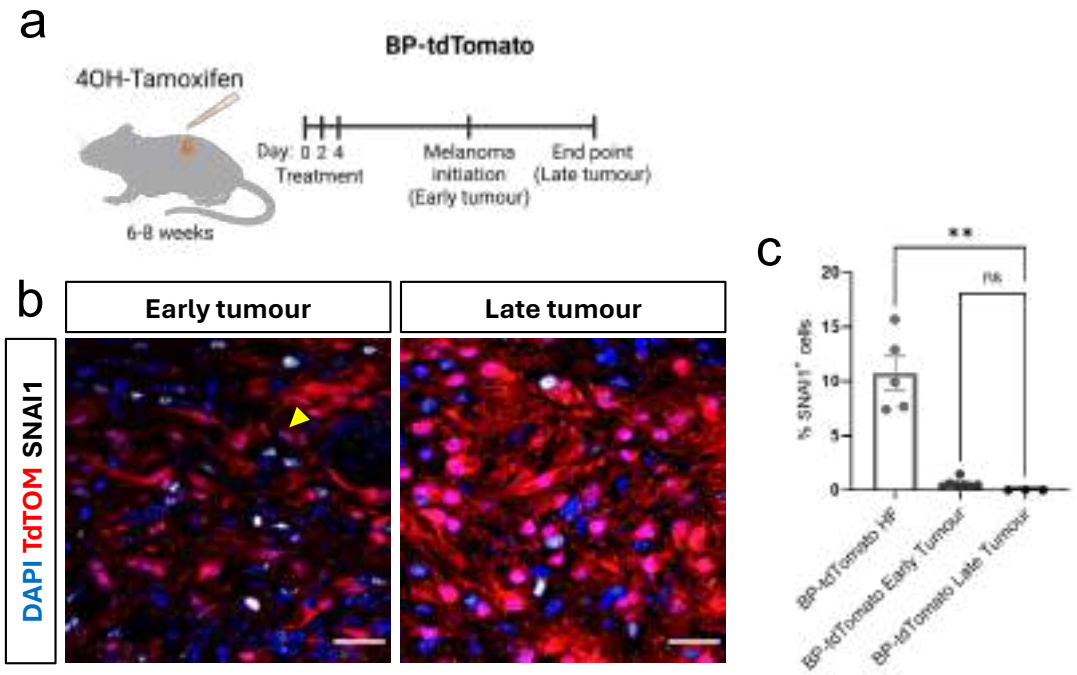

Figure 16. Snai1 expression can be detected in early melanomas. (**a**) Schematic representation of the treatment performed in mice to generate melanomas and the different tumour stages analysed. (**b**) Representative images of immunolabeling for SNAI1 (white) in melanomas from BP-tdTomato mice (tdTomato$^+$ cells labelled in red). Early tumours (2mm width, left) and late tumours (experiment end point, right). Yellow arrowheads indicate SNAI1 expression in tdTomato$^+$ cells. (**c**) Graph showing percentage of SNAI1$^+$/tdTomato$^+$ of total tdTomato$^+$ cells in the bulb of hair follicle (HF) in anagen (n=5), early tumours (n=7) and late tumours (n=3) in BP-tdTomato mouse model. Data are represented by Mean ± SEM and statistically significant differences are tested by unpaired two-tailed Mann-Whitney test. Each dot represents one animal (* = $p < 0.05$, ** = $p < 0.01$, *** = $p < 0.001$, **** = $p < 0.0001$). Scale bars: 25 µm. Illustrations created with BioRender.com.

8.3.1 Generation and validation of loss-of-function of Snai1 melanoma mouse model

To investigate the function of Snai1 in melanoma initiation, we next generated a conditionally activated melanoma reporter murine model with loss-of-function of *Snai1*. This model was generated by crossing our BP-tdTomato mice with the Snai1^{cKO} (*Snai1*$^{loxP/loxP}$) model.

Following the same strategy described in Section 8.2.3 for the validation of the Cre-recombinase, we treated BP-tdTomato and BP-tdTomato/Snai1^{cKO} mice with 4-HT to generate melanomas (**Figure 17a**). These samples were collected and subjected to FACS to isolate tdTomato$^+$ melanoma cells. Sorted cells were used for gDNA extraction and PCR to confirm recombination.

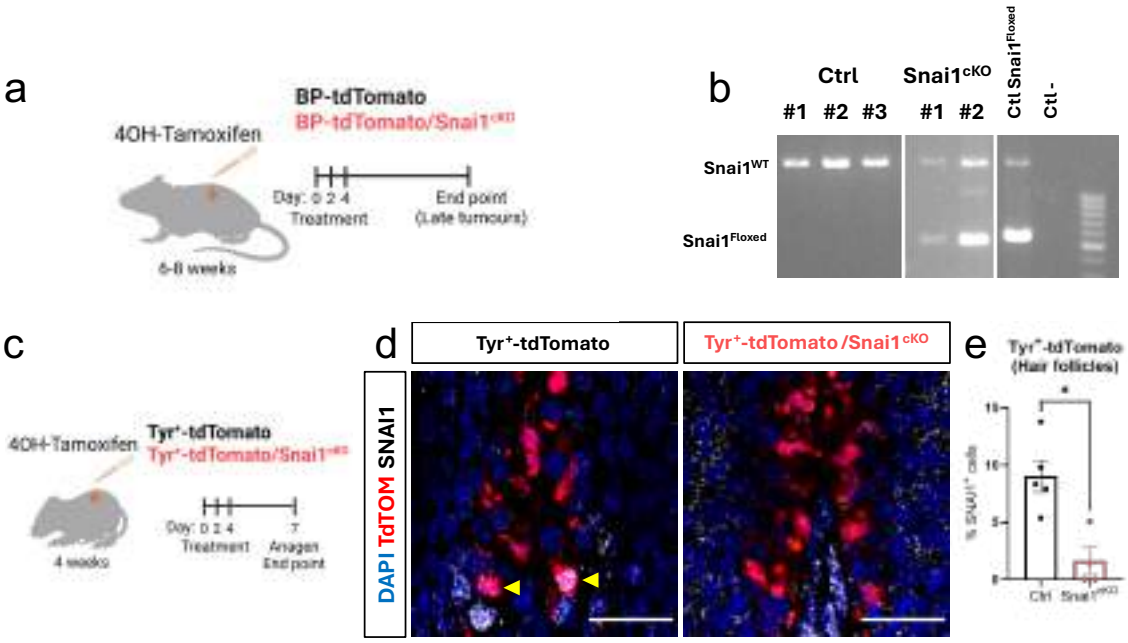

Figure 17. Generation and validation of Snai1 loss-of-function mouse melanoma model. (**a**) Schematic representation of the treatment performed in BP-tdTomato/Snai1^{cKO} mice to generate melanomas. (**b**) DNA gel electrophoresis confirming CRE-ER^{T2}-dependent recombination of Snai1^{loxP} gene, shown by the presence of Snai1^{Floxed} band. Molecular weight marker of 100bp. (**c**) Schematic representation of the treatment performed in Tyr^{+}-tdTomato and Tyr^{+}-tdTomato/Snai1^{cKO} mice in which hair follicle samples were analysed. (**d**) Representative images of immunolabeling for SNAI1 (white) in hair follicles (HF) in anagen from Tyr^{+}-tdTomato and Tyr^{+}-tdTomato/Snai1^{cKO} mice. tdTomato^{+} cells labelled in red. Yellow arrowheads indicate SNAI1 expression in tdTomato^{+} cells. (**e**) Graph showing percentage of SNAI1^{+}/tdTomato+ of total tdTomato^{+} cells in the bulb of the hair follicle (HF) in anagen in samples from Tyr^{+}-tdTomato and Tyr^{+}-tdTomato/Snai1^{cKO} mouse models (n=5, n=4). Data are represented by Mean ± SEM and statistically significant differences are tested by unpaired two-tailed Mann-Whitney test. Each dot represents one animal (* = $p < 0.05$, ** = $p < 0.01$, *** = $p < 0.001$, **** = $p < 0.0001$). Scale bars: 25 µm. Illustrations created with BioRender.com.

Imaging of the gels upon DNA staining and electrophoresis, showed that while control melanoma cells from BP-tdTomato mice showed the presence of the wild type allele (*Snai1*^{WT}), melanoma cells from BP-tdTomato/Snai1^{cKO} tumour present a band corresponding to the recombined allele (*Snai1*^{Floxed}), confirming Cre activity at the Snai1 locus (**Figure 17b**).

To investigate Snai1 depletion at protein level, we moved to hair follicles (**Figure 17c**), where the higher number of SNAI1^{+}/tdTomato^{+} cells could be previously detected (**Figure 7**). Analysis of the hair bulb in anagen confirmed the reduction in the number of SNAI1^{+}/tdTomato^{+} cells in Tyr^{+}-tdTomato/Snai1^{cKO} model compared to control (**Figure 17d, e**).

This data indicates that Cre-recombinase activity is present in our Snai1 loss of function newly generated models, making them suitable for further experiments.

8.3.2 Snai1 depletion delays melanomagenesis

We next investigated the impact of Snai1 depletion in melanoma development. For this, we treated 6-8 weeks BP and BP/Snai1^{cKO} mice with 4-HT and animals were monitored during melanoma progression until end point (**Figure 18a**). Check Materials and methods for further details.

Kaplan-Meier survival plot showed a delay in tumour initiation in BP/Snai1^{cKO} models compared to BP controls, as the mean melanoma-free survival for BP/Snai1^{cKO} mice was 103 days compared to the 94.5 days of BP control mice (**Figure 18b**). However, some of the BP/Snai1^{cKO} mice never developed melanoma, in contrast to BP or BP/Prrx1^{cKO} mice with a 100% melanoma penetrance. Although, no significant differences in the number of tumours between the BP and the BP/Snai1^{cKO} mice were found (**Figure 18c**).

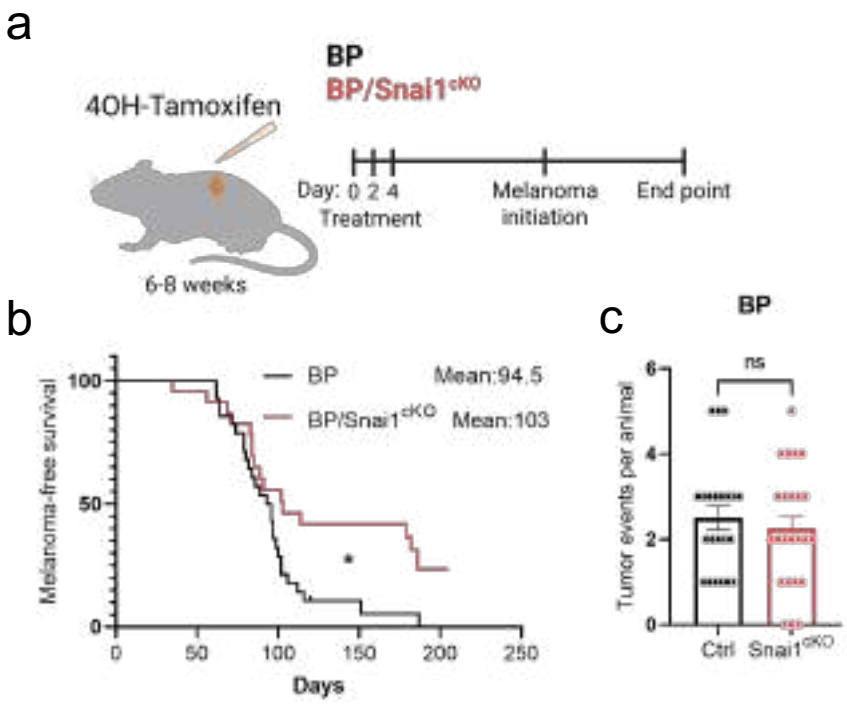

Figure 18. Snai1 depletion delays melanomagenesis. (**a**) Schematic representation of the treatment performed in BP and BP/Snai1^{cKO} mice to generate melanomas. (**b**) Kaplan-Meier plot showing melanoma-free survival since the start of the 4-HT treatment in the BP and BP/Snai1^{cKO} melanoma models (n=28, n=23). (**c**) Quantification of tumours developed in BP and BP/Snai1^{cKO} mice (n=22, n=24). Data are represented by Mean ± SEM and statistically significant differences are tested by unpaired two-tailed Mann-Whitney test. Each dot represents one animal (* = $p < 0.05$, ** = $p < 0.01$, *** = $p < 0.001$, **** = $p < 0.0001$). Illustrations created with BioRender.com.

Additionally, as performed previously and explained in Section 8.2.5, we next analysed BP/Snai1^{cKO} late melanomas (**Figure 19a**). As in tumours from BP/Prrx1^{cKO} mice, haematoxylin-eosin contrast staining showed no major differences at histological level between BP and BP/Snai1^{cKO} melanomas (**Figure 19d left**). Similarly, analysis of the number of KI67^{+} cells (**Figure 19b**, **d middle**) or IBA1^{+} cells (**Figure 19c**, **d right**) in melanomas showed no significant differences between BP and BP/Snai1^{cKO} mice.

All these findings suggest that Snai1 contributes to melanoma initiation.

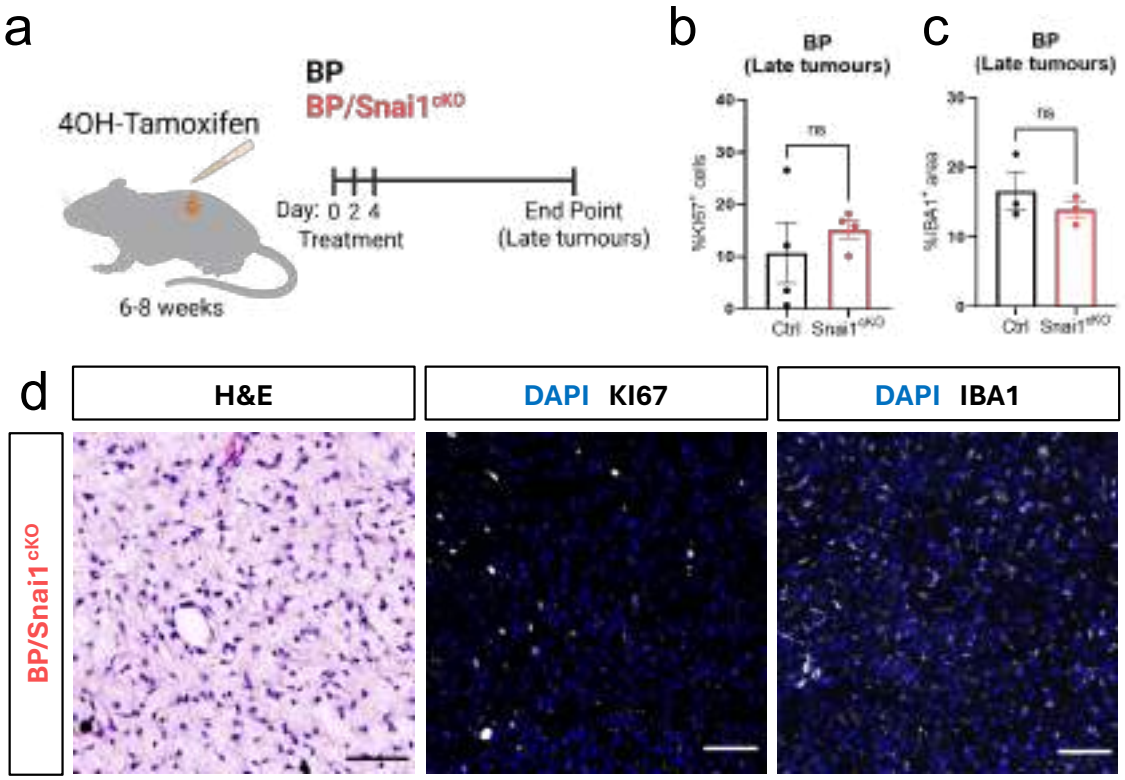

Figure 19. Snai1 depletion does not impact on tumour histopathological characteristics or proliferation. (**a**) Schematic representation of the treatment performed in BP and BP/Snai1^{cKO} mice to generate melanomas. (**b**) Graph showing percentages of KI67^{+} cells in tumour cells in melanomas from BP and BP/Snai1^{cKO} mice. (**c**) Graph showing percentages of IBA1^{+} cells in tumour cells in melanomas from BP and BP/Snai1^{cKO} mouse models. (**d**) Representative images of haematoxylin-eosin (H&E) staining (left), KI67 immunolabeling (white, middle) and IBA1(white, right) in melanomas from BP/Snai1^{cKO} mice. Data are represented by Mean ± SEM and statistically significant differences are tested by unpaired two-tailed Mann-Whitney test. Each dot represents one animal (* = $p < 0.05$, ** = $p < 0.01$, *** = $p < 0.001$, **** = $p < 0.0001$). Scale bars: 50 µm. Illustrations created with BioRender.com.

8.3.3 Loss of Snai1 in melanoma cells does not upregulate Prrx1

As previous research indicate, a mutual inhibitory loop between Prrx1 and Snai1 plays a critical role in embryonic development and some carcinomas (Fazilaty et al., 2019). Our data in the Prrx1^{cKO} mouse model, indicate that this regulatory loop is at least in part, present in melanoma cells, since Prrx1 depletion promotes Snai1 upregulation. Thus, we next investigated whether Prrx1 could also regulate Snai1 expression in melanoma.

To do this, BP-tdTomato and BP-tdTomato/Snai1^{cKO} mice were treated with 4-HT and early melanomas collected (**Figure 20a**). Contrary to what we hypothesised, immunolabeling for PRRX1 in melanoma early tumours showed that the number of PRRX1^{+}/tdTomato^{+} cells in BP-tdTomato/Snai1^{cKO} was very similar to that in BP-tdTomato control mice (**Figure 20b**), as we could not find any statistically significant differences between these tumours (**Figure 20c**).

We also compared Prrx1 expression in hair follicles from Tyr^{+}-tdTomato and Tyr^{+}-tdTomato/Snai1^{cKO} mice (**Figure 20d**). In line with the situation in early melanomas, immunolabeling for PRRX1 in hair bulbs in anagen showed no significant changes in the number of PRRX1^{+}/tdTomato^{+} cells in both models (**Figure 20e, f**).

These results indicate that Snai1 downregulation does not impact on Prrx1 expression in melanocytic cells *in vivo*.

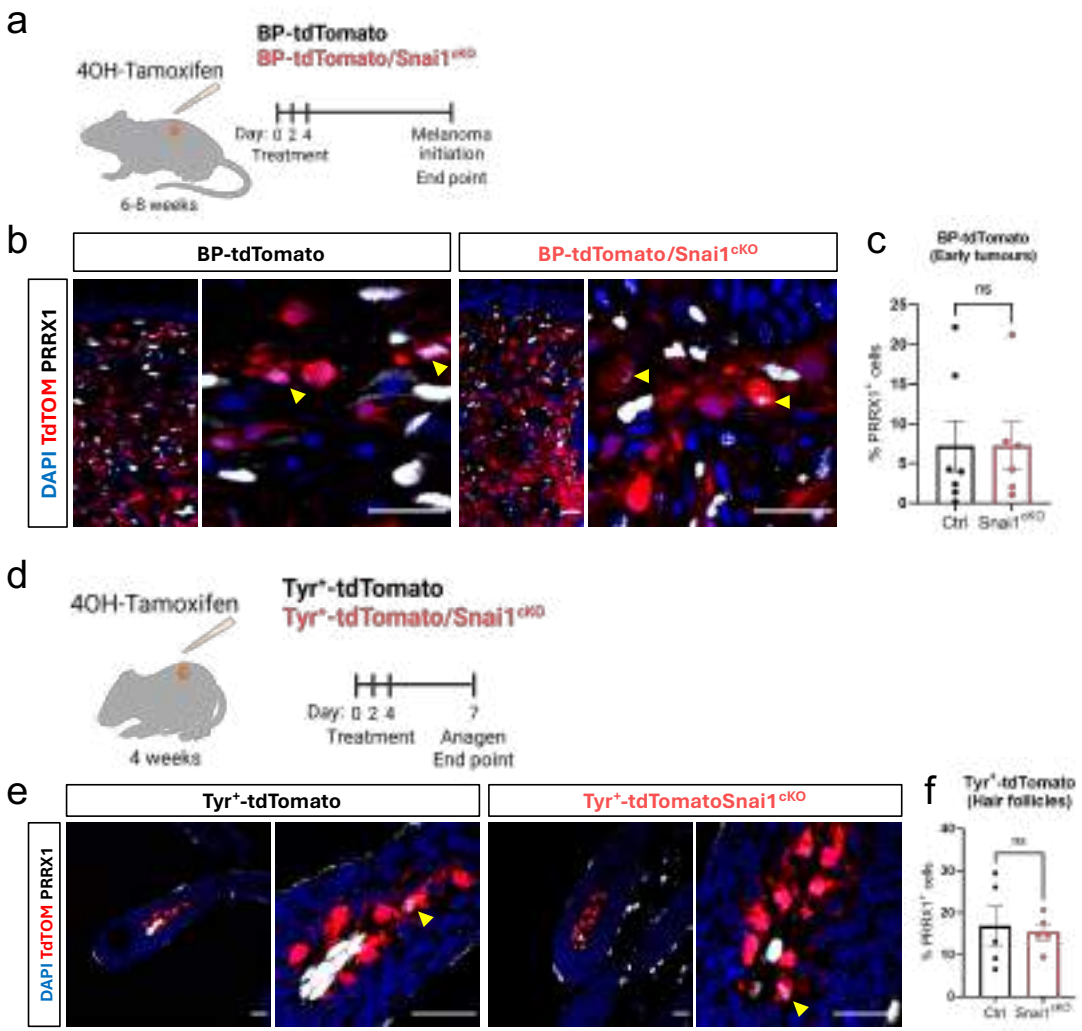

Figure 20. Loss of Snai1 in melanoma cells does not upregulate Prrx1. (**a**) Schematic representation of the treatment performed in BP-tdTomato and BP-tdTomato/Snai1^{cKO} mice to generate early melanomas. (**b**) Representative images of immunolabeling for PRRX1 (white) in early melanomas from BP-tdTomato and BP-tdTomato/Snai1^{cKO} mice (tdTomato$^+$ cells labelled in red). Yellow arrowheads indicate PRRX1 expression in tdTomato$^+$ cells. (**c**) Graph showing percentages of PRRX1$^+$/tdTomato$^+$ cells of total tdTomato$^+$ cells in early tumours on BP-tdTomato and BP-tdTomato/Snai1^{cKO} mouse models (n=6, n=5). PRRX1$^+$/tdTomato$^+$ melanoma cells appear in BP-tdTomato and BP-tdTomato/Snai1^{cKO} melanoma tumours in a similar proportion. (**d**) Schematic representation of the treatment performed in Tyr$^+$-tdTomato and Tyr$^+$-tdTomato/Snai1^{cKO} mice in which hair follicle samples were analysed. (**e**) Representative images of immunolabeling for PRRX1 (white) in hair follicles (HF) in anagen from Tyr$^+$-tdTomato and Tyr$^+$-tdTomato/Snai1^{cKO} mice. tdTomato$^+$ cells labelled in red. Yellow arrowheads indicate PRRX1 expression in tdTomato$^+$ cells. (**f**) Graph showing percentages of PRRX1$^+$/tdTomato$^+$ of total tdTomato$^+$ cells in the bulb of the hair follicle (HF) in anagen in samples from Tyr$^+$-tdTomato and Tyr$^+$-tdTomato/Snai1^{cKO} mice (n=5, n=5). Data are represented by Mean ± SEM and statistically significant differences are tested by unpaired two-tailed Mann-Whitney test. Each dot represents one animal (* = $p < 0.05$, ** = $p < 0.01$, *** = $p < 0.001$, **** = $p < 0.0001$). Scale bars: 25 µm. Illustrations created with BioRender.com.

8.4 Analysis of Prrx1 and Snai1 in melanocytes *in vitro*

Our animal experiments show a role of Prrx1 and Snai1 in melanoma initiation. To investigate in more detail these cell-intrinsic regulatory mechanisms we next moved to an *in vitro* context.

8.4.1 Prrx1 to Snai1 repressive axis in melanocytes *in vitro*

Our *in vivo* experiments showed that melanoma onset was accelerated and enhanced in a loss-of-function of Prrx1 context, which may be induced by an increase in Snai1 expression in melanocytic cells. To confirm that Prrx1 is repressing Snai1, we next used the immortalized murine melanocyte cell line Melan-a.

As mentioned previously, it has been shown that the EMT-TFs Prrx1 and Snai1 can function as part of a mutually repressive regulatory loop in embryonic development, adult injured tissues and carcinomas (Fazilaty et al., 2019; Youssef et al., 2024). The regulatory loop proposed in Fazilaty et al., 2019 showed that Prrx1 expression depends on a balance between the direct upregulation by itself and the repression by the EMT-TF Snai1. Interestingly, Snai1 can repress Prrx1 transcription by direct DNA binding in this context. However, Prrx1 attenuates Snai1 transcription by activating the expression of members of the miR-15 miRNA family (**Figure 21a**).

In our *in vivo* melanocytic models, upregulation of Prrx1 upon Snai1 depletion could not be detected (**Figure 20**). However, we found that Prrx1 depletion increased Snai1 expression (**Figure 14**). To investigate this *in vitro*, we transfected Melan-a cells with siRNA against *Prrx1 or Snai1* and checked *Prrx1* and *Snai1* mRNA expression levels by qRT-PCR. We first confirmed efficient downregulation upon transfection in both cases. Critically, we confirmed Snai1 increase after Prrx1 downregulation, but no changes in Prrx1 expression upon Snai1 targeting. By contrast, no differences in Prrx1 expression were found upon Snai1 silencing (**Figure 21b**).

Next, to investigate whether regulation of Snai1 by Prrx1 in melanocytes was regulated by the miR-15 family of miRNA, we performed a short-term inhibition of the *Prrx1* gene by siRNA in Melan-a cells. Upon transfection, samples were collected and processed to obtain mature miRNAs. TaqMan™ probes against the miR-15 family members *Mir15a*, *Mir15b* and *Mir195a* were used to investigate miRNA levels by qPCR. Our results indicate that, upon *Prrx1* downregulation, miR-15 family members expression was reduced in Melan-a cells compared to control (**Figure 21c**).

These results further confirmed that, in contrast to the mutual repressive loop described in other contexts, in melanocytes only Prrx1 regulates Snai1 expression. Interestingly, as described before, Prrx1 downregulation also promotes a decrease in the levels of members of the miR15 family, that have been shown to attenuate Snai1

expression. Further, the presence of this Prrx1-Snai1 regulatory axis helps to explain the increase of Snai1 expression in melanomas from BP-tdTomato/Prrx1^{cKO} mice.

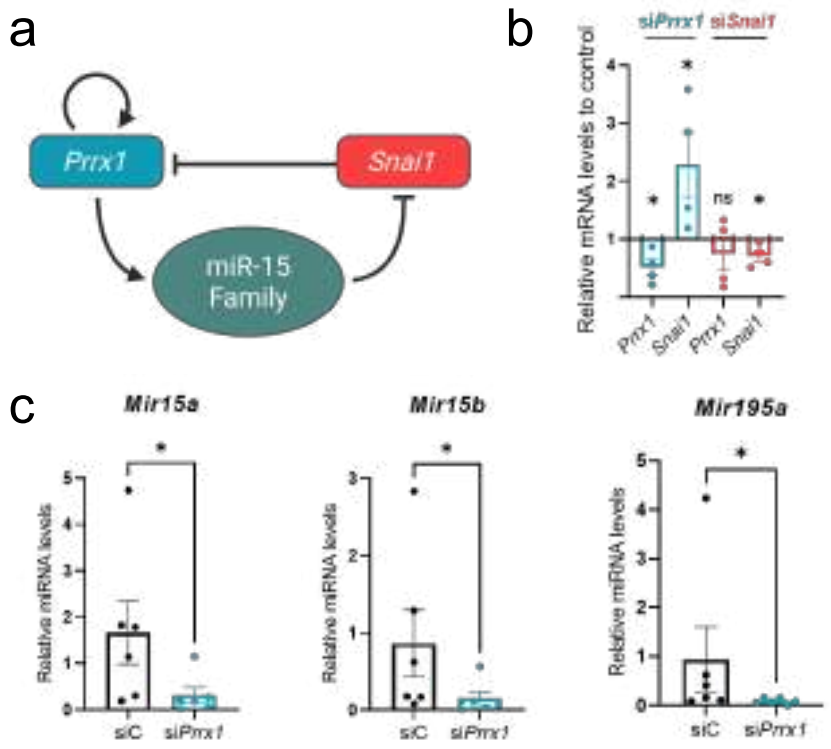

Figure 21. Prrx1 to Snai1 repressive loop in melanocytes *in vitro*. (**a**) Graphical representation of a gene regulatory network highlighting mutual transcriptional inhibition between Prrx1 and Snai1, forming a bidirectional repressive loop, in which members of mir-15 miRNA family are implicated (Fazilaty et al., 2019). (**b**) Relative *Prrx1* and *Snai1* mRNA levels assessed by quantitative RT-PCR in Melan-a cells upon *Prrx1* and *Snai1* siRNA transfection, represented by log2 fold change relative to control (set to 1). Cells were collected 24 hours after transfection. Each dot represents one *in vitro* experiment. (**c**) Analysis of mir-15 family members mRNA levels assessed by quantitative RT-PCR in Melan-a cells upon *Prrx1* siRNA transfection (n=5). Each dot represents one *in vitro* experiment. Data are represented by Mean ± SEM and statistically significant differences are tested by unpaired two-tailed Mann-Whitney test (* = $p < 0.05$, ** = $p < 0.01$, *** = $p < 0.001$, **** = $p < 0.0001$). Illustrations created with BioRender.com.

8.4.2 Prrx1 depletion and Snai1 overexpression increases stem-like properties in melanocytes

As shown above, loss-of-function of *Prrx1* in mouse melanoma models accelerates tumour initiation and increases tumour number. Upon characterization of tumours, we could not detect major changes in histopathological characteristics or proliferation rates. However, we detected an upregulation of *Snai1* expression in early melanoma tumours. Interestingly, Snai1 expression is associated with tumour initiating capabilities and stem-like properties in cancer cells (Cano et al., 2000; Dang et al., 2011; Nieto & Cano, 2012), but the capacity of *Snai1* to induce these effects in melanocytes remains to be elucidated.

To investigate this, we first characterize the ability of Melan-a cells to grow as spheres in soft agar, an experimental approach to investigate stemness and tumour-initiating potential. For this, we transfected Melan-a cells with siRNA against *Prrx1 or Snai1*, that were seeded in soft-agar 24 hours post-transfection.

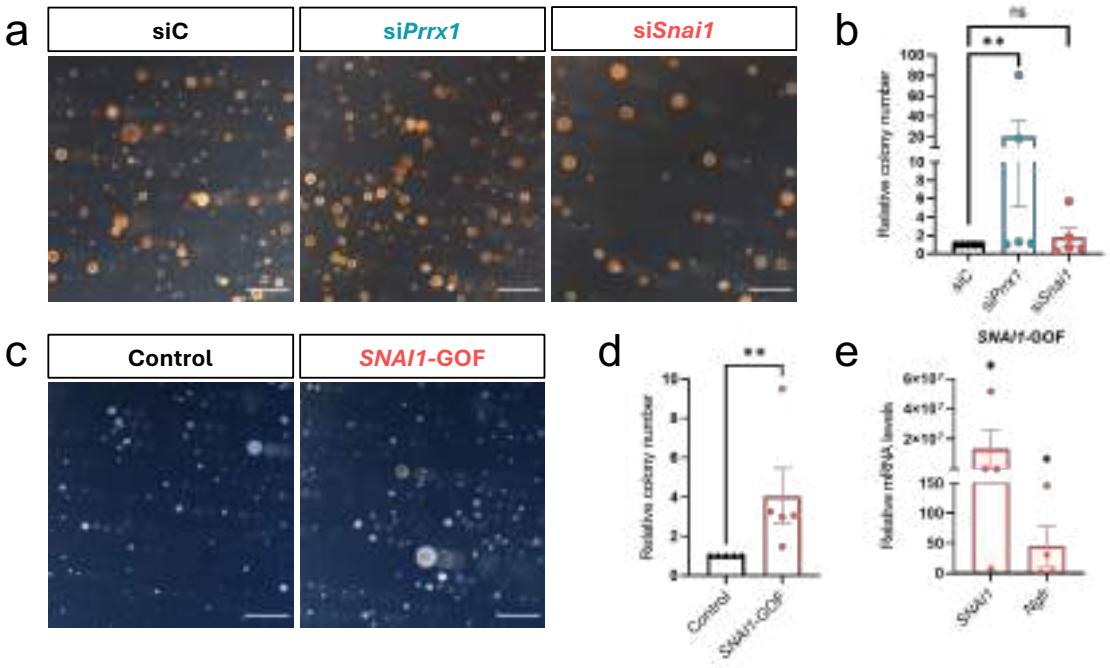

Figure 22. Overexpression of Snai1 and inhibition of Prrx1 increase tumour initiating capabilities in melanocytes *in vitro*. (**a**) Representative images of Melan-a cells grown in soft-agar assay in different conditions (**b**) Quantification of soft-agar colony formation in Melan-a upon transfection with *Prrx1* and *Snai1* siRNAs. Cells were seeded 24 h after transfection. Each dot represents one *in vitro* experiment. Relative colony number has been normalized to mean of controls for each experiment (**c**) Representative images of MelanA cells grown in soft-agar assay upon Snai1 overexpression. Cells were seeded 24 h after transfection. (**d, e**) *SNAI1* and *Ngfr* mRNA levels assessed by quantitative RT-PCR in Melan-a. Data is represented log2 fold change relative to control (set to 1). Cells were collected 24 hours after transfection. Each dot represents one *in vitro* experiment. Data are represented by Mean ± SEM and statistically significant differences are tested by unpaired two-tailed Mann-Whitney test (* = $p < 0.05$, ** = $p < 0.01$, *** = $p < 1$, **** = $p < 0.0001$). Scale bars: 1 mm.

In line with our *in vivo* results, analysis of the number of spheres showed an increase in the spheres upon Prrx1 depletion. In contrast no significant changes in the number of spheres were found upon *Snai1* downregulation (**Figure 22a, b**).

To confirm that the mechanism by which Prrx1 downregulation increases the number spheres could be mediated by Snai1 upregulation, we next assessed whether *Snai1* expression was sufficient to enhance tumour initiating capabilities in untransformed melanocytic cells. To do this, we overexpressed *SNAI1* gene in Melan-a cells. Analysis of the ability of Melan-a to generate spheres in soft agar, showed an increase in the number of spheres in *SNAI1* overexpressing Melan-a cells compared to control (**Figure 22c, d**). This increase in sphere-forming abilities was accompanied by an

increase in *Ngfr* mRNA levels, a well stablished melanoma stemness marker (Boiko et al., 2010; Redmer et al., 2014), in the *SNAI1*-GOF condition compared to control (**Figure 22e**).

These results suggest that an increase in *Snai1* expression levels in melanocytes is sufficient to induce an increase in their ability to form spheres and stem-like properties.

8.5 Prrx1 silencing accelerates melanoma formation through Snai1 expression

Our results in experiments *in vivo* and *in vitro* indicate that Prrx1 could be acting as a protective factor by repressing Snai1 expression during melanoma development. When Prrx1 is downregulated, Snai1 enhanced expression may increase tumour initiating capacities and stemness properties of melanocytic cells, thus leading to acceleration of tumour initiation and increase in tumour number.

To confirm this, and to investigate whether acceleration in melanomagenesis and increased number of tumours upon Prrx1 depletion could be reverted by blocking Snai1 expression, we generated a BP/Snai1^{cKO}/Prrx1^{cKO} model. These animals were treated 6-8 weeks post birth and monitored (**Figure 23a**).

Kaplan-Meier survival plot showed that the mean melanoma-free survival for BP/Snai1^{cKO}/Prrx1^{cKO} mice was 84 days, very similar to the BP mice, thus rescuing the Prrx1 depletion phenotype (**Figure 23b**).

Further, analysis of the number of tumours generated in the BP/Snai1^{cKO}/Prrx1^{cKO} model (mean = 3.5) showed no statistically significant differences compared to control BP animals (**Figure 23c**).

As done previously, we also investigated histopathological changes (**Figure 23d left**), proliferation rates (**Figure 23d middle, e**) and myeloid infiltration (**Figure 23d right, f**) in melanomas from BP/Snai1^{cKO}/Prrx1^{cKO}. Again, no major differences were found when compared with BP mice.

These findings indicate that Prrx1 regulation of melanomagenesis is driven by Snai1 expression.

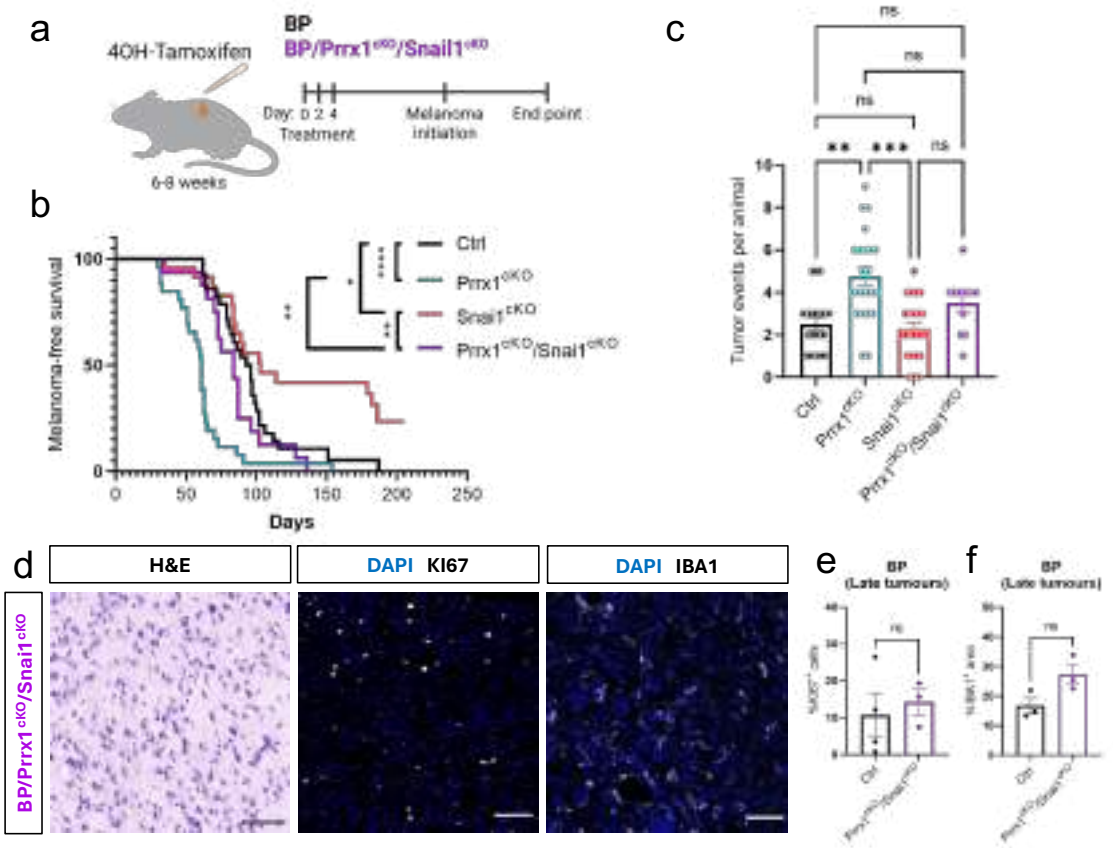

Figure 23. Prrx1 silencing accelerates melanoma formation through Snai1 expression. (**a**) Schematic representation of the treatment performed in BP and BP/Prrx1^{cKO}/Snai1^{cKO} mice to generate melanomas. (**b**) Kaplan-Meier plot showing melanoma-free survival since the start of the 4-HT treatment in BP, BP/Prrx1^{cKO}, BP/Snai1^{cKO} and BP/Prrx1^{cKO}/Snai1^{cKO} melanoma models (n=28, n=27, n=23, n=15). (**c**) Quantification of tumour-events number in BP, BP/Prrx1^{cKO}, BP/Snai1^{cKO} and BP/Prrx1^{cKO}/Snai1^{cKO} melanoma models (n=22, n=23, n=24, n=12). (**d**) Representative image of haematoxylin-eosin (H&E) staining (left) and immunolabeling from Ki67 (white, middle) and IBA1 (white, right) in melanomas from BP/Prrx1^{cKO}/Snai1^{cKO} mice. (**e**) Graph showing percentages of KI67^{+} cells in tumour cells in melanomas from BP and BP/Prrx1^{cKO}/Snai1^{cKO} mice. (**f**) Graph showing percentages of IBA1^{+} cells in tumour cells in melanomas from BP and BP/Prrx1^{cKO}/Snai1^{cKO} mice. Data are represented by Mean ± SEM and statistically significant differences are tested by unpaired two-tailed Kruskal-Wallis or Mann-Whitney test. Each dot represents one animal (* = $p < 0.05$, ** = $p < 0.01$, *** = $p < 0.001$, **** = $p < 0.0001$). Scale bars: 50 µm. Illustrations created with BioRender.com.

9 Discussion

Melanoma represents one of the most aggressive and therapy-resistant forms of skin cancer, which originates in melanocytes, pigment-producing cells derived from the neural crest during embryo development (Centeno et al., 2023). While early-stage melanomas are potentially curable via surgical excision, advanced disease remains clinically challenging due to its high metastatic potential and marked phenotypic heterogeneity (Davis et al., 2019; Garbe et al., 2022). During the last decades, we have witnessed significant advances in the understanding of melanoma molecular drivers (Shain & Bastian, 2016), but the precise mechanisms that govern melanoma initiation and the earliest transformation of melanocytes into malignant cells, remain incompletely understood.

One critical aspect emerging from recent studies is the notion that melanoma initiation is not only genetically driven but tightly regulated by the differentiation state and plasticity of the cell of origin. Melanocyte stem cells (MSC), transit-amplifying (TA) cells and even differentiated melanocytes have been implicated in transformation events under specific oncogenic and microenvironmental conditions (Baggiolini et al., 2021; Köhler et al., 2017; Q. Sun et al., 2019). This plasticity is particularly evident in melanoma due to its neural crest origin and lineage program flexibility (Rambow et al., 2018; Wouters et al., 2020). Recent findings indicate that this melanoma plasticity can be modulated by dynamic changes in the expression of EMT-TFs, with most evidence supporting a switch from Zeb2/Snail2 expressing proliferative cells towards Zeb1/Twist1 expressing invasive melanoma cells (Caramel et al., 2013; Vandamme et al., 2020). In fact, in the hair follicle during anagen, melanocytes located in the lower portion of the hair bulb, committed to differentiation and melanin production, express Zeb2, that in this case is responsible for maintaining their differentiated state (Denecker et al., 2014). Here we show that Prrx1 and Snail 1 can also be expressed in the hair follicle and a novel transcriptional switch from Prrx1 to Snail1 that triggers melanoma initiation.

Our analyses of hair follicles indicate that Prrx1 and Snail1 are expressed during anagen in melanocytic cells in the hair bulb compartment. After years of controversy, the ability of MSCs in mouse hair follicles to generate melanomas is accepted (Moon et al., 2017; Q. Sun et al., 2019). Interestingly, adult stem cells in mammalian tissues have been described as stationary cells, residing within specialized microenvironments known as niches. Within these niches, they generate transiently proliferative progenitor cells, commonly referred to as transit-amplifying cells, which subsequently migrate and differentiate to maintain tissue homeostasis. MSCs were classically thought to behave like this, residing in a defined region of the hair follicle comprising the bulge and the hair germ. From this location, they were believed to give

rise to melanocytes that migrate to the follicular base during the anagen phase of the hair cycle to facilitate pigmentation. Briefly, in anagen, when hair growth begins, MSCs move downwards towards the base of the hair follicle. During this movement, this transient-amplifying population begin to differentiate and express gene markers characteristic of melanocytes, such as pigmentation genes (Schneider et al., 2009; Q. Sun et al., 2023). However, very recently, lineage tracing and intravital imaging approaches to monitor individual MSCs in single hair follicles, revealed that these cells can reverse this program, dedifferentiating back to MSCs in the bulge. From the bulge, they can later re-enter the hair germ or differentiate into mature melanocytes in the hair bulb (Sun et al., 2023), showing that MSCs behave differently from adult stem-cell populations described previously.

Prrx1 or Snail1 expression could mostly be detected in the hair bulb in anagen, which is the location where MSCs that have initiated the differentiation process transform into mature, functional melanocytes responsible for hair pigmentation. However, the ability of MSCs to fully reverse differentiation, indicates that MSCs are a highly dynamic plastic population. Moreover, the mechanisms by which intermediate MSCs choose their final fate are not yet understood highlighting the complexity and heterogeneity of melanocytic cells in the hair follicles and the need for robust clonal lineage tracing experiments to characterize in what specific populations Prrx1 and Snail1 are expressed.

Interestingly, single cell transcriptional analyses have linked the expression of Prrx1 with MSCs programmes in human samples (Belote et al., 2021). Other transcriptional analyses in MSCs detected Snail1 as a differentially expressed gene in different MSCs subpopulations during telogen (Joshi et al., 2019), linking Snail1 expression with stem cell maintenance in the melanocytic lineage, compatible with our *in vitro* results. Although we could not detect Snail1 at protein level at telogen stages, its expression could be not sufficient for immunolabeling detection, thus indicating that further analyses are needed.

Previous studies in melanoma suggest that, during earlier stages of melanocyte transformation, EMT-TFs expression appear to transition from Zeb2 expressing differentiated melanocytes towards Zeb1 expressing invasive and dedifferentiated melanoma (Caramel et al., 2013; Denecker et al., 2014; Durand et al., 2024). This expression switch seems to be maintained during primary tumour progression, but can be reverted upon metastatic colonization (Denecker et al., 2014). However, in contrast to Zeb1 expression found in early and late tumours, Snail1 and Prrx1 were detected only during the earliest stages of melanoma. This implies that these transcription factors may be involved in the early transformation of melanocytes but are dispensable or actively repressed in later tumour progression. In our mouse melanoma model. PRRX1^{+} melanoma cells were mostly localized in interfollicular

areas close to epidermal cells, under the basal lamina of epidermis, or adjacent to the hair follicle outer root sheath. Interestingly, in line with our mouse models, we also detected PRRX1^{+} /HMB45^{+} cells in human early melanomas at similar anatomical sites,

Critically, we have found that Prrx1 loss accelerates melanoma development. At first, we hypothesized that this could be mediated by an increase in the proliferation rate in the tumours. Even though we could not detect Snail1 and rarely Prrx1 expression in melanoma cells in late tumours, there is a possibility that their expression levels are so low that could not be detected at protein level (Fazilaty et al., 2019). Some studies in xenografts and *in vitro* suggest that Prrx1 downregulation in melanoma modify cells towards a more proliferative/melanocytic state, and that Prrx1 knock-down also drives a reduction in Snail1 expression (Ferreres et al., 2024), but these results were obtained in melanoma cell lines that behave differently from our *in vivo* transgenic models were no differences in the proliferation of tumour cells were found. Further, as EMT have been associated with inflammation and macrophages in tumours (Y. Guo et al., 2021; Hsu et al., 2014; Johansson et al., 2015; Youssef et al., 2024), we also checked whether the infiltration of myeloid cells was altered upon Prrx1 depletion. However, this could not be detected in our tumours.

Interestingly, further analysis of the tumours showed that in line with the previously described repressive loop (Fazilaty et al., 2019), Prrx1 loss induces Snail1 expression in melanoma cells. As described above, we found that Prrx1 was present in the hair bulb compartment, where transient-amplifying and differentiated melanocytes are located. These melanocytic cells are dividing and transitioning towards a differentiated state, even though they retain plasticity and can de-differentiate. (Q. Sun et al., 2023). Previous studies in BP mice showed that melanoma onset in the hair follicle arise during anagen phase, as MSCs exits the quiescent state (Q. Sun et al., 2019), but this process could be induced by UV-radiation independently of the stage of the hair follicle, as MSCs get activated in response to UV stress (Moon et al., 2017). As occurs with UV radiation, in our Prrx1 loss-of-function models transition from Prrx1 towards Snail1 expression may induce a similar activation, leading to melanoma initiation independently of hair cycle stage. In addition, UV-stress activation of MSCs and translocation to the epidermis seems to be mediated by inflammatory mechanisms (Moon et al., 2017), and Snail1 expression has been linked to the regulation of inflammation in carcinomas (Youssef et al., 2024). This suggests that Snail1 besides from increasing the probability of melanomagenesis by enhancing the stem cell-like potential in melanocytic cells as shown in our *in vitro* experiments, may be inducing similar activation patterns as UV-dependent inflammation in MSCs. However, to confirm this hypothesis, further experiments are necessary.

A major difficulty when studying the role of EMT-TFs in cancer and, particularly how they regulate tumour cells biology, is their wide expression in different populations from the tumour microenvironment. That is the reason we decided to generate a reporter melanoma mouse model in which melanoma cells are labelled in red. Using this model, we found that in late melanomas Prrx1 and Snail1 expression was very rarely detected in tumour cells but was very abundant in a big proportion of cells in the tumour microenvironment. These results are compatible with available transcriptional analyses of human melanoma samples, that suggested that Prrx1 and Snail1 were expressed in advanced melanomas; However, those analyses were unable to discriminate Prrx1 or Snail1 expression in melanoma or stromal cells. Taking advantage of these datasets, some studies indicate that Prrx1 in melanoma is linked to survival in patients (Ferreres et al., 2024). However, another study describes that Prrx1 expression in cancer-associated fibroblasts enhances myofibroblast functions leading to increased tumorigenicity and aggressiveness (Lee et al., 2022). Thus, Prrx1 levels in the stroma could also influence survival in patients. This highlights the need to characterize in more detail in which cell populations Prrx1 is expressed in patients, as our characterization of late melanomas indicate that the majority of Prrx1 expression comes from stromal cells.

Additionally, other studies in established melanomas from Nras-mutant mice suggested that a population of melanoma cells that expresses Prrx1 could be responsible for metastatic dissemination (Karras et al., 2022), compatible with other studies in carcinomas (Ocaña et al., 2012) and in melanoma (Ferreres et al., 2024). The mouse model used for this study carries a Cre-ER coupled to the GFP gene under the control of the Prrx1 promoter, a Nras-mutant construct under the control of the Tyr promoter and a tdTomato gene with loxP-flanked Stop codon that is ubiquitously expressed. Prrx1-expressing cells are labelled in green, and under tamoxifen treatment, these cells begin to express tdTomato and can retain this expression at the protein level even if Prrx1 is downregulated. Critically, this model is unable to discriminate stromal from melanoma cells. Even though some of the Prrx1 expressing cells may be melanoma and are compatible with our results, this data raises the possibility that the Prrx1-expressing cells identified in this study in late melanomas by tdTomato expression, may be derived from cells that have expressed Prrx1 at earlier stages, indicating that Prrx1 may not be a specific marker for melanoma metastatic dissemination.

The EMT-TFs follow a hierarchical regulatory mechanism during EMT induction, being Snail1 a promoter of this process though transcriptional repression of epithelial markers (Nieto et al., 2016; Youssef & Nieto, 2024), leading to progression of cell state towards a mesenchymal state, that is controlled by Prrx1 expression (Youssef et al., 2024). Among the regulatory loops that fine tune the regulation and maintenance of EMT-TFs, the Prrx1/Snail1 mutual repressive loop is responsible for maintaining

distinct subpopulations with the leading expression of one or the other (Fazilaty et al., 2019; Youssef et al., 2024).

From our *in vitro* results in Melan-a cells, we detected the expression of miR-15 family members, microRNAs responsible for Snail1 transcriptional attenuation, (Fazilaty et al., 2019). When Prrx1 is downregulated, miR-15 members are also downregulated, which is compatible with the activation of Snail1 expression in melanocytic cells observed in our *in vitro* and *in vivo* experiments. Interestingly, upregulation of Snail1 was confirmed upon Prrx1 knock-down in Melan-a cells but downregulation of Snail1 did not enhance Prrx1 expression in *in vivo* nor *in vitro* experiments, contrary to what has been described in other models. Interestingly, in Fazilaty et al., 2019, members of the TGF-β superfamily were the signal inducing Snail1 and Prrx1 expression. However, our preliminary data indicates that Melan-a cells do not respond to TGF-β as epithelial cells do, and Snail1 or Prrx1 expression levels did not change (not shown). Additional experiments including the analysis of different TGF-β receptors could help to understand the differences found in this mutually repressive loop in the different contexts.

In our mouse models, Prrx1 depletion leads to increase of Snail1 expressing melanocytic cells. Critically, the acceleration in the ability of melanocytic cells to generate melanomas and the higher number of tumours upon Prrx1 depletion is abrogated when Snail1 upregulation is blocked, supporting that this is the mechanism by which Prrx1 loss promote melanomagenesis. As mentioned, Snail1 promote stemness in different contexts (Dang et al., 2011; W. Guo et al., 2012; Nieto et al., 2016). As such, an enhancement in the stem cell-like potential in melanocytes could explain increased melanomagenesis. Compatible with this, in Snai1^{cKO} models, this potentiality is reduced, since melanoma initiation is delayed by Snail1 depletion. Furthermore, using Melan-a cells, we confirmed that Prrx1 downregulation or Snail1 overexpression increases sphere forming capabilities of these cells. Additionally, Snail1 overexpression induced an increase in *Ngfr* expression levels, a marker related to stemness acquisition and therapy resistance in melanoma (Boiko et al., 2010; Redmer et al., 2014). Thus, our results *in vitro* support the notion that Snail1-dependent acquisition of stemness capabilities is responsible for the phenotype of increased tumorigenesis upon Prrx1 depletion in melanoma models.

In this study, we describe a novel Prrx1/Snail1 switch in melanoma development, responsible for accelerating tumour initiation and increased propensity to tumour formation (**Figure 24**). Prrx1 and Snail1 expression are present in melanocytic cells in the hair bulb compartment during anagen phase, and in early melanomas, but this expression is lost as tumour progresses. Furthermore, our findings indicate that Prrx1 acts as a melanoma suppressor, as it attenuates Snail1 expression and this is

mediated at least in part by miR-15 family members, restraining melanoma cells from acquiring enhanced stemness properties from Snail1 activity.

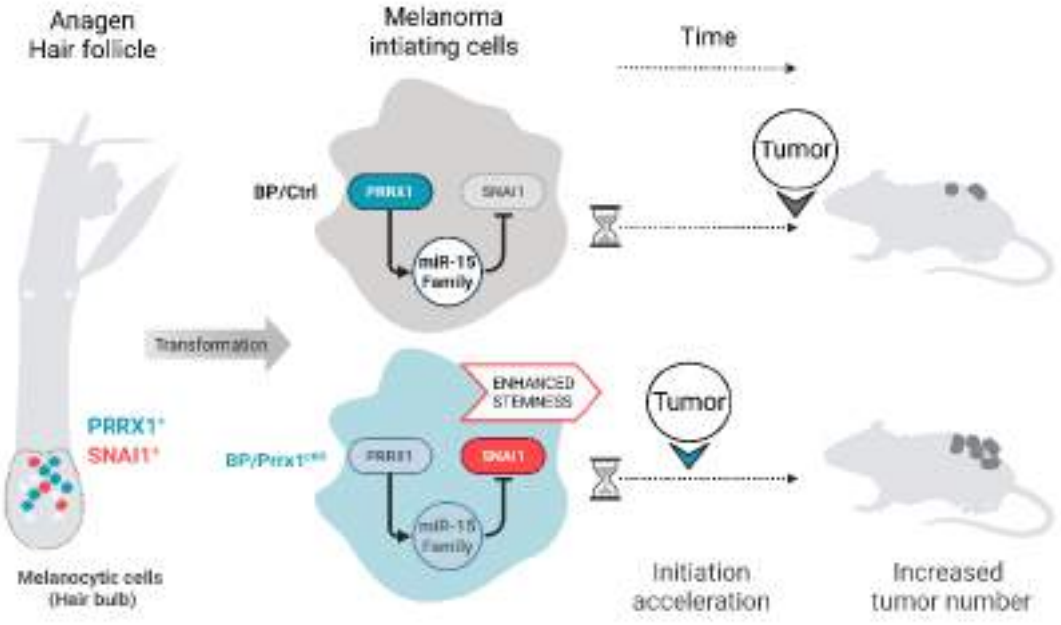

Figure 24. Schematic illustration of the key findings in the Prrx1/Snail1 expression switch during melanoma initiation. Briefly, melanocytic cells in the hair bulb express Prrx1 and Snail1 during anagen phase. Upon transformation, this expression is retained briefly and lost as tumour progresses. Upon Prrx1 downregulation, Snail1 attenuation through miR-15 family is impaired, enhancing stemness capabilities of melanocytic cells, thus accelerating tumour initiation and increasing tumour number.

10 Conclusions

1. **Prrx1 and Snail1 are expressed in melanocytic cells of the hair follicle during the anagen phase**, both under physiological (homeostatic) conditions and in the presence of oncogenic mutations.
2. During melanoma development, both **Prrx1 and Snail1 are transiently expressed in early tumour stages**, but their expression is **progressively lost as the tumour progressed**.
3. **Prrx1 depletion accelerates melanoma onset and increases tumor number**, without significantly affecting cell proliferation.
4. **Loss of Prrx1 results in upregulation of Snail1**, confirming a regulatory relationship between these two EMT-TFs. However, Snail1 depletion does not alter Prrx1 expression, indicating the presence of a unidirectional regulatory axis.
5. Prrx1 downregulation leads to decreased expression of microRNAs belonging to the miR-15 family, suggesting that **Prrx1 may supress Snail1 levels indirectly through miR-15-mediated post-transcriptional regulation**.
6. **Snail1 overexpression is sufficient to induce tumour-initiating traits in non-transformed melanocytic cells**. This supports its potential role as a driver of early melanomagenesis.
7. **Simultaneous deletion of Prrx1 and Snail1 rescues the accelerated tumor phenotype observed in Prrx1-deficient models**, confirming that the pro-tumorigenic effect of Prrx1 loss is mediated by Snail1. This genetic interaction highlights the functional relevance of the Prrx1–Snail1 axis in melanoma initiation.

11 Conclusiones

1. **Prrx1 y Snail1 se expresan en células melanocíticas del folículo piloso durante la fase anágena**, tanto en condiciones fisiológicas (homeostáticas) como en presencia de mutaciones oncogénicas.
2. Durante el desarrollo del melanoma, tanto **Prrx1 como Snail1 se expresan de forma transitoria en las fases tempranas del tumor**, pero su **expresión se pierde progresivamente** a medida que el tumor crece.
3. **La depleción de Prrx1 acelera la aparición del melanoma y aumenta el número de tumores generados**, sin afectar significativamente a la proliferación celular.
4. **La pérdida de Prrx1 induce una sobreexpresión de Snail1**, lo que confirma la regulación reguladora entre estos dos factores de transcripción asociados a EMT. Sin embargo, la pérdida de Snail1 no altera la expresión de Prrx1, lo que indica una regulación unidireccional.
5. La inhibición de Prrx1 reduce la expresión de microARNs que pertenecen a la familia miR-15, lo que sugiere que **Prrx1 podria suprimir los niveles de Snail1 de manera indirecta a través de la regulación postranscripcional mediada por los miembros de la familia miR-15**.
6. **La sobreexpresión de Snail1 es suficiente para inducir características iniciadoras de tumor en células melanocíticas no transformadas**. Esto respalda su potencial como un factor que promueve la melanomagénesis.
7. **La eliminación simultanea de Prrx1 y Snail1 revierte el fenotipo de aceleración del inicio del melanoma observado en los modelos deficientes de Prrx1**, confirmando que el efecto pro-tumoral de la perdida de Prrx1 esta mediado por Snail1. Esta interacción genética resalta la importancia del eje Prrx1-Snail1 en la iniciación del melanoma.

12 Bibliography

Adameyko, I., Lallemend, F., Aquino, J. B., Pereira, J. A., Topilko, P., Müller, T., Fritz, N., Beljajeva, A., Mochii, M., Liste, I., Usoskin, D., Suter, U., Birchmeier, C., & Ernfors, P. (2009). Schwann Cell Precursors from Nerve Innervation Are a Cellular Origin of Melanocytes in Skin. *Cell*, *139*(2), 366–379. https://doi.org/10.1016/j.cell.2009.07.049

Aiello, N. M., & Kang, Y. (2019). Context-dependent EMT programs in cancer metastasis. *Journal of Experimental Medicine*, *216*(5), 1016–1026. https://doi.org/10.1084/jem.20181827

Akbani, R., Akdemir, K. C., Aksoy, B. A., Albert, M., Ally, A., Amin, S. B., Arachchi, H., Arora, A., Auman, J. T., Ayala, B., Baboud, J., Balasundaram, M., Balu, S., Barnabas, N., Bartlett, J., Bartlett, P., Bastian, B. C., Baylin, S. B., Behera, M., … Zou, L. (2015). Genomic Classification of Cutaneous Melanoma. *Cell*, *161*(7), 1681–1696. https://doi.org/10.1016/j.cell.2015.05.044

Arnold, M., de Vries, E., Whiteman, D. C., Jemal, A., Bray, F., Parkin, D. M., & Soerjomataram, I. (2018). Global burden of cutaneous melanoma attributable to ultraviolet radiation in 2012. *International Journal of Cancer*, *143*(6), 1305–1314. https://doi.org/10.1002/ijc.31527

Arozarena, I., & Wellbrock, C. (2019). Phenotype plasticity as enabler of melanoma progression and therapy resistance. *Nature Reviews Cancer*, *19*(7), 377–391. https://doi.org/10.1038/s41568-019-0154-4

Arumi-Planas, M., Rodriguez-Baena, F. J., Cabello-Torres, F., Gracia, F., Lopez-Blau, C., Nieto, M. A., & Sanchez-Laorden, B. (2023). Microenvironmental Snail1-induced immunosuppression promotes melanoma growth. *Oncogene*, *42*(36), 2659–2672. https://doi.org/10.1038/s41388-023-02793-5

Baggiolini, A., Callahan, S. J., Montal, E., Weiss, J. M., Trieu, T., Tagore, M. M., Tischfield, S. E., Walsh, R. M., Suresh, S., Fan, Y., Campbell, N. R., Perlee, S. C., Saurat, N., Hunter, M. V., Simon-Vermot, T., Huang, T.-H., Ma, Y., Hollmann, T., Tickoo, S. K., … White, R. M. (2021). Developmental chromatin programs determine oncogenic competence in melanoma. *Science*, *373*(6559), eabc1048. https://doi.org/10.1126/science.abc1048

Bedogni, B., & Paus, R. (2020). Hair(y) Matters in Melanoma Biology. *Trends in Molecular Medicine*, *26*(5), 441–449. https://doi.org/10.1016/j.molmed.2020.02.005

Belote, R. L., Le, D., Maynard, A., Lang, U. E., Sinclair, A., Lohman, B. K., Planells-Palop, V., Baskin, L., Tward, A. D., Darmanis, S., & Judson-Torres, R. L. (2021). Human melanocyte development and melanoma dedifferentiation at single-cell

resolution. *Nature Cell Biology*, *23*(9), 1035–1047. https://doi.org/10.1038/s41556-021-00740-8

Bennett, D. C., Cooper, P. J., & Hart, I. R. (1987). A line of non-tumorigenic mouse melanocytes, syngeneic with the B16 melanoma and requiring a tumour promoter for growth. *International Journal of Cancer*, *39*(3), 414–418. https://doi.org/10.1002/ijc.2910390324

Blanpain, C., & Sotiropoulou, P. A. (2010). A Dominant Role of the Hair Follicle Stem Cell Niche in Regulating Melanocyte Stemness. *Cell Stem Cell*, *6*(2), 95–96. https://doi.org/10.1016/j.stem.2010.01.006

Boiko, A. D., Razorenova, O. V., van de Rijn, M., Swetter, S. M., Johnson, D. L., Ly, D. P., Butler, P. D., Yang, G. P., Joshua, B., Kaplan, M. J., Longaker, M. T., & Weissman, I. L. (2010). Human melanoma-initiating cells express neural crest nerve growth factor receptor CD271. *Nature*, *466*(7302), 133–137. https://doi.org/10.1038/nature09161

Breslow, A. (1970). Thickness, Cross-Sectional Areas and Depth of Invasion in the Prognosis of Cutaneous Melanoma. *Annals of Surgery*, *172*(5), 902.

Brombin, A., & Patton, E. E. (2024). Melanocyte lineage dynamics in development, growth and disease. *Development*, *151*(15), dev201266. https://doi.org/10.1242/dev.201266

Campbell, N. R., Rao, A., Hunter, M. V., Sznurkowska, M. K., Briker, L., Zhang, M., Baron, M., Heilmann, S., Deforet, M., Kenny, C., Ferretti, L. P., Huang, T.-H., Perlee, S., Garg, M., Nsengimana, J., Saini, M., Montal, E., Tagore, M., Newton-Bishop, J., … White, R. M. (2021). Cooperation between melanoma cell states promotes metastasis through heterotypic cluster formation. *Developmental Cell*, *56*(20), 2808-2825.e10. https://doi.org/10.1016/j.devcel.2021.08.018

Candido-Ferreira, I. L., Lukoseviciute, M., & Sauka-Spengler, T. (2023). Multi-layered transcriptional control of cranial neural crest development. *Seminars in Cell & Developmental Biology*, *138*, 1–14. https://doi.org/10.1016/j.semcdb.2022.07.010

Cano, A., Pérez-Moreno, M. A., Rodrigo, I., Locascio, A., Blanco, M. J., Del Barrio, M. G., Portillo, F., & Nieto, M. A. (2000). The transcription factor Snail controls epithelial–mesenchymal transitions by repressing E-cadherin expression. *Nature Cell Biology*, *2*(2), 76–83. https://doi.org/10.1038/35000025

Caramel, J., Papadogeorgakis, E., Hill, L., Browne, G. J., Richard, G., Wierinckx, A., Saldanha, G., Osborne, J., Hutchinson, P., Tse, G., Lachuer, J., Puisieux, A., Pringle, J. H., Ansieau, S., & Tulchinsky, E. (2013). A Switch in the Expression of Embryonic EMT-Inducers Drives the Development of Malignant Melanoma. *Cancer Cell*, *24*(4), 466–480. https://doi.org/10.1016/j.ccr.2013.08.018

Centeno, P. P., Pavet, V., & Marais, R. (2023). The journey from melanocytes to melanoma. *Nature Reviews Cancer*, *23*(6), 372–390. https://doi.org/10.1038/s41568-023-00565-7

Chan, P. Y., & Corrie, P. G. (2024). Curing Stage IV Melanoma: Where Have We Been and Where Are We? *American Society of Clinical Oncology Educational Book*, *44*(3), e438654. https://doi.org/10.1200/EDBK_438654

Chou, W. C., Takeo, M., Rabbani, P., Hu, H., Lee, W., Chung, Y. R., Carucci, J., Overbeek, P., & Ito, M. (2013). Direct migration of follicular melanocyte stem cells to the epidermis after wounding or UVB irradiation is dependent on Mc1r signaling. *Nature Medicine*, *19*(7), 10.1038/nm.3194. https://doi.org/10.1038/nm.3194

Chudnovsky, Y., Khavari, P. A., & Adams, A. E. (2005). Melanoma genetics and the development of rational therapeutics. *The Journal of Clinical Investigation*, *115*(4), 813–824. https://doi.org/10.1172/JCI24808

Clark, W. H., Elder, D. E., Guerry, D., Epstein, M. N., Greene, M. H., & Van Horn, M. (1984). A study of tumor progression: The precursor lesions of superficial spreading and nodular melanoma. *Human Pathology*, *15*(12), 1147–1165. https://doi.org/10.1016/S0046-8177(84)80310-X

Curti, B. D., & Faries, M. B. (2021). Recent Advances in the Treatment of Melanoma. *New England Journal of Medicine*, *384*(23), 2229–2240. https://doi.org/10.1056/NEJMra2034861

Dang, H., Ding, W., Emerson, D., & Rountree, C. B. (2011). Snail1 induces epithelial-to-mesenchymal transition and tumor initiating stem cell characteristics. *BMC Cancer*, *11*(1), 396. https://doi.org/10.1186/1471-2407-11-396

Dankort, D., Curley, D. P., Cartlidge, R. A., Nelson, B., Karnezis, A. N., Damsky Jr, W. E., You, M. J., DePinho, R. A., McMahon, M., & Bosenberg, M. (2009). BrafV600E cooperates with Pten loss to induce metastatic melanoma. *Nature Genetics*, *41*(5), 544–552. https://doi.org/10.1038/ng.356

Davis, L. E., Shalin, Sara C., & and Tackett, A. J. (2019). Current state of melanoma diagnosis and treatment. *Cancer Biology & Therapy*, *20*(11), 1366–1379. https://doi.org/10.1080/15384047.2019.1640032

Denecker, G., Vandamme, N., Akay, Ö., Koludrovic, D., Taminau, J., Lemeire, K., Gheldof, A., De Craene, B., Van Gele, M., Brochez, L., Udupi, G. M., Rafferty, M., Balint, B., Gallagher, W. M., Ghanem, G., Huylebroeck, D., Haigh, J., Van Den Oord, J., Larue, L., … Berx, G. (2014). Identification of a ZEB2-MITF-ZEB1 transcriptional network that controls melanogenesis and melanoma progression. *Cell Death & Differentiation*, *21*(8), 1250–1261. https://doi.org/10.1038/cdd.2014.44

Díaz-López, A., Moreno-Bueno, G., & Cano, A. (2014). Role of microRNA in epithelial to mesenchymal transition and metastasis and clinical perspectives. *Cancer Management and Research*, *6*, 205–216. https://doi.org/10.2147/CMAR.S38156

Dongre, A., & Weinberg, R. A. (2019). New insights into the mechanisms of epithelial–mesenchymal transition and implications for cancer. *Nature Reviews Molecular Cell Biology*, *20*(2), 69–84. https://doi.org/10.1038/s41580-018-0080-4

Durand, S., Tang, Y., Pommier, R. M., Benboubker, V., Grimont, M., Boivin, F., Barbollat-Boutrand, L., Cumunel, E., Dupeuble, F., Eberhardt, A., Plaschka, M., Dalle, S., & Caramel, J. (2024). ZEB1 controls a lineage-specific transcriptional program essential for melanoma cell state transitions. *Oncogene*, *43*(20), 1489–1505. https://doi.org/10.1038/s41388-024-03010-7

Erdmann, F., Lortet-Tieulent, J., Schüz, J., Zeeb, H., Greinert, R., Breitbart, E. W., & Bray, F. (2013). International trends in the incidence of malignant melanoma 1953–2008—Are recent generations at higher or lower risk? *International Journal of Cancer*, *132*(2), 385–400. https://doi.org/10.1002/ijc.27616

Fazilaty, H., Rago, L., Kass Youssef, K., Ocaña, O. H., Garcia-Asencio, F., Arcas, A., Galceran, J., & Nieto, M. A. (2019). A gene regulatory network to control EMT programs in development and disease. *Nature Communications*, *10*(1), 5115. https://doi.org/10.1038/s41467-019-13091-8

Ferreres, J. R., Vinyals, A., Campos-Martin, R., Espín, R., Podlipnik, S., Ramos, R., Bertran, E., Carrera, C., Marcoval, J., Malvehy, J., Fabregat, I., Puig, S., & Fabra, À. (2024). PRRX1 silencing is required for metastatic outgrowth in melanoma and is an independent prognostic of reduced survival in patients. *Molecular Oncology*, *18*(10), 2471–2494. https://doi.org/10.1002/1878-0261.13688

Filho, A. M., Laversanne, M., Ferlay, J., Colombet, M., Piñeros, M., Znaor, A., Parkin, D. M., Soerjomataram, I., & Bray, F. (2025). The GLOBOCAN 2022 cancer estimates: Data sources, methods, and a snapshot of the cancer burden worldwide. *International Journal of Cancer*, *156*(7), 1336–1346. https://doi.org/10.1002/ijc.35278

Florian Rambow, Rambow, F., Jean-Christophe Marine, Marine, J.-C., Colin R. Goding, & Goding, C. R. (2019). Melanoma plasticity and phenotypic diversity: Therapeutic barriers and opportunities. *Genes & Development*, *33*, 1295–1318. https://doi.org/10.1101/gad.329771.119

Frasier, K., Hash, M. G., Werpachowski, N., & Fritts, H. (2025). The Blind Spots of Artificial Intelligence in Skin Cancer Diagnosis. *Dermis*, *5*(2), 1–7.

Garbe, C., Amaral, T., Peris, K., Hauschild, A., Arenberger, P., Basset-Seguin, N., Bastholt, L., Bataille, V., Marmol, V. del, Dréno, B., Fargnoli, M. C., Forsea, A.-M.,

Grob, J.-J., Höller, C., Kaufmann, R., Kelleners-Smeets, N., Lallas, A., Lebbé, C., Lytvynenko, B., … Lorigan, P. (2022). European consensus-based interdisciplinary guideline for melanoma. Part 1: Diagnostics: Update 2022. *European Journal of Cancer*, *170*, 236–255. https://doi.org/10.1016/j.ejca.2022.03.008

Garbe, C., & Eigentler, T. K. (2007). Diagnosis and treatment of cutaneous melanoma: State of the art 2006. *Melanoma Research*, *17*(2), 117–127. https://doi.org/10.1097/CMR.0b013e328042bb36

Gerdes, J., Schwab, U., Lemke, H., & Stein, H. (1983). Production of a monoclonal antibody mouse reactive with a human nuclear antigen associated with cell proliferation. *International Journal of Cancer*, *31*(1), 13–20. https://doi.org/10.1002/ijc.2910310104

Glover, J. D., Knolle, S., Wells, K. L., Liu, D., Jackson, I. J., Mort, R. L., & Headon, D. J. (2015). Maintenance of distinct melanocyte populations in the interfollicular epidermis. *Pigment Cell & Melanoma Research*, *28*(4), 476–480. https://doi.org/10.1111/pcmr.12375

Gown, A. M., Vogel, A. M., Hoak, D., Gough, F., & McNutt, M. A. (1986). Monoclonal antibodies specific for melanocytic tumors distinguish subpopulations of melanocytes. *The American Journal of Pathology*, *123*(2), 195–203.

Grande, M. T., Sánchez-Laorden, B., López-Blau, C., De Frutos, C. A., Boutet, A., Arévalo, M., Rowe, R. G., Weiss, S. J., López-Novoa, J. M., & Nieto, M. A. (2015). Snail1-induced partial epithelial-to-mesenchymal transition drives renal fibrosis in mice and can be targeted to reverse established disease. *Nature Medicine*, *21*(9), 989–997. https://doi.org/10.1038/nm.3901

Guo, W., Keckesova, Z., Donaher, J. L., Shibue, T., Tischler, V., Reinhardt, F., Itzkovitz, S., Noske, A., Zürrer-Härdi, U., Bell, G., Tam, W. L., Mani, S. A., van Oudenaarden, A., & Weinberg, R. A. (2012). Slug and Sox9 Cooperatively Determine the Mammary Stem Cell State. *Cell*, *148*(5), 1015–1028. https://doi.org/10.1016/j.cell.2012.02.008

Guo, Y., Lu, X., Chen, Y., Rendon, B., Mitchell, R. A., Cuatrecasas, M., Cortés, M., Postigo, A., Liu, Y., & Dean, D. C. (2021). Zeb1 induces immune checkpoints to form an immunosuppressive envelope around invading cancer cells. *Science Advances*, *7*(21), eabd7455. https://doi.org/10.1126/sciadv.abd7455

Gupta, P. B., Kuperwasser, C., Brunet, J.-P., Ramaswamy, S., Kuo, W.-L., Gray, J. W., Naber, S. P., & Weinberg, R. A. (2005). The melanocyte differentiation program predisposes to metastasis after neoplastic transformation. *Nature Genetics*, *37*(10), 1047–1054. https://doi.org/10.1038/ng1634

Hirobe, T. (1984). Histochemical survey of the distribution of the epidermal melanoblasts and melanocytes in the mouse during fetal and postnatal periods. *The Anatomical Record*, *208*(4), 589–594. https://doi.org/10.1002/ar.1092080414

Hodis, E., Watson, I. R., Kryukov, G. V., Arold, S. T., Imielinski, M., Theurillat, J.-P., Nickerson, E., Auclair, D., Li, L., Place, C., DiCara, D., Ramos, A. H., Lawrence, M. S., Cibulskis, K., Sivachenko, A., Voet, D., Saksena, G., Stransky, N., Onofrio, R. C., … Chin, L. (2012). A Landscape of Driver Mutations in Melanoma. *Cell*, *150*(2), 251–263. https://doi.org/10.1016/j.cell.2012.06.024

Hoek, K. S., Eichhoff, O. M., Schlegel, N. C., Döbbeling, U., Kobert, N., Schaerer, L., Hemmi, S., & Dummer, R. (2008). In vivo Switching of Human Melanoma Cells between Proliferative and Invasive States. *Cancer Research*, *68*(3), 650–656. https://doi.org/10.1158/0008-5472.CAN-07-2491

Horton, L., Fakhoury, J. W., Manwar, R., Rajabi-Estarabadi, A., Turk, D., O'Leary, S., Fotouhi, A., Daveluy, S., Jain, M., Nouri, K., Mehregan, D., & Avanaki, K. (2025). Review of Non-Invasive Imaging Technologies for Cutaneous Melanoma. *Biosensors*, *15*(5), Article 5. https://doi.org/10.3390/bios15050297

Hsu, D. S.-S., Wang, H.-J., Tai, S.-K., Chou, C.-H., Hsieh, C.-H., Chiu, P.-H., Chen, N.-J., & Yang, M.-H. (2014). Acetylation of Snail Modulates the Cytokinome of Cancer Cells to Enhance the Recruitment of Macrophages. *Cancer Cell*, *26*(4), 534–548. https://doi.org/10.1016/j.ccell.2014.09.002

Huang, X., Huang, W., Wu, K., Lin, Q., & Chen, G. (2022). PRRX1/FOXM1 reduces gemcitabin-induced cytotoxicity by regulating autophagy in bladder cancer. *Translational Andrology and Urology*, *11*(8), 1116–1129. https://doi.org/10.21037/tau-22-415

Jakob, J. A., Bassett Jr., R. L., Ng, C. S., Curry, J. L., Joseph, R. W., Alvarado, G. C., Rohlfs, M. L., Richard, J., Gershenwald, J. E., Kim, K. B., Lazar, A. J., Hwu, P., & Davies, M. A. (2012). NRAS mutation status is an independent prognostic factor in metastatic melanoma. *Cancer*, *118*(16), 4014–4023. https://doi.org/10.1002/cncr.26724

Jerby-Arnon, L., Shah, P., Cuoco, M. S., Rodman, C., Su, M.-J., Melms, J. C., Leeson, R., Kanodia, A., Mei, S., Lin, J.-R., Wang, S., Rabasha, B., Liu, D., Zhang, G., Margolais, C., Ashenberg, O., Ott, P. A., Buchbinder, E. I., Haq, R., … Regev, A. (2018). A Cancer Cell Program Promotes T Cell Exclusion and Resistance to Checkpoint Blockade. *Cell*, *175*(4), 984-997.e24. https://doi.org/10.1016/j.cell.2018.09.006

Johansson, J., Tabor, V., Wikell, A., Jalkanen, S., & Fuxe, J. (2015). TGF-β1-Induced Epithelial-Mesenchymal Transition Promotes Monocyte/Macrophage

Properties in Breast Cancer Cells. *Frontiers in Oncology*, *5*. https://doi.org/10.3389/fonc.2015.00003

Joshi, S. S., Tandukar, B., Pan, L., Huang, J. M., Livak, F., Smith, B. J., Hodges, T., Mahurkar, A. A., & Hornyak, T. J. (2019). CD34 defines melanocyte stem cell subpopulations with distinct regenerative properties. *PLOS Genetics*, *15*(4), e1008034. https://doi.org/10.1371/journal.pgen.1008034

Karras, P., Bordeu, I., Pozniak, J., Nowosad, A., Pazzi, C., Van Raemdonck, N., Landeloos, E., Van Herck, Y., Pedri, D., Bervoets, G., Makhzami, S., Khoo, J. H., Pavie, B., Lamote, J., Marin-Bejar, O., Dewaele, M., Liang, H., Zhang, X., Hua, Y., … Marine, J.-C. (2022). A cellular hierarchy in melanoma uncouples growth and metastasis. *Nature*, *610*(7930), 190–198. https://doi.org/10.1038/s41586-022-05242-7

Kaucka, M., Szarowska, B., Kavkova, M., Kastriti, M. E., Kameneva, P., Schmidt, I., Peskova, L., Joven Araus, A., Simon, A., Kaiser, J., & Adameyko, I. (2021). Nerve-associated Schwann cell precursors contribute extracutaneous melanocytes to the heart, inner ear, supraorbital locations and brain meninges. *Cellular and Molecular Life Sciences*, *78*(16), 6033–6049. https://doi.org/10.1007/s00018-021-03885-9

Kaufhold, S., & Bonavida, B. (2014). Central role of Snail1 in the regulation of EMT and resistance in cancer: A target for therapeutic intervention. *Journal of Experimental & Clinical Cancer Research*, *33*(1), 62. https://doi.org/10.1186/s13046-014-0062-0

Kaufman, C. K., Mosimann, C., Fan, Z. P., Yang, S., Thomas, A. J., Ablain, J., Tan, J. L., Fogley, R. D., Van Rooijen, E., Hagedorn, E. J., Ciarlo, C., White, R. M., Matos, D. A., Puller, A.-C., Santoriello, C., Liao, E. C., Young, R. A., & Zon, L. I. (2016). A zebrafish melanoma model reveals emergence of neural crest identity during melanoma initiation. *Science*, *351*(6272), aad2197. https://doi.org/10.1126/science.aad2197

Kemper, K., de Goeje, P. L., Peeper, D. S., & van Amerongen, R. (2014). Phenotype Switching: Tumor Cell Plasticity as a Resistance Mechanism and Target for Therapy. *Cancer Research*, *74*(21), 5937–5941. https://doi.org/10.1158/0008-5472.CAN-14-1174

Kim, J. E., Leung, E. Y., Baguley, B. C., & Finlay, G. J. (2013). Heterogeneity of expression of epithelial–mesenchymal transition markers in melanocytes and melanoma cell lines. *Frontiers in Genetics*, *4*. https://doi.org/10.3389/fgene.2013.00097

Köhler, C., Nittner, D., Rambow, F., Radaelli, E., Stanchi, F., Vandamme, N., Baggiolini, A., Sommer, L., Berx, G., Oord, J. J. van den, Gerhardt, H., Blanpain, C., & Marine, J.-C. (2017). Mouse Cutaneous Melanoma Induced by Mutant BRaf Arises

from Expansion and Dedifferentiation of Mature Pigmented Melanocytes. *Cell Stem Cell*, *21*(5), 679-693.e6. https://doi.org/10.1016/j.stem.2017.08.003

Kudo-Saito, C., Shirako, H., Takeuchi, T., & Kawakami, Y. (2009). Cancer Metastasis Is Accelerated through Immunosuppression during Snail-Induced EMT of Cancer Cells. *Cancer Cell*, *15*(3), 195–206. https://doi.org/10.1016/j.ccr.2009.01.023

Lade-Keller, J., Riber-Hansen, R., Guldberg, P., Schmidt, H., Hamilton-Dutoit, S. J., & Steiniche, T. (2013). E- to N-cadherin switch in melanoma is associated with decreased expression of phosphatase and tensin homolog and cancer progression. *British Journal of Dermatology*, *169*(3), 618–628. https://doi.org/10.1111/bjd.12426

Lee, K.-W., Yeo, S.-Y., Gong, J.-R., Koo, O.-J., Sohn, I., Lee, W. Y., Kim, H. C., Yun, S. H., Cho, Y. B., Choi, M.-A., An, S., Kim, J., Sung, C. O., Cho, K.-H., & Kim, S.-H. (2022). PRRX1 is a master transcription factor of stromal fibroblasts for myofibroblastic lineage progression. *Nature Communications*, *13*(1), 2793. https://doi.org/10.1038/s41467-022-30484-4

Lin, J. Y., & Fisher, D. E. (2007). Melanocyte biology and skin pigmentation. *Nature*, *445*(7130), 843–850. https://doi.org/10.1038/nature05660

Madisen, L., Zwingman, T. A., Sunkin, S. M., Oh, S. W., Zariwala, H. A., Gu, H., Ng, L. L., Palmiter, R. D., Hawrylycz, M. J., Jones, A. R., Lein, E. S., & Zeng, H. (2010). A robust and high-throughput Cre reporting and characterization system for the whole mouse brain. *Nature Neuroscience*, *13*(1), 133–140. https://doi.org/10.1038/nn.2467

Mani, S. A., Guo, W., Liao, M.-J., Eaton, E. Ng., Ayyanan, A., Zhou, A. Y., Brooks, M., Reinhard, F., Zhang, C. C., Shipitsin, M., Campbell, L. L., Polyak, K., Brisken, C., Yang, J., & Weinberg, R. A. (2008). The Epithelial-Mesenchymal Transition Generates Cells with Properties of Stem Cells. *Cell*, *133*(4), 704–715. https://doi.org/10.1016/j.cell.2008.03.027

Melnikova, V. O., Bolshakov, S. V., Walker, C., & Ananthaswamy, H. N. (2004). Genomic alterations in spontaneous and carcinogen-induced murine melanoma cell lines. *Oncogene*, *23*(13), 2347–2356. https://doi.org/10.1038/sj.onc.1207405

Michalak-Mićka, K., Büchler, V. L., Zapiórkowska-Blumer, N., Biedermann, T., & Klar, A. S. (2022). Characterization of a melanocyte progenitor population in human interfollicular epidermis. *Cell Reports*, *38*(9), 110419. https://doi.org/10.1016/j.celrep.2022.110419

Miller, A. J., & Mihm, M. C. (2006). Melanoma. *New England Journal of Medicine*, *355*(1), 51–65. https://doi.org/10.1056/NEJMra052166

Moon, H., Donahue, L. R., Choi, E., Scumpia, P. O., Lowry, W. E., Grenier, J. K., Zhu, J., & White, A. C. (2017). Melanocyte Stem Cell Activation and Translocation

Initiate Cutaneous Melanoma in Response to UV Exposure. *Cell Stem Cell*, *21*(5), 665-678.e6. https://doi.org/10.1016/j.stem.2017.09.001

Morel, A.-P., Lièvre, M., Thomas, C., Hinkal, G., Ansieau, S., & Puisieux, A. (2008). Generation of Breast Cancer Stem Cells through Epithelial-Mesenchymal Transition. *PLoS ONE*, *3*(8), e2888. https://doi.org/10.1371/journal.pone.0002888

Mort, R. L., Jackson, I. J., & Patton, E. E. (2015). The melanocyte lineage in development and disease. *Development*, *142*(4), 620–632. https://doi.org/10.1242/dev.106567

Müller-Röver, S., Foitzik, K., Paus, R., Handjiski, B., Van Der Veen, C., Eichmüller, S., McKay, I. A., & Stenn, K. S. (2001). A Comprehensive Guide for the Accurate Classification of Murine Hair Follicles in Distinct Hair Cycle Stages. *Journal of Investigative Dermatology*, *117*(1), 3–15. https://doi.org/10.1046/j.0022-202x.2001.01377.x

Nieto, M. A., & Cano, A. (2012). The epithelial–mesenchymal transition under control: Global programs to regulate epithelial plasticity. *Seminars in Cancer Biology*, *22*(5), 361–368. https://doi.org/10.1016/j.semcancer.2012.05.003

Nieto, M. A., Huang, R. Y.-J., Jackson, R. A., & Thiery, J. P. (2016). EMT: 2016. *Cell*, *166*(1), 21–45. https://doi.org/10.1016/j.cell.2016.06.028

Nishimura, E. K., Jordan, S. A., Oshima, H., Yoshida, H., Osawa, M., Moriyama, M., Jackson, I. J., Barrandon, Y., Miyachi, Y., & Nishikawa, S.-I. (2002). Dominant role of the niche in melanocyte stem-cell fate determination. *Nature*, *416*(6883), 854–860. https://doi.org/10.1038/416854a

Nishimura, E. K., Suzuki, M., Igras, V., Du, J., Lonning, S., Miyachi, Y., Roes, J., Beermann, F., & Fisher, D. E. (2010). Key Roles for Transforming Growth Factor β in Melanocyte Stem Cell Maintenance. *Cell Stem Cell*, *6*(2), 130–140. https://doi.org/10.1016/j.stem.2009.12.010

Ocaña, O. H., Córcoles, R., Fabra, Á., Moreno-Bueno, G., Acloque, H., Vega, S., Barrallo-Gimeno, A., Cano, A., & Nieto, M. A. (2012). Metastatic Colonization Requires the Repression of the Epithelial-Mesenchymal Transition Inducer Prrx1. *Cancer Cell*, *22*(6), 709–724. https://doi.org/10.1016/j.ccr.2012.10.012

Ocaña, O. H., Coskun, H., Minguillón, C., Murawala, P., Tanaka, E. M., Galcerán, J., Muñoz-Chápuli, R., & Nieto, M. A. (2017). A right-handed signalling pathway drives heart looping in vertebrates. *Nature*, *549*(7670), 86–90. https://doi.org/10.1038/nature23454

Paraiso, K. H. T., Xiang, Y., Rebecca, V. W., Abel, E. V., Chen, Y. A., Munko, A. C., Wood, E., Fedorenko, I. V., Sondak, V. K., Anderson, A. R. A., Ribas, A., Palma, M. D.,

Nathanson, K. L., Koomen, J. M., Messina, J. L., & Smalley, K. S. M. (2011). PTEN Loss Confers BRAF Inhibitor Resistance to Melanoma Cells through the Suppression of BIM Expression. *Cancer Research*, *71*(7), 2750–2760. https://doi.org/10.1158/0008-5472.CAN-10-2954

Pastushenko, I., & Blanpain, C. (2019). EMT Transition States during Tumor Progression and Metastasis. *Trends in Cell Biology*, *29*(3), 212–226. https://doi.org/10.1016/j.tcb.2018.12.001

Peinado, H., Olmeda, D., & Cano, A. (2007). Snail, Zeb and bHLH factors in tumour progression: An alliance against the epithelial phenotype? *Nature Reviews Cancer*, *7*(6), 415–428. https://doi.org/10.1038/nrc2131

Piorońska, W., Nwosu, Z. C., Han, M., Büttner, M., Ebert, M. P., Dooley, S., & Meyer, C. (2021). Dysregulated paired related homeobox 1 impacts on hepatocellular carcinoma phenotypes. *BMC Cancer*, *21*(1), 1006. https://doi.org/10.1186/s12885-021-08637-3

Poser, I., Domínguez, D., Herreros, A. G. de, Varnai, A., Buettner, R., & Bosserhoff, A. K. (2001). Loss of E-cadherin Expression in Melanoma Cells Involves Up-regulation of the Transcriptional Repressor Snail *. *Journal of Biological Chemistry*, *276*(27), 24661–24666. https://doi.org/10.1074/jbc.M011224200

Pozniak, J., Pedri, D., Landeloos, E., Van Herck, Y., Antoranz, A., Vanwynsberghe, L., Nowosad, A., Roda, N., Makhzami, S., Bervoets, G., Maciel, L. F., Pulido-Vicuña, C. A., Pollaris, L., Seurinck, R., Zhao, F., Flem-Karlsen, K., Damsky, W., Chen, L., Karagianni, D., … Marine, J.-C. (2024). A TCF4-dependent gene regulatory network confers resistance to immunotherapy in melanoma. *Cell*, *187*(1), 166-183.e25. https://doi.org/10.1016/j.cell.2023.11.037

Qing, F., Xue, J., Sui, L., Xiao, Q., Xie, T., Chen, Y., Huang, J., & Liu, Z. (2023). Intestinal epithelial SNAI1 promotes the occurrence of colorectal cancer by enhancing EMT and Wnt/β-catenin signaling. *Medical Oncology*, *41*(1), 34. https://doi.org/10.1007/s12032-023-02253-w

Rabbani, P., Takeo, M., Chou, W., Myung, P., Bosenberg, M., Chin, L., Taketo, M. M., & Ito, M. (2011). Coordinated Activation of Wnt in Epithelial and Melanocyte Stem Cells Initiates Pigmented Hair Regeneration. *Cell*, *145*(6), 941–955. https://doi.org/10.1016/j.cell.2011.05.004

Rago, L., Castroviejo, N., Fazilaty, H., Garcia-Asencio, F., Ocaña, O. H., Galcerán, J., & Nieto, M. A. (2019). MicroRNAs Establish the Right-Handed Dominance of the Heart Laterality Pathway in Vertebrates. *Developmental Cell*, *51*(4), 446-459.e5. https://doi.org/10.1016/j.devcel.2019.09.012

Raimondi, S., Suppa, M., & Gandini, S. (2020). Melanoma Epidemiology and Sun Exposure. *Acta Dermato-Venereologica*, *100*(11), Article 11. https://doi.org/10.2340/00015555-3491

Rambow, F., Rogiers, A., Marin-Bejar, O., Aibar, S., Femel, J., Dewaele, M., Karras, P., Brown, D., Chang, Y. H., Debiec-Rychter, M., Adriaens, C., Radaelli, E., Wolter, P., Bechter, O., Dummer, R., Levesque, M., Piris, A., Frederick, D. T., Boland, G., … Marine, J.-C. (2018). Toward Minimal Residual Disease-Directed Therapy in Melanoma. *Cell*, *174*(4), 843-855.e19. https://doi.org/10.1016/j.cell.2018.06.025

Redmer, T., Welte, Y., Behrens, D., Fichtner, I., Przybilla, D., Wruck, W., Yaspo, M.-L., Lehrach, H., Schäfer, R., & Regenbrecht, C. R. A. (2014). The Nerve Growth Factor Receptor CD271 Is Crucial to Maintain Tumorigenicity and Stem-Like Properties of Melanoma Cells. *PLOS ONE*, *9*(5), e92596. https://doi.org/10.1371/journal.pone.0092596

Redondo-Muñoz, M., Rodriguez-Baena, F. J., Aldaz, P., Caballé-Mestres, A., Moncho-Amor, V., Otaegi-Ugartemendia, M., Carrasco-Garcia, E., Olias-Arjona, A., Lasheras-Otero, I., Santamaria, E., Bocanegra, A., Chocarro, L., Grier, A., Dzieciatkowska M, M., Bigas, C., Martin, J., Urdiroz-Urricelqui, U., Marzo, F., Santamaria, E., … Arozarena, I. (2023). Metabolic rewiring induced by ranolazine improves melanoma responses to targeted therapy and immunotherapy. *Nature Metabolism*, *5*(9), 1544–1562. https://doi.org/10.1038/s42255-023-00861-4

Restifo, N. P., Smyth, M. J., & Snyder, A. (2016). Acquired resistance to immunotherapy and future challenges. *Nature Reviews Cancer*, *16*(2), 121–126. https://doi.org/10.1038/nrc.2016.2

Richard, G., Dalle, S., Monet, M., Ligier, M., Boespflug, A., Pommier, R. M., de la Fouchardière, A., Perier-Muzet, M., Depaepe, L., Barnault, R., Tondeur, G., Ansieau, S., Thomas, E., Bertolotto, C., Ballotti, R., Mourah, S., Battistella, M., Lebbé, C., Thomas, L., … Caramel, J. (2016). ZEB1-mediated melanoma cell plasticity enhances resistance to MAPK inhibitors. *EMBO Molecular Medicine*, *8*(10), 1143–1161. https://doi.org/10.15252/emmm.201505971

Robert, C., Grob, J. J., Stroyakovskiy, D., Karaszewska, B., Hauschild, A., Levchenko, E., Sileni, V. C., Schachter, J., Garbe, C., Bondarenko, I., Gogas, H., Mandalá, M., Haanen, J. B. A. G., Lebbé, C., Mackiewicz, A., Rutkowski, P., Nathan, P. D., Ribas, A., Davies, M. A., … Long, G. V. (2019). Five-Year Outcomes with Dabrafenib plus Trametinib in Metastatic Melanoma. *New England Journal of Medicine*, *381*(7), 626–636. https://doi.org/10.1056/NEJMoa1904059

Rodríguez, C. I., & Setaluri, V. (2014). Cyclic AMP (cAMP) signaling in melanocytes and melanoma. *Archives of Biochemistry and Biophysics*, *563*, 22–27. https://doi.org/10.1016/j.abb.2014.07.003

Rodriguez-Baena, F. J., Marquez-Galera, A., Ballesteros-Martinez, P., Castillo, A., Diaz, E., Moreno-Bueno, G., Lopez-Atalaya, J. P., & Sanchez-Laorden, B. (2025). Microglial reprogramming enhances antitumor immunity and immunotherapy response in melanoma brain metastases. *Cancer Cell*, *43*(3), 413-427.e9. https://doi.org/10.1016/j.ccell.2025.01.008

Roh, M. R., Eliades, P., Gupta, S., & Tsao, H. (2015). Genetics of melanocytic nevi. *Pigment Cell & Melanoma Research*, *28*(6), 661–672. https://doi.org/10.1111/pcmr.12412

Rowe, R. G., Li, X.-Y., Hu, Y., Saunders, T. L., Virtanen, I., de Herreros, A. G., Becker, K.-F., Ingvarsen, S., Engelholm, L. H., Bommer, G. T., Fearon, E. R., & Weiss, S. J. (2009). Mesenchymal cells reactivate Snail1 expression to drive three-dimensional invasion programs. *Journal of Cell Biology*, *184*(3), 399–408. https://doi.org/10.1083/jcb.200810113

Rowling, E. J., Miskolczi, Z., Nagaraju, R., Wilcock, D. J., Wang, P., Telfer, B., Li, Y., Lasheras-Otero, I., Redondo-Muñoz, M., Sharrocks, A. D., Arozarena, I., & Wellbrock, C. (2020). Cooperative behaviour and phenotype plasticity evolve during melanoma progression. *Pigment Cell & Melanoma Research*, *33*(5), 695–708. https://doi.org/10.1111/pcmr.12873

Sacco, A., Forgione, L., Carotenuto, M., De Luca, A., Ascierto, P. A., Botti, G., & Normanno, N. (2020). Circulating Tumor DNA Testing Opens New Perspectives in Melanoma Management. *Cancers*, *12*(10), Article 10. https://doi.org/10.3390/cancers12102914

Sade-Feldman, M., Jiao, Y. J., Chen, J. H., Rooney, M. S., Barzily-Rokni, M., Eliane, J.-P., Bjorgaard, S. L., Hammond, M. R., Vitzthum, H., Blackmon, S. M., Frederick, D. T., Hazar-Rethinam, M., Nadres, B. A., Van Seventer, E. E., Shukla, S. A., Yizhak, K., Ray, J. P., Rosebrock, D., Livitz, D., … Hacohen, N. (2017). Resistance to checkpoint blockade therapy through inactivation of antigen presentation. *Nature Communications*, *8*(1), 1136. https://doi.org/10.1038/s41467-017-01062-w

Schneider, M. R., Schmidt-Ullrich, R., & Paus, R. (2009). The Hair Follicle as a Dynamic Miniorgan. *Current Biology*, *19*(3), R132–R142. https://doi.org/10.1016/j.cub.2008.12.005

Shain, A. H., & Bastian, B. C. (2016). From melanocytes to melanomas. *Nature Reviews Cancer*, *16*(6), 345–358. https://doi.org/10.1038/nrc.2016.37

Shain, A. H., Yeh, I., Kovalyshyn, I., Sriharan, A., Talevich, E., Gagnon, A., Dummer, R., North, J., Pincus, L., Ruben, B., Rickaby, W., D'Arrigo, C., Robson, A., & Bastian, B. C. (2015). The Genetic Evolution of Melanoma from Precursor Lesions. *New England Journal of Medicine*, *373*(20), 1926–1936. https://doi.org/10.1056/NEJMoa1502583

Siegel, R. L., Kratzer, T. B., Giaquinto, A. N., Sung, H., & Jemal, A. (2025). Cancer statistics, 2025. *CA: A Cancer Journal for Clinicians*, *75*(1), 10–45. https://doi.org/10.3322/caac.21871

Slominski, A., Tobin, D. J., Shibahara, S., & Wortsman, J. (2004). Melanin Pigmentation in Mammalian Skin and Its Hormonal Regulation. *Physiological Reviews*, *84*(4), 1155–1228. https://doi.org/10.1152/physrev.00044.2003

Sun, Q., Lee, W., Hu, H., Ogawa, T., De Leon, S., Katehis, I., Lim, C. H., Takeo, M., Cammer, M., Taketo, M. M., Gay, D. L., Millar, S. E., & Ito, M. (2023). Dedifferentiation maintains melanocyte stem cells in a dynamic niche. *Nature*, *616*(7958), 774–782. https://doi.org/10.1038/s41586-023-05960-6

Sun, Q., Lee, W., Mohri, Y., Takeo, M., Lim, C. H., Xu, X., Myung, P., Atit, R. P., Taketo, M. M., Moubarak, R. S., Schober, M., Osman, I., Gay, D. L., Saur, D., Nishimura, E. K., & Ito, M. (2019). A novel mouse model demonstrates that oncogenic melanocyte stem cells engender melanoma resembling human disease. *Nature Communications*, *10*(1), 5023. https://doi.org/10.1038/s41467-019-12733-1

Sun, Y., Shen, Y., Liu, Q., Zhang, H., Jia, L., Chai, Y., Jiang, H., Wu, M., & Li, Y. (2025). Global trends in melanoma burden: A comprehensive analysis from the Global Burden of Disease Study, 1990-2021. *Journal of the American Academy of Dermatology*, *92*(1), 100–107. https://doi.org/10.1016/j.jaad.2024.09.035

Sun, Y., Ying, K., Sun, J., Wang, Y., Qiu, L., Ji, M., Sun, L., & Chen, J. (2024). PRRX1-OLR1 axis supports CAFs-mediated lung cancer progression and immune suppression. *Cancer Cell International*, *24*(1), 247. https://doi.org/10.1186/s12935-024-03436-9

Sung, H., Ferlay, J., Siegel, R. L., Laversanne, M., Soerjomataram, I., Jemal, A., & Bray, F. (2021). Global Cancer Statistics 2020: GLOBOCAN Estimates of Incidence and Mortality Worldwide for 36 Cancers in 185 Countries. *CA: A Cancer Journal for Clinicians*, *71*(3), 209–249. https://doi.org/10.3322/caac.21660

Tang, Y., Durand, S., Dalle, S., & Caramel, J. (2020). EMT-Inducing Transcription Factors, Drivers of Melanoma Phenotype Switching, and Resistance to Treatment. *Cancers*, *12*(8), 2154. https://doi.org/10.3390/cancers12082154

TheJacksonLab—BRaf[CA], Pten[loxP], Tyr::CreER[T2] Strain Details. (n.d.). Retrieved 28 June 2025, from https://www.jax.org/strain/013590

Tirosh, I., Izar, B., Prakadan, S. M., Wadsworth, M. H., Treacy, D., Trombetta, J. J., Rotem, A., Rodman, C., Lian, C., Murphy, G., Fallahi-Sichani, M., Dutton-Regester, K., Lin, J.-R., Cohen, O., Shah, P., Lu, D., Genshaft, A. S., Hughes, T. K., Ziegler, C. G. K., … Garraway, L. A. (2016). Dissecting the multicellular ecosystem of metastatic melanoma by single-cell RNA-seq. *Science*, *352*(6282), 189–196. https://doi.org/10.1126/science.aad0501

Tsirigoti, C., Ali, M. M., Maturi, V., Heldin, C.-H., & Moustakas, A. (2022). Loss of SNAI1 induces cellular plasticity in invasive triple-negative breast cancer cells. *Cell Death & Disease*, *13*(9), 1–17. https://doi.org/10.1038/s41419-022-05280-z

Valluet, A., Druillennec, S., Barbotin, C., Dorard, C., Monsoro-Burq, A. H., Larcher, M., Pouponnot, C., Baccarini, M., Larue, L., & Eychène, A. (2012). B-Raf and C-Raf Are Required for Melanocyte Stem Cell Self-Maintenance. *Cell Reports*, *2*(4), 774–780. https://doi.org/10.1016/j.celrep.2012.08.020

van der Veen, C., Handjiski, B., Paus, R., Müller-Röver, S., Maurer, M., Eichmüller, S., Ling, G., Hofmann, U., Foitzik, K., & Mecklenburg, L. (1999). A Comprehensive Guide for the Recognition and Classification of Distinct Stages of Hair Follicle Morphogenesis. *Journal of Investigative Dermatology*, *113*(4), 523–532. https://doi.org/10.1046/j.1523-1747.1999.00740.x

Vandamme, N., Denecker, G., Bruneel, K., Blancke, G., Akay, Ö., Taminau, J., De Coninck, J., De Smedt, E., Skrypek, N., Van Loocke, W., Wouters, J., Nittner, D., Köhler, C., Darling, D. S., Cheng, P. F., Raaijmakers, M. I. G., Levesque, M. P., Mallya, U. G., Rafferty, M., … Berx, G. (2020). The EMT Transcription Factor ZEB2 Promotes Proliferation of Primary and Metastatic Melanoma While Suppressing an Invasive, Mesenchymal-Like Phenotype. *Cancer Research*, *80*(14), 2983–2995. https://doi.org/10.1158/0008-5472.CAN-19-2373

Vázquez-Naharro, A., Alberto Vázquez-Naharro, José Bustos-Tauler, José Bustos-Tauler, Floristán, A., Alfredo Floristán, Yuste, L., Lourdes Yuste, Sara S. Oltra, Silvestre Oltra, Vinyals, A., Antònia Vinyals, Moreno-Bueno, G., Gema Moreno-Bueno, Àngels Fabra, Àngels Fabra, Portillo, F., Francisco Portillo, Cano, A., … Patricia G. Santamaría. (2022). Loxl3 Promotes Melanoma Progression and Dissemination Influencing Cell Plasticity and Survival. *Cancers*, *14*(5), 1200–1200. https://doi.org/10.3390/cancers14051200

Viros, A., Sanchez-Laorden, B., Pedersen, M., Furney, S. J., Rae, J., Hogan, K., Ejiama, S., Girotti, M. R., Cook, M., Dhomen, N., & Marais, R. (2014). Ultraviolet radiation accelerates BRAF-driven melanomagenesis by targeting TP53. *Nature*, *511*(7510), 478–482. https://doi.org/10.1038/nature13298

Warzecha, C. C., & Carstens, R. P. (2012). Complex changes in alternative pre-mRNA splicing play a central role in the epithelial-to-mesenchymal transition (EMT). *Seminars in Cancer Biology*, *22*(5), 417–427. https://doi.org/10.1016/j.semcancer.2012.04.003

Wong, S. L., Balch, C. M., Hurley, P., Agarwala, S. S., Akhurst, T. J., Cochran, A., Cormier, J. N., Gorman, M., Kim, T. Y., McMasters, K. M., Noyes, R. D., Schuchter, L. M., Valsecchi, M. E., Weaver, D. L., & Lyman, G. H. (2012). Sentinel Lymph Node Biopsy for Melanoma: American Society of Clinical Oncology and Society of Surgical Oncology Joint Clinical Practice Guideline. *Journal of Clinical Oncology*, *30*(23), 2912–2918. https://doi.org/10.1200/JCO.2011.40.3519

Wouters, J., Kalender-Atak, Z., Minnoye, L., Spanier, K. I., De Waegeneer, M., Bravo González-Blas, C., Mauduit, D., Davie, K., Hulselmans, G., Najem, A., Dewaele, M., Pedri, D., Rambow, F., Makhzami, S., Christiaens, V., Ceyssens, F., Ghanem, G., Marine, J.-C., Poovathingal, S., & Aerts, S. (2020). Robust gene expression programs underlie recurrent cell states and phenotype switching in melanoma. *Nature Cell Biology*, *22*(8), 986–998. https://doi.org/10.1038/s41556-020-0547-3

Yan, S., Yu, Z., Primiero, C., Vico-Alonso, C., Wang, Z., Yang, L., Tschandl, P., Hu, M., Ju, L., Tan, G., Tang, V., Ng, A. B., Powell, D., Bonnington, P., See, S., Magnaterra, E., Ferguson, P., Nguyen, J., Guitera, P., … Ge, Z. (2025). A multimodal vision foundation model for clinical dermatology. *Nature Medicine*. https://doi.org/10.1038/s41591-025-03747-y

Yang, J., Antin, P., Berx, G., Blanpain, C., Brabletz, T., Bronner, M., Campbell, K., Cano, A., Casanova, J., Christofori, G., Dedhar, S., Derynck, R., Ford, H. L., Fuxe, J., García de Herreros, A., Goodall, G. J., Hadjantonakis, A.-K., Huang, R. Y. J., Kalcheim, C., … Sheng, G. (2020). Guidelines and definitions for research on epithelial–mesenchymal transition. *Nature Reviews Molecular Cell Biology*, *21*(6), 341–352. https://doi.org/10.1038/s41580-020-0237-9

Youssef, K. K., Narwade, N., Arcas, A., Marquez-Galera, A., Jiménez-Castaño, R., Lopez-Blau, C., Fazilaty, H., García-Gutierrez, D., Cano, A., Galcerán, J., Moreno-Bueno, G., Lopez-Atalaya, J. P., & Nieto, M. A. (2024). Two distinct epithelial-to-mesenchymal transition programs control invasion and inflammation in segregated tumor cell populations. *Nature Cancer*, *5*(11), 1660–1680. https://doi.org/10.1038/s43018-024-00839-5

Youssef, K. K., & Nieto, M. A. (2024). Epithelial–mesenchymal transition in tissue repair and degeneration. *Nature Reviews Molecular Cell Biology*, *25*(9), 720–739. https://doi.org/10.1038/s41580-024-00733-z

Zhong, L., Tan, W., Yang, Q., Zou, Z., Zhou, R., Huang, Y., Qiu, Z., Zheng, K., & Huang, Z. (2022). PRRX1 promotes colorectal cancer stemness and chemoresistance via the JAK2/STAT3 axis by targeting IL-6. *Journal of Gastrointestinal Oncology*, *13*(6), 2989–3008. https://doi.org/10.21037/jgo-22-1137

13 Acknowledgments

Quiero dedicar este apartado de la tesis para agradecer a todas las personas que me han ayudado durante este largo proceso que es la tesis doctoral. Ha habido momentos difíciles y momentos felices, y se ha hecho un poco más cuesta arriba llegando al final, pero gracias a vosotros puedo llegar a dar fin a esta etapa.

En primer lugar, quiero agradecer a mi mentora y directora de tesis **Berta L. Sánchez-Laorden**. Gracias por abrirme las puertas y por darme la oportunidad de formar parte de este proyecto en el laboratorio. Gracias por haber tenido paciencia conmigo cuando aún estaba "muy verde" y de ayudarme a crecer en el ámbito científico y personal. Me has enseñado a ver que siempre podemos mejorar y nunca es tarde para cambiar lo que sea necesario, y que con esfuerzo podemos llegar a nuestras metas. Gracias también por darme libertad para explorar aquellas ideas y enfoques de los que no estábamos seguros de que funcionarían. Me alegra haber formado parte de tu grupo de investigación desde los orígenes y ser testigo del crecimiento y la trayectoria que ha tenido bajo tu liderazgo, y estoy seguro de que ese camino estará lleno de éxitos. Gracias por apoyarme y entenderme en los momentos difíciles, ya que sin tu ayuda nada de esto habría sido posible.

También quiero agradecer a **Angela Nieto**, por la experiencia, conocimiento e inspiración que transmite en cada reunión, que me han ayudado a afrontar las dificultades de la tesis. A **Joan Galceran**, por estar dispuesto siempre a darme consejos de cómo realizar y mejorar las técnicas de biología molecular. Todas vuestras sugerencias y aportaciones han sido de gran ayuda.

Quiero también agradecer a todos los miembros del laboratorio de Berta y de Angela, por el apoyo, el compañerismo y el ambiente que habéis tan agradable que habéis creado. Es una alegría para mi haber podido formar parte de este equipo tan grande y me llevo conmigo un cachito de todos vosotros.

A **Javi**. Estuviste conmigo desde el principio cuando entramos al laboratorio, y siempre has sido un apoyo que no tiene precio. Gracias por siempre estar dispuesto a escuchar mis dudas científicas y no tan científicas, a veces demasiado rebuscadas. Me ayudaste a aprender a valorar mi trabajo y a ganar confianza en mí mismo. Tus consejos siempre han sido de vital ayuda y me han ayudado a lo largo de este largo camino. Siempre has sabido darle alegría al laboratorio cuando más lo necesitábamos. Nunca olvidaré los retreats, las horas de confocal, los jueves, los festivales ni los coches del pasado. Gracias por todo.

A **Marta**. Como tú ya dijiste, has sido mi compañera de batallas desde que entraste en el laboratorio. Aunque llegaste después de mí, siempre has sido la primera en enfrentarte a las dificultades que teníamos por delante, y no me extraña que por eso

te marchases antes. Gracias por el apoyo mutuo durante esta travesía. Gracias por tus saludos largos, tus risas esporádicas y tus locuras. Gracias por nuestras sesiones musicales de cultivos y todos los ratos que pasamos en los microscopios. No quiero dejar sin mencionar los "papelitos", la niebla y todos los cafés de emergencia.

A **Pablo**. Gracias por siempre estar pendiente de todos nosotros, de mantener esa motivación constante y de transmitir esa energía y disciplina. Por aguantar mi música y estar siempre dispuesto a debatir nuestras teorías. Por nuestros saludos de fusión que para mí son muy especiales. Por saber que siempre podía contar contigo para cualquier cosa, en cualquier momento, fuese o no del laboratorio. Por reírte conmigo de nuestras desgracias. Por lo que he dicho y lo que queda por decir, muchas gracias.

A **Fran Quiles**. Recuerdo aquellos dias que entraste al laboratorio y comenzaste a aprender conmigo en cultivos; tardaste poco en superarme. Gracias por estar dispuesto a ayudar siempre, de ser un ejemplo de autodeterminación y por llenar las tardes de energía "tikitiki". Por compartir conmigo los dramas de la qPCR. Por todos esos buenos momentos que hemos vivido.

A **Sonia**. Por ayudarme y enseñarme tanto en cultivos. Por tus consejos de cómo organizarme y llevar a cabo los experimentos. Por toda la amabilidad que siempre tuviste conmigo.

A **Cris**. Gracias por todos los "Una cosa, Cris…", que nunca eran fáciles ni rápidos. Por todo el empeño en enseñarme cuando hizo falta. Por siempre sacar ese lado divertido. Por todas mis liadas de novato que conseguimos solucionar. Por todas las veces que nos veremos en el Leyendas.

A **Alba**. Gracias por darnos tus alegrías y resoplidos, por tu espontaneidad y tu facilidad de encontrar el lado divertido de las cosas. Y no olvides que un post-it bien colocado tapa bien el sol.

A **Khalil** y **Raúl**. Me habéis ayudado en el diseño y la ejecución de un montón de experimentos. Siempre habéis tenido tiempo para pararos a contestar mis dudas, y no dudabais en aportar ideas a la hora de mejorar lo que estábamos haciendo. Vuestra aportación ha sido fundamental para poder desarrollar mi tesis doctoral. Os agradezco muchísimos todo el apoyo que me habéis brindado.

A **Ana**, por llenar de sonrisas y buenos recuerdos todos los dias del laboratorio, los consejos, tus enseñanzas y estar ahí como una madre postiza, y a **Gema**, siempre pendiente de si podía ayudar en algo más y por esa energía positiva contagiosa. Por todos desayunos y los Springs que estuvimos, y en los que nos volveremos a ver. A **Marilyn**, por todas las bromas y buenos ratos que pasamos juntos. A Macarena, que, aunque has llegado más tarde, no has dejado de poner sonrisas y dulces en todos nosotros.

A **Aida**, porque siempre encontraste algun hueco para enseñarme más sobre bioinformática, por introducirme en el mundillo del New Romance y por siempre volver para vernos. A **Auxi, Fara, Diana, Mariángeles, Hassan, Andrea, Andrés, David, Ismael, Beate**, **Maria, José** y **Paloma**, con quienes he coincidido menos tiempo en el laboratorio y de quien me llevo un pedacito de vosotros.

To **Nitin**, thanks for being always ready to help me with all my questions about transcriptomics with a smile on your face. A **Aurelia**, por apoyarme desde el primer momento y a lo largo del camino que estoy emprendiendo.

A **Noemi, Fran Garcia, Ainara, Lucia, Aysha, Bea** y **Alicia**. A **Juan, Oscar** y **Selene**. Por los ratos en el instituto y fuera del instituto. Por nuestros festivales. Por todo vuestro apoyo y vuestro entendimiento. A **Mari**, por todas las veces que dijimos de quedar y no quedamos, y por todas nuestras charlas que vienen de lejos.

A las personas que trabajan en las unidades de apoyo del instituto. A **Antonio**, y las horas que hemos pasado en el citómetro. A **Trini** y las sonrisas que nos saca por las mañanas cuando llega con su carrito. A **Sara** y nuestras conversaciones en la oficina de cultivos.

También quiero agradecer a todas esas personas que, aunque no han colaborado directamente en el desarrollo de la tesis, han sido muy importantes para poder avanzar a lo largo de esta etapa.

A los del pueblo, **Albert, Maria Isabel** y **Carolina**, siempre dispuestos a buscar una forma de reencontrarnos, aunque llevemos meses sin vernos. A los de Murcia, **Marina, Emilio, Alicia, Paco, Juan, Alfredo, Franky** y **Sofia**, que a pesar del tiempo y que cada uno esté en un sitio distinto, hacemos lo posible para volver a reencontrarnos. A **Elena**, que supo ayudarme a avanzar y llegar al final de esta etapa.

A **Alex, Carla** y **Raquel**. Por todas las salidas a la puerta, los cafés, las conversaciones y los apoyos. Por todas las ideas y sugerencias. Por todos los buenos y los malos ratos que hemos pasado juntos. Por estar siempre dispuestos a escucharme. Y porque, aunque la distancia ponga barreras, siempre estaremos juntos de una forma u otra. A **Adri**, porque aun estando lejos todo este tiempo, siempre has estado presente y dispuesto a venir a las tierras del metal. Gracias a todos vosotros, por todas las aventuras que hemos vivido juntos y las quedan aún por vivir; me habéis hecho crecer como persona.

A los del rol, **Javi, Edu, Javier, Tatín, Juanma** y **Antonio**, sin olvidar a **Alex, Adri, Carla** y **Raquel**. Por todas las aventuras que hemos vivido durante estos años, y por hacer más fácil la tesis. A los del tatuaje, **Adri, Carla, Iris, Vero** y **Sara**, por siempre estar ahí, aunque la distancia, el tiempo y las circunstancias hayan hecho difícil que estemos juntos. A **Paqui, Edu** y **Diego**, por estar siempre dispuestos a ayudar en lo

que sea, aunque ya no esté entre ellos. Y a todos aquellos que llegaron y se fueron muy pronto; me hubiera gustado pasar más tiempo con vosotros.

A mi familia, por estar presente y por el apoyo durante todo este trayecto aun estando a cientos de kilómetros. Por entender mis circunstancias y buscar siempre la forma de juntarnos todos cuando era posible. Por todas las provisiones con las que volvía para hacerme más fácil la tesis. Por estar siempre ahí.

Y a ti **Nacho**, que has sido el mayor apoyo que he tenido durante todo este proceso. Gracias por aguantarme y hacer lo posible para animarme cuando todo se hacía cuesta arriba. Gracias por facilitarme siempre las cosas, por guiarme cuando no encontraba una razón y por darme fuerzas para llegar al final de este arduo camino. Gracias por empujarme cuando no tenía fuerzas para hacerlo yo mismo. Gracias por todo lo que haces, por lanzarte conmigo a nuestros proyectos y por estar siempre cerca de mí. Te quiero.

Al final, todo este proceso no ha sido resultado únicamente de mi esfuerzo personal, sino del trabajo conjunto y el apoyo de todas las personas que me han rodeado durante estos últimos años. Me es imposible agrupar todo lo que podria decir de vosotros en unas pocas páginas. Sin vosotros, nada de esto habría sido posible. Muchas gracias de corazón.